Fall 12-20-2013

A Numerical Study of High Temperature and High Velocity Gaseous Hydrogen Flow in a Cooling Channel of a NTR Core

Sajan B. Singh
sbsingh@uno.edu

A Numerical Study of High Temperature and High Velocity Gaseous Hydrogen Flow in a Cooling Channel of a NTR Core

A Thesis

Submitted to the Graduate faculty of
University of New Orleans
in partial fulfillment of the
requirements for the degree of

Master of Science
In
Mechanical Engineering
Thermal Fluids Science

by

Sajan Bikram Singh

B.Sc., University of New Orleans, 2010

December, 2013

Dedication

This research study is dedicated to my wonderful mother, Chandra Devi Singh, and to my love, Prashiddhi Chand, for their infinite love and continuous support.

Acknowledgements

I would like to attribute the success of this project to Dr. Kazim M. Akyuzlu, Professor of Mechanical Engineering. Dr. Akyuzlu with his strong intellect and motivating personality inculcated a positive attitude in me. The present thesis would not have been possible without his elaborate guidance and full encouragement. I would also like to thank Dr. Uttam Chakravarty, Associate Professor of Mechanical Engineering, for serving on my thesis committee.

I would like to express my sincere thanks to Dr. Paul D. Herrington, Professor of Mechanical Engineering, and Dr. David Hui, Professor of Mechanical Engineering for serving in my thesis committee and their help in courses and projects. I would also like to thank the Department of Mechanical Engineering at the University of New Orleans for providing financial assistance.

I am extremely grateful to my classmate Wesley and Jose for their help in developing the models used in this study. I would also like to thank my friends Harish, Binod, Dipankar, Rameel, Rich, Bishal and Krishna for their encouragement and support throughout my studies. Special thanks goes to my friends and roommates Barsha, Shashank, Tshering, Subin, Sajen and Aditya for being so understanding and supportive of me during this journey.

I feel indebted to my family for their never ending care and encouragement. I would like to thank especially my love, Prashiddhi Chand. Her support, inspiration, and constant love have sustained me throughout this journey.

Table of contents

Nomenclature

Symbols

A_c	cross sectional area
AR	channel aspect ratio (L/D)
C_f	friction coefficient
c_p	specific heat at constant pressure
D	diameter of the pipe
t	thickness of the pipe
F	frictional losses, shape factor
f	Fanning friction coefficient
k	thermal conductivity
K	turbulence kinetic energy
L	axial length of the channel
m	mass flow rate
n	Stoichiometric constant
p	pressure of the gas
Pr	Prandtl number
Ma	Mach number
q	heat flux
Q_H	heat input
R	gas constant

Re	Reynolds number
T	time
T	temperature
u_x	axial velocity
x	axial coordinate
r	radial coordinate
n_f	radial mesh layers in the fluid domain
n_s	radial mesh layers in the solid domain

Greek Symbols

ε	turbulence dissipation function, roughness factor
β	area ratio
β_R	radiative diffusion mean extinction coefficient
μ	Absolute viscosity
v	kinematic viscosity
ρ	density
τ	shear stress
σ	Stephan Boltzmann constant, transformed coordinate in r-direction

Subscripts

abs	absolute
eff	effective
rad	radiative
t	turbulent
i	inlet
e	exit
cst	constant

max	maximum
f	fluid
s	solid
m	mean
dot	*rate*

List of Figures

List of Tables

Abstract

Two mathematical models (a one and a three-dimensional) were adopted to study, numerically, the thermal hydrodynamic behavior of flow inside a single cooling channel of a Nuclear Thermal Rocket (NTR) engine. The first model assumes the flow in the cooling channel to be one-dimensional, unsteady, compressible, turbulent, and subsonic. The working fluid (GH_2) is assumed to be compressible. The governing equations of the 1-D model are discretized using a second order accurate finite difference scheme. Also, a commercial CFD code is used to study the same problem. Numerical experiments, using both codes, simulated the flow and heat transfer in a cooling channel of the reactor. The steady state predictions of both models were compared to the existing experimental results and it is concluded that both models successfully predict the steady state fluid temperature distribution in the NTR cooling channel.

Keywords: Thermal Hydrodynamic, Unsteady, Compressible, Turbulent, CFD Models, Discretization

Chapter 1

Introduction

The main objective of this thesis is to study the flow of gaseous hydrogen in the cooling channel of a NTR core and to simulate the flow to achieve the results identical to the ones from the experiment. A one-dimensional mathematical model is developed to predict the temperature and pressure change in a flow inside a cooling channel of a NTR reactor. Also, a three-dimensional commercial CFD model is adopted to calibrate the one-dimensional model in terms of pressure and temperature.

A typical NTR engine (see Figure 1) is composed turbo-pumps to pressurize the cryogenic hydrogen, external shield, nuclear reactor (reactor core, control drum, internal shield), nozzle, and the nozzle extension. The flow diagram for the hydrogen is shown in Figure 2. See reference [1, 2, 3, and 4].

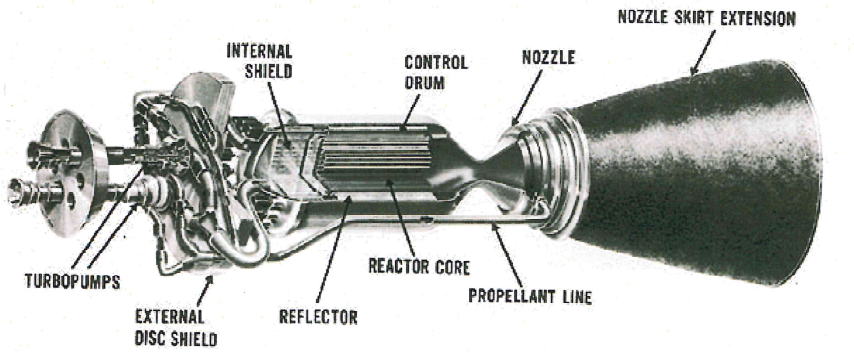

Figure 1 - Typical NERVA Derived NTR Engine [2]

The nuclear core is composed of a matrix of fuel elements with cooling channels through which the pressurized cryogenic fluid (hydrogen) flows (see Figure 2.) Typical fuel elements are hexagonal shape and made of composite fuel (UC_2 coated with ZrC) graphite matrix shown in the same figure. The fuel matrix could also be in coated particle matrix form or as a composite matrix form. The cooling channels are one tenth of an inch (2.54 mm) in diameter and each fuel element has 16 of them as shown in Figure 3 and Figure 4. The fuel core also contains tie tubes which extracts additional thermal energy from the nuclear core to drive the turbo-pumps (TPA) [4].

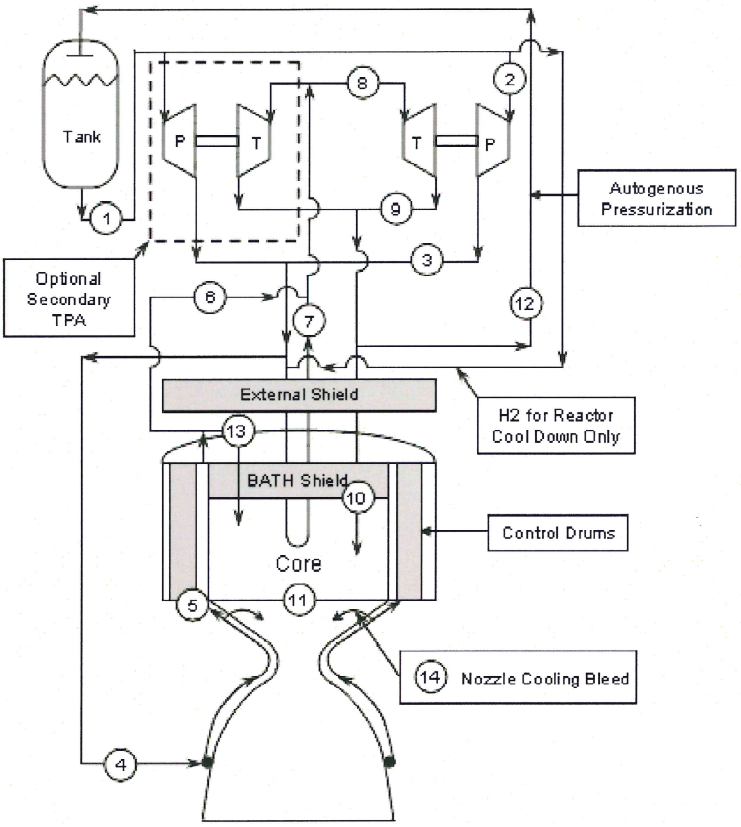

Figure 2 - Typical NTR - GH2 Expander Cycle Flow Diagram [3]

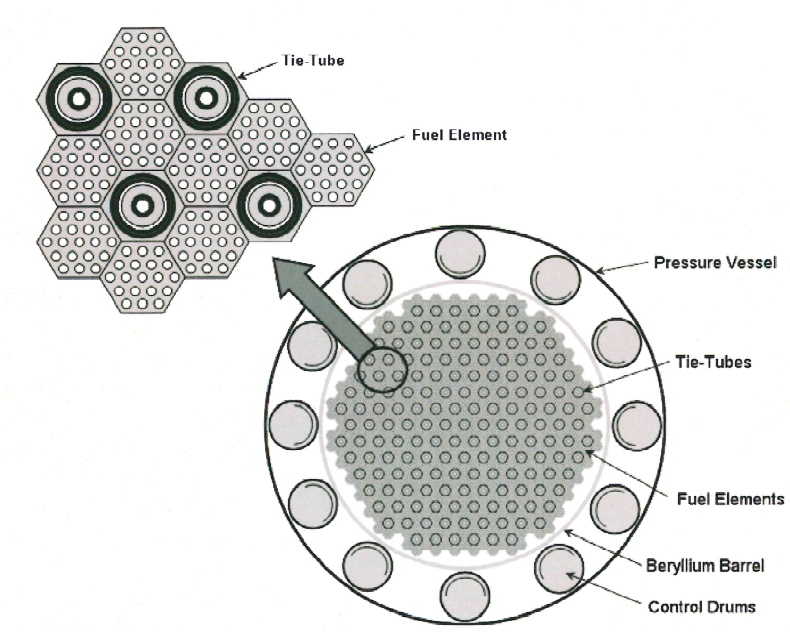

Figure 3 - NTR Fission Reactor Cross-Section [4]

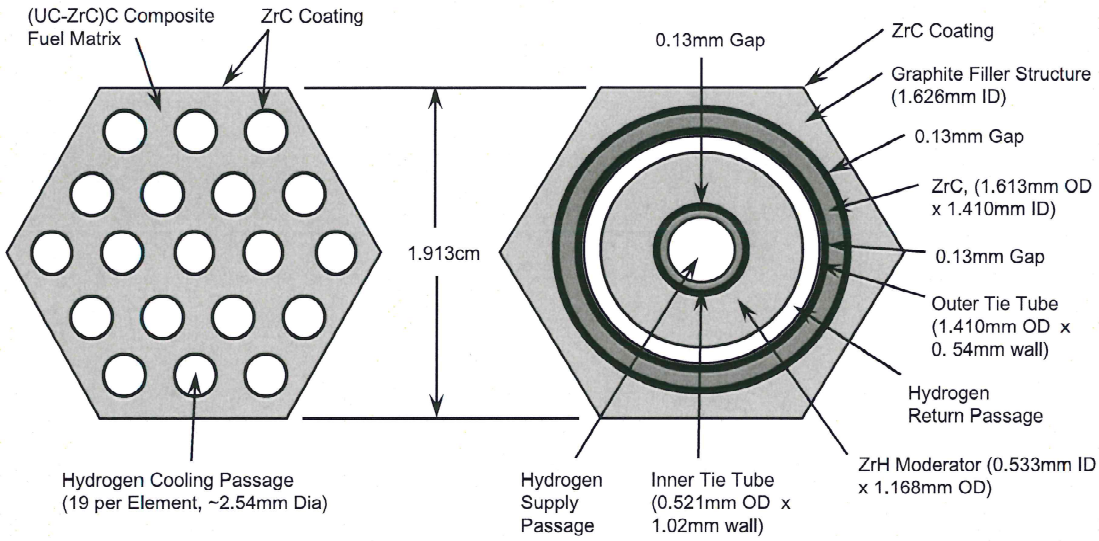

Figure 4 - NTR Fission Reactor Fuel Element and Tie Tube Cross-Sections [3]

The fluid attains high temperatures while passing through the cooling channels of the core and then expands in the converging–diverging nozzle. Temperatures in the core can reach to reach 2500 degree Kelvin. Maximum hydrogen temperature is very close to this value. The operating pressure of a typical NTR core is around 3 MPa. Some experimental NTRs have operated at higher pressures. Thermal power of the nuclear reactor which creates a thrust of 337 kN is 1570 Mw for the NERVA engine. Hydrogen flow rate is 41.6 kg/sec and expansion ratio through the

nozzle is 100:1. Chamber pressure and temperature for this engine is 3.1 MPa and 2360 degree Kelvin, respectively [5 and 6]. The power, hydrogen, and wall temperature distributions of a typical NTR engine are shown in Figure 5 [5]. During the development of the NTR engines under the Rover program various fuel material problems were observed that were not completely resolved. These material problems limit the performance and the reliability of these engines. The results of the NERVA engine tests indicated that these problems were not due to the irradiation from fission process. Basically the damage to the fuel elements was due to the high temperatures attained at the fuel surface. It is now understood that many interrelated and competing physical mechanisms do act in concert to grade the structural integrity of the fuel element and accelerate the fuel mass loss. Among these processes are the (i) melting of the fuel (formation of liquid), (ii) vaporization/ sublimation, (iii) creep of material cracks, (iv) corrosion, and (v) structural degradation.

The challenge for a high performance NTR engine requires the understanding of these complex physical phenomena and then develop core materials fuel matrix and coating that can stand high temperature (greater than 3000 degree K) and high mass flow rates (greater than 50 kg/sec) of hydrogen environment with minimum corrosion under high pressures (greater than 3 MPa) that can stand breakage from vibration and thermally induced stresses [7, 8, and 9].

Figure 5 shows the power input, wall temperature, and hydrogen temperature distributions in a typical NTR engine. Present study aims at understanding the basic thermal-hydrodynamic processes involved with the expansion of gaseous hydrogen in a Nuclear Thermal Rocket engine. For this purpose, the existing one-dimensional and three-dimensional CFD models are modified and adopted to the study of hot gaseous hydrogen flow through the cooling channels of the reactor core. Simulations were carried out at conditions similar to the ones experienced in

nuclear thermal reactors like NERVA using all these models to predict the temperature in the gaseous hydrogen.

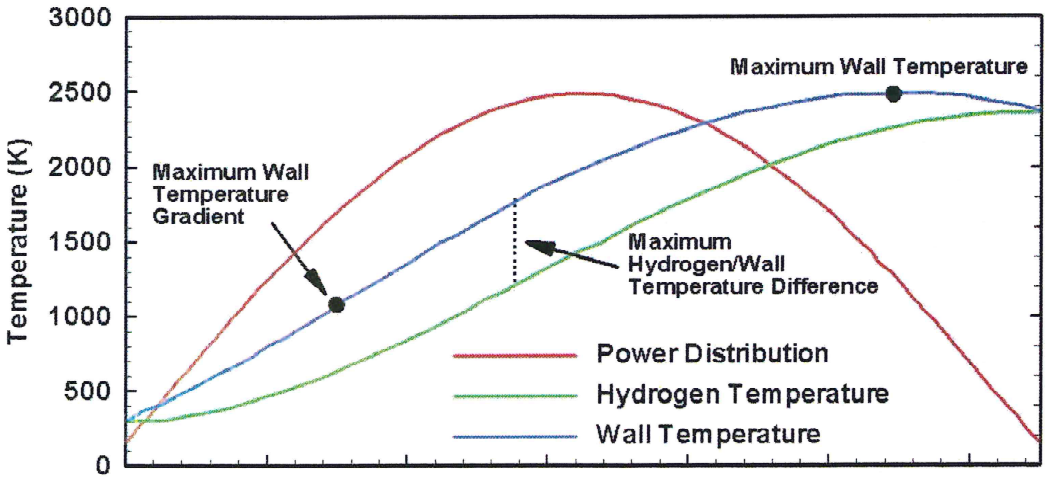

Figure 5 – Temperature and Heat Input distribution in a NTR Fuel Element [5]

A review of the experiences gained from the Space Nuclear Rocket Program (Rover) is given by Koenig [1]. Research on NTRs started in 1959 and went until 1972. The research engines developed during this period were in two categories, small like Kiwi type engines, and full size ones like Phoebus which had a thermal power of 5320 Mw and a thrust of 1123 KN.

Also under NERVA, program which covered the period from 1964 to 1969, various types of nuclear reactors and engines for NTR were build and tested (like NRX, XE, and XEXF.) The description/specs of these engines and the test results of the experiments on these engines can be found in a final report by Koenig [1].

NASA has also developed simulations codes to study various NTR vehicle concepts and carry on mission analysis studies using theses codes. One, which was developed by NASA Glen research Center at Ohio, is called the Nuclear Engine System Simulation (NESS) code. This code was developed in 1970s and now has been upgraded to perform high fidelity NTR propulsion system analysis and design and estimate the weight, performance, size and operating characteristics of the propulsion system components including the nuclear reactor. Code outputs include engine cycle parameters like pressures, temperatures, and mass flow rates. The hydrogen temperature, channel wall temperature, fuel temperature, and fuel heat generation rate distributions inside a NERVA SNRE engine as predicted by the NESS code is presented in Figure 5.

Since the degradation of the fuel elements and the structural failure of the nuclear reactor core is believed not to be caused by irradiation from the fission process, the development and testing of new fuel matrices, fuel coatings, compatibility of the fuel and coating materials, and resistance of other reactor and engine parts to high temperature gas flow can be studied in a non-nuclear test environment provided that the hydrogen gas flow has comparable (preferably higher) temperature and pressures to those attained in a typical NTR engine. Secondly, radiation and residual radioactivity associated with nuclear reactors impose significant constraints on technology and system development programs due to radiation safety, environmental

contamination, and nuclear security concerns; therefore testing of these NRT engines at laboratory scale (or full scale) in a non-nuclear environment is very desirable. Since it is technically sound and also desirable from environmental point of view, NASA has invested in design and construction of various NTR Environment simulators in various NASA centers to understand the mechanisms that are involved in the failure of fuel elements and also test new fuel materials for fuel matrices that may ultimately improve the performance, reliability, and durability of NTR engines [10].

One of such test facilities is located at the Idaho National Laboratory [11]. The Hot Hydrogen Test Facility (HHTF) is suitable to test core materials in 2500 degree C hydrogen flowing at 15000 liters per minute. This facility is intended to test non-uranium containing materials and therefore is suitable to test potential fuel cladding and coating materials. It can also be used to understand the thermal-hydrodynamic behavior and stability of the core, reflector, moderator, and the shielding materials.

NASA MSFC has also been active in developing simulators to test candidate fuel elements for NTRs under the program called Nuclear Thermal Rocket Element Environment Simulator or NTREES [12]. The initial simulator had a power capacity of 50 kW for the inductor heating system, operated at a 35 gm/sec flow rate of hydrogen and attained test article temperatures greater than 3000 degree K.

MSFC also designed and constructed a 1 Mw Multi-Gas Arc-Heater unit in which small material specimen can be exposed to long durations of hot hydrogen gas. This unit has a view port where the effects of the hot gases on the specimen can be observed during the tests. The test done on a candidate fuel element (CERMET) has yielded very important information on degradation of this fuel under long durations of hypo thermal gas flow.

The most recent simulator at NASA MSFC is powered by a 1.5 Mw unit and is capable of providing hydrogen at 300 degree K and 1000 psi. This unit has a pyrometer suite to measure fuel temperature profiles, and a mass spectrometer to measure the mass loss from the fuel element during the test period.

A one-dimensional model is developed to study the effects of heat input in a cooling channel of a nuclear thermal reactor engine. An extensive literature survey conducted on NTRs is included in Chapter 2. These include journal and conference publications and the final reports by various NASA centers. The ones relevant to this study are listed in the references section of this report. A compressible, turbulent, viscous flow inside a cooling channel of a NTR engine with variable het flux and constant mass flow rate is simulated for the present study. A more detailed description of the physical model of the NTR cooling channel is given in Chapter 3.

A physics based mathematical model is developed to obtain numerical solutions for the study by assuming the thermodynamic and transport properties of the fluid to be functions of temperature. The mathematical model comprises of conservation of mass, momentum, and energy equations. Formulations of conservation equations in terms of the primitive variables of the problem (u, v, p, and T) together with the appropriate boundary conditions and assumptions are provided in Chapter 4.

The discretization of the conservation equations are given in Chapter 5. This chapter also includes the numerical solution and algorithm employed to predict the values of the primitive variables of the problem. A detailed description of the modified MacCormack scheme used in the solution algorithm, which is second order accurate in time differencing, is also given in this chapter. The accuracy of the numerical code is verified by applying the developed code to

predict the results of a benchmark case study. Grid independence and time convergence studies carried out to verify the solution algorithm are presented in Chapter 6.

The study of the second order accurate in time model is also provided including the grid independence and time convergence studies and then compared to the 3-D commercial CFD model in Chapter 7. In Chapter 8, parametric studies were conducted to determine the effect of various parameters such as mass flow rate, wall heat flux, and inlet temperature on temperature and velocity distributions. Finally, results for unsteady flow using a 1-D model are discussed in Chapter 9.

The conclusions drawn from the results of the present study are presented in Chapter 10 and the recommendations to improve the mathematical and solution procedure proposed in this study are given in Chapter 11. A list of references used in the literature survey is provided in the "List of References" section of the thesis.

Chapter 2

Literature Survey

Thermohydraulic and Neutronic modeling of nuclear thermal rocket propulsion engines have been carried out by various national laboratories and NASA centers including Idaho National Laboratory, Los Alamos National Laboratory, NASA Marshall Space Flight Center, and NASA Glenn Research Center.

In 1992, M.L. Hall et al. studied the thermohydraulics of the gaseous flow in the nuclear core using KLAXON code [13]. They investigated the hydrogen flow from the storage tanks through the reactor core out of the NTR nozzle using an integral model. A shock-capturing numerical methodology was used to model the gas flow in the cooling channels. Their one-dimensional model was able to predict the pressure distribution from the inlet of the reactor core to the exit of the converging-diverging nozzle. They also predicted the steady-state Mach number distribution for a generic Nuclear Thermal Rocket.

E. Schmidt and et al. used KINETIC (which is a collection of computer programs written for the purpose of analyzing start-up transients in nuclear reactor) system code to analyze the transients experienced in NTR engines [14]. This code consists of a point reactor model and nodes to describe the fluid dynamics and heat transfer mechanics in the cooling channel of the NTR. With this code they were able to carry out a viable transient analysis of a start-up and shutdown behavior of the NTR engine.

J.E. Fittje of NASA Glenn Research Center used an updated version of the Nuclear Engine System Simulation (NESS) code to conduct integrated neutronic and thermal-fluid-

structural analysis of the NTR reactor core components [15]. This code uses the Monte Carlo N-Particle (MCNP) transport code to determine the reactor inputs. Data obtained from the MCNP is used to carry out the fuel elements heat transfer analysis and propellant flow rate determination.

J.A. Webb and et al. used the MCNP code to determine the volumetric heating rates within the nuclear core [16]. The heating rates were then imported to STAR-CCM+ fluids code to carry out the thermal hydraulic analysis of the cooling channels of the nuclear core. Successful coupling of these two codes enabled the authors to determine the spatial steady-state temperature profile within the coolant channels. This information was used to determine the optimum coolant channel surface area to volume ratio to cool the rocket engine operating at a high specific impulse.

Dr. Akyuzlu of University of New Orleans Cryogenics Lab used a one-dimensional mathematical model of the hybrid rocket motor to investigate the instabilities due to coupling of acoustics and hydrodynamic oscillations. The author also used the model to conduct numerical simulations of thermal hydrodynamic transients in the cooling channels of the nuclear thermal propulsion engine. Also, an analytical study was carried out to explore the fluid structure in a nuclear thermal rocket [17, 18, and 19].

Chapter 3

Description of a Physical Model

In the present study, a cooling channel of the NTR core is considered. The cooling channel is 1.2 meters long Stainless Steel pipe with an inner diameter of 2.54 meters (0.1inches). The thickness on the cooling channel is 0.125 mm. The left end of the pipe is the inlet through which the fluid (gaseous hydrogen) comes in at a constant temperature and mass flow rate and the right end of the pipe is the outlet, where the exit pressure is maintained at constant. Initially, hydrogen gas at the inlet is at 300 degree Kelvin. As the flow comes into the cooling channel with a mass flow rate of 0.005 kg/s, the temperature and the velocity of the fluid in the channel gradually increases due to the heat flux from the NTR core. Considering the Mach number and Reynolds's number, the flow in the pipe can be categorized as turbulent and subsonic. The physical model of the cooling channel of the NTR core is shown in Figure 7.

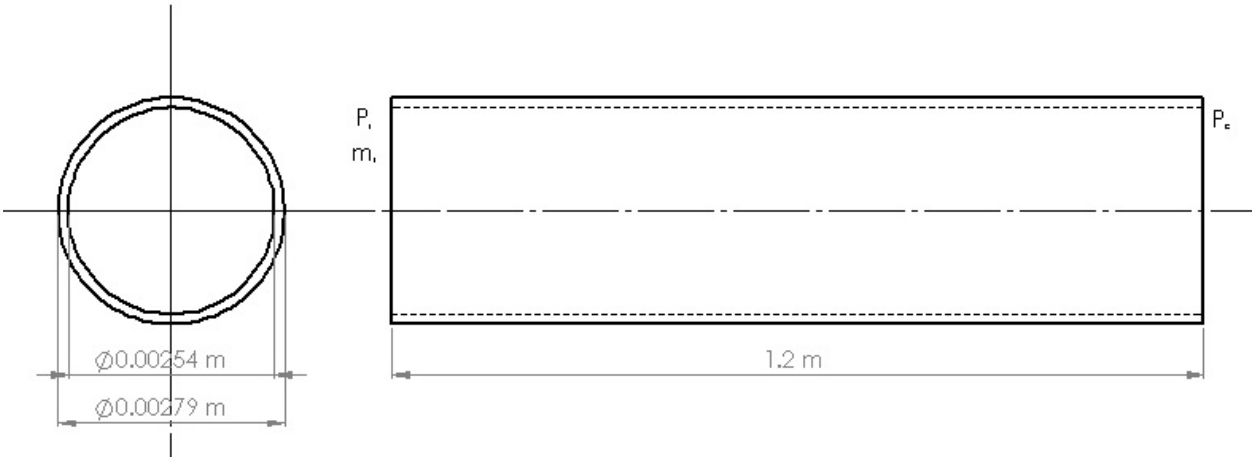

Figure 6 - Schematic of a cooling channel of a NTR engine

No slip conditions are assumed on the wall of the pipe and the wall s are assumed to be impermeable. Mass flow rate and wall heat flux are the major factors affecting the thermodynamic and transport properties of the fluid. Heat is transferred from hot wall to the adjacent gaseous hydrogen molecules flowing inside the pipe, thus decreasing the density of the fluid which in turn decreases the inlet pressure as well through ideal gas relation. Since, the mass flow rate and the cross-sectional area of the pipe are same, decreasing density results in the increase of velocity and temperature.

Figure 7 shows the heat flux distribution along the length of the cooling channel in the experiment. The 1-D and the CFD models are modified and adopted to study the flow of hydrogen gas through the cooling channel of the NTR core under the effect of similar non-uniform heat flux created based on a sine function (Appendix). The results for temperature and velocity distribution from the study are then compared to the ones from the experiment.

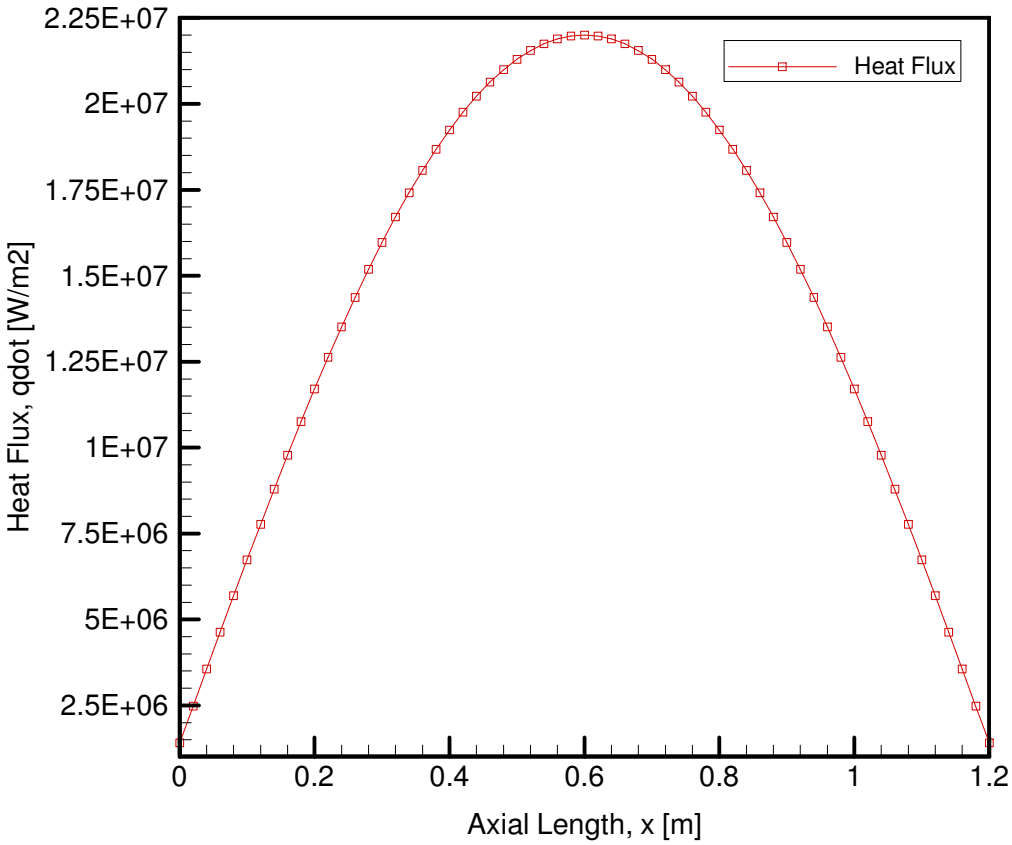

Figure 7 - Heat Flux Distribution along the cooling channel of a NTR core

Chapter 4

Description of Mathematical Model

The mathematical formulation of the conservation equations together with the initial and boundary conditions in first order and second order accurate in time models are given below. The dimensional governing equations were derived from the respective vector form (refer to Appendix I) and together with the initial and boundary conditions were then transformed into non-dimensional form. The non-dimensional forms of these equations as well as the assumptions made in the derivation of these equations are presented in this chapter.

4.1 One-Dimensional Models: Steady and Unsteady State

4.1.1 Assumption of 1-D Mathematical Model

The following assumptions were made for the present study.

1. The physical domain is one-dimensional and the equations are in Cartesian co-ordinates
2. The working fluid forms a continuum
3. The flow is unsteady, turbulent, and viscous
4. The working fluid (gaseous hydrogen) is compressible (the density of the fluid is a function of temperature and pressure) and can be treated as an ideal gas
5. The working fluid behaves like a Newtonian fluid with stokes assumptions
6. Pressure work term is negligible in the energy equation
7. Effects of viscous dissipation in the energy equation are insignificant

8. The kinetic and potential energy terms in the energy equations are neglected

9. Radiation heat transfer is ignored

10. There are no internal heat sources

11. Heat conduction within the fluid follows Fourier's law

12. The physical properties of the fluid are assumed to be constant

13. Thermodynamic and transport properties are assumed to be function of temperature

4.1.2 Mathematical Formulation for 1-D Model

i. Governing Differential Equations

The conservation equations for one-dimensional, unsteady, viscous, compressible, subsonic turbulent flow in the pipe can be written in terms of primitive variables *ρ, u, T, and p* as follows:

Continuity:

$$\frac{\partial(\rho)}{\partial t} + \frac{\partial}{\partial x}(\rho u) = 0 \qquad (1)$$

Momentum:

$$\frac{\partial(\rho u)}{\partial t} + \frac{\partial}{\partial x}(\rho u) = -\frac{\partial(P)}{\partial x} - \tau'_w \qquad (2)$$

Energy:

$$\frac{\partial}{\partial t}\left(\rho c_v T\right)+\frac{\partial}{\partial x}\left(\rho u c_v T\right)-P\frac{\partial u}{\partial x}=\frac{\partial}{\partial x}(k\frac{\partial T}{\partial x})+q_w^{'} \qquad (3)$$

The equation of state

$$P=\rho\ R\ T \qquad (4)$$

is used for the closure of the one dimensional compressible viscous flow model described by the conservation laws.

Wall shear stress per volume in Eq. 2 is given by

$$\tau_w'=4\frac{\tau_w}{D} \qquad (5)$$

where,

$$\tau_w=\frac{1}{8}f\rho\ u^2 \qquad (6)$$

The friction factor f is determined from

$$f=\frac{0.316}{\mathrm{Re}^{0.25}} \qquad (7)$$

or, fully turbulent flow with high Reynolds numbers in smooth pipes.

And the heat input per volume of fluid in Eq. 3 is defined as

$$q'_w = 4\frac{q_w}{D} \tag{8}$$

ii. Initial and Boundary Conditions

To complete the mathematical formulation, the following initial conditions were used.

$$\rho = \rho_o \text{ @ } t=0 \quad \text{for } 0 < x > L$$

$$u = u_o \text{ @ } t=0 \text{ for } 0 < x > L$$

$$T_i = T_o \text{ @ } t=0 \text{ for } 0 < x > L$$

$$P_i = P_o \text{ @ } t=0 \text{ for } 0 < x > L$$

And, the boundary conditions used were

$$P = P_e \text{ @ } x = L \text{ for } t >= 0$$

$$T = T_o \text{ @ } x = 0 \text{ for } t >= 0$$

$$\frac{\partial T}{\partial x} = 0 \text{ @ } x = 0 \text{ for } t >= 0$$

4.2 3-Dimensional General CFD Model – Steady State

Two different 3-Dimensional CFD models are created to effectively study the flow in the cooling channel and achieve the results identical to the experiment. The models are further discussed in details in the sections below.

4.2.1 Assumptions for the 3-D Models

The following assumptions were made for the study with 3-D CFD models:

1. The physical domain is two-dimensional computational domain and the equations are in cylindrical co-ordinates

2. The working fluid forms a continuum

3. The flow is steady, turbulent, and viscous

4. The working fluid (gaseous hydrogen) is compressible (the density of the fluid is a function of temperature and pressure) and can be treated as an ideal gas

5. The working fluid behaves like a Newtonian fluid with stokes assumptions

6. Pressure work term is negligible in the energy equation

7. Effects of viscous dissipation in the energy equation are insignificant

8. The kinetic and potential energy terms in the energy equations are neglected

9. Radiation heat transfer is insignificant

10. There are no internal heat sources

11. Heat conduction within the fluid follows Fourier's law

12. Thermodynamic and transport properties are assumed to be function of temperature

13. No slip condition and stationary walls

4.2.2 Mathematical Formulation for 3-D Two-Domain Model: Fluid

The flow through the two-dimensional computational domain is considered to be compressible and turbulent. The conservation equations for steady, viscous, compressible, subsonic turbulent flow are given as follows:

Continuity:

$$\frac{\partial}{\partial x}(\rho u) + \frac{1}{r}\frac{\partial}{\partial r}(\rho r v) = 0 \qquad (9)$$

r-momentum:

$$v\frac{\partial(\rho v)}{\partial r}+\ u\frac{\partial(\rho v)}{\partial x}=F_r-\ \frac{\partial P}{\partial r}+\ \mu_{eff}\left(\frac{\partial^2 v}{\partial r^2}+\frac{1}{r}\frac{\partial v}{\partial r}-\frac{v}{r^2}+\frac{\partial^2 v}{\partial x^2}\right) \tag{10}$$

x-momentum:

$$v\frac{\partial(\rho u)}{\partial r}+\ u\frac{\partial(\rho u)}{\partial x}=F_x-\ \frac{\partial P}{\partial x}+\ \mu_{eff}\left(\frac{\partial^2 u}{\partial r^2}+\frac{1}{r}\frac{\partial u}{\partial r}+\frac{\partial^2 u}{\partial x^2}\right) \tag{11}$$

The effective viscosity in the above equations is defined as

$$\mu_{eff}=\mu\ +\mu_t \tag{12}$$

where the eddy viscosity is given by

$$\mu_t=\rho C_\mu\frac{K^2}{\varepsilon} \tag{13}$$

The turbulent kinetic energy is determined from:

$$\frac{\partial(\rho uK)}{\partial x}+\frac{\partial(\rho vK)}{\partial r}=\frac{\partial}{\partial x}\left(\left(\mu+\frac{\mu_t}{Pr_K}\right)\frac{\partial K}{\partial x}\right)+\frac{\partial}{\partial r}\left(\left(\mu+\frac{\mu_t}{Pr_t}\right)\frac{\partial K}{\partial r}\right)+$$
$$\mu_t\left(\left(\frac{\partial u}{\partial r}+\frac{\partial v}{\partial x}\right)^2+2\left(\frac{\partial u}{\partial x}\right)^2+2\left(\frac{\partial v}{\partial r}\right)^2\right)-\rho\varepsilon \tag{14}$$

The turbulent dissipation energy is determined from:

$$\frac{\partial(\rho u\varepsilon)}{\partial x}+\frac{\partial(\rho v\varepsilon)}{\partial r}=\frac{\partial}{\partial x}\left(\left(\mu+\frac{\mu_t}{Pr_\varepsilon}\right)\frac{\partial \varepsilon}{\partial x}\right)+\frac{\partial}{\partial r}\left(\left(\mu+\frac{\mu_t}{Pr_\varepsilon}\right)\frac{\partial \varepsilon}{\partial r}\right)+$$
$$C_{\varepsilon 1}\mu_t\frac{\varepsilon}{K}\left(\left(\frac{\partial u}{\partial r}+\frac{\partial v}{\partial x}\right)^2+2\left(\frac{\partial u}{\partial x}\right)^2+2\left(\frac{\partial v}{\partial r}\right)^2\right)-C_{\varepsilon 2}\rho\frac{\varepsilon^2}{K} \tag{15}$$

The constants of the K-ε model adopted for this study are: C_μ = *0.09,* Pr_K = 1.0, Pr_ε = 1.3. $C_{\varepsilon 1}$ = 1.55 and $C_{\varepsilon 2}$ = 2.0

The energy equation is given by:

$$v\frac{\partial(\rho c_p T)}{\partial r} + u\frac{\partial(\rho c_p T)}{\partial x} = k_{eff}\left(\frac{\partial^2 T}{\partial r^2} + \frac{1}{r}\frac{\partial T}{\partial r} + \frac{\partial^2 T}{\partial x^2}\right) + \mu_{eff}\left(2\left(\frac{\partial v}{\partial r}\right)^2 + \left(\frac{\partial u}{\partial x}\right)^2\right) + \left(\frac{\partial v}{\partial x} + \frac{\partial u}{\partial r}\right)^2 \quad (16)$$

Where the effective thermal conductivity is given by

$$k_{eff} = k_{rad} + k_t + k_{abs} \quad (17)$$

The radiative and turbulent thermal conductivities in these equations are given by

$$k_{rad} = \frac{16n^2\sigma T^3}{3\beta_R} \quad (18)$$

$$k_t = {}^{c_p\mu_t}/_{Pr_t} \quad (19)$$

4.2.3 Mathematical Formulation for 3-D Two-Domain Model: Solid

For the case of a stationary solid such as the flow in a pipe, we can neglect the convective terms in the total derivatives. Also because the flow rate in the pipe is subsonic (M<0.3) we can neglect viscous dissipation and pressure work in the energy equation because Ec << 1. Therefore, there is no heat generation and the energy equation for the solid is given by

$$\frac{\partial(\rho c_p T)}{\partial t} = \frac{\partial}{\partial x}\left(k_s \frac{\partial T_s}{\partial x}\right) - \frac{\partial}{\partial r}\left(k_s \frac{\partial T_s}{\partial r}\right) \tag{20}$$

4.3 Thermodynamic and Transport Properties

The thermodynamic and transport properties are assumed to be the function of temperature. The equations for thermal conductivity, specific heat and viscosity for gaseous hydrogen (GH_2) are obtained using figures from Appendix III [20].

Thermal conductivity, k_t:

$$k(x) = 0.1554 + 0.00047x \tag{21}$$

Specific heat, c_p:

$$c_p(x) = 14219.231 + 248.232x - 55.172x^2 + 7.066x^3 - 0.360x^4 + 0.008x^5 \tag{22}$$

And, for viscosity, ν:

$$v(x) = 1 \times 10^{-5} - 3 \times 10^{-6}x + 3 \times 10^{-6}x^2 - 6 \times 10^{-7}x^3 + 8 \times 10^{-8}x^4 - 5 \times 10^{-9}x^5 + 1 \times 10^{-10}x^6 \tag{23}$$

Chapter 5

Numerical Formulation and Solution Procedure for 1-D Model

5.1 1-D Mathematical Model

5.1.1 Discretization of the Governing Differential Equations

In this study, a second order accurate in time and space numerical scheme (modified MacCormack) is used to solve the conservation of mass, momentum, and energy equations given in the previous section. The discretization method was used for the inner points of the computational domains, which is represented by a uniform orthogonal structured mesh. The computational cell used for the discretization is shown in Figure 8. This technique is well suited to solve compressible flow equations for high velocities. It is two-step numerical schemes where the primitive variables of the problem are first predicted using a forward in time scheme and then are corrected using a backward in time scheme.

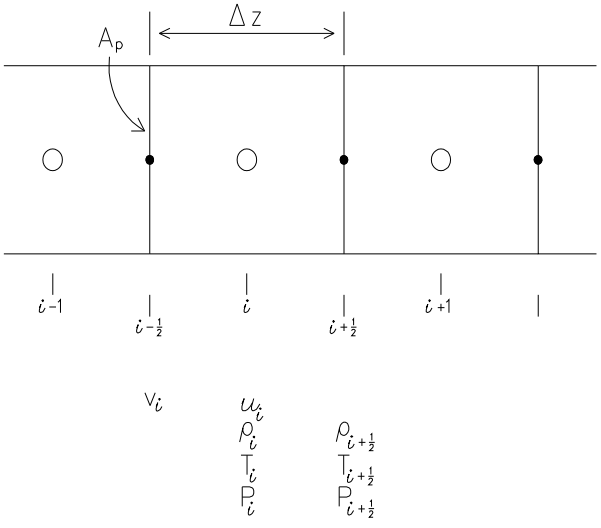

Figure 8- Spatial Discretization of the Pipe for Finite Differential approximations

The numerical stability criterion for the MacCormack scheme is given by

$$\Delta t \le \frac{\sigma(\Delta t)_{CFL}}{1+2/\mathrm{Re}_{\Delta}} \tag{24}$$

where σ is the safety factor and this factor is taken as 0.9. The Courant-Frederics-Levy stability condition is given by :

$$(\Delta t)_{CFL} \le \frac{\Delta x}{a+|u|} \tag{25}$$

where "a" is the local speed of sound. "Re_{Δ}" is the minimum mesh Reynolds number given by

$$\mathrm{Re}_{\Delta} = \min(\mathrm{Re}_{\Delta x}) \quad \text{where} \quad \mathrm{Re}_{\Delta x} = \frac{u\,\Delta x}{\nu} \tag{26}$$

To verify the grid size independence of the results, the computations were carried out for different number of nodes in axial direction for the full length of the coolant channel 31, 41, and 51. The changes in the velocity field due to this change in cell size were found insignificant. Therefore the study was carried out with a 41 node computational domain.

Convergence of the numerical results for different time increments was also studied. It was concluded that time increments smaller than $1\text{x}10^{-5}$ resulted in no significant changes in the temperature and velocity distributions with the coolant channel therefore this non-dimensional time step was used in all of the numerical simulations reported in this study.

5.1.2 Solutions Technique

The solution of the coupled differential equations for the present problem requires a specific procedure to be followed. First, the mass flow rate at the inlet of the pipe is used to calculate the velocity of the gaseous Hydrogen at the inlet. Then the governing equations of the turbulent compressible flow through the cooling channel (Eqs. 9, 10, 11, 12) are solved. This results in the determination of the density and velocity field at the exit of the cooling channel which is used to update the pressure at the inlet of the cooling channel.

5.2 3-D Models

A commercial CFD package (Fluent) was used to predict the temperature distribution inside the fluid and the pipe. These distributions are used in calculating the radial temperature gradients in the solid and in the GH_2 along the gas-solid interface. Conservation equations are solved using pressure-velocity coupling. Second order upwind scheme is used in the discretization of the conservation equations and the K-ε turbulence model equations. The mesh for the computational domain (fluid and the solid) are generated using the Wokrbench mesh generator and has around 300K cells. As boundary conditions, the mass flow rate and temperature of the GH_2 are specified at the inlet, and the pressure is specified at the exit of the pipe.

Table 1- Fluent Solver Setting

CFD SOLVER SETTINGS	
Description	**Settings**
Problem Setup – Solver	Pressure-Based
Turbulence Model	*k-ε*
Viscous	Standard
Viscous Heating	ON
Pressure-Velocity Coupling	Coupled
Gradient Discretization	Least Square Cell-Based
Pressure Discretization	Standard
Density Discretization	Second Order Upwind
Momentum Discretization	Second Order Upwind
Turbulent *k-ε* Discretization	Second Order Upwind
Energy	Second Order Upwind
Residual: Criteria	1E-08

Chapter 6

Validation of the Solution Code and Study of Various Cases

In this study, various numerical studies have been carried out to establish the validity of the solution code. When numerical methods are used to solve differential equations, getting a numerical stable solution does not immediately imply that this is the correct one. A time convergence study and grid independence study requires that there are not significant changes in the results when the computational time increment and grid size are varied. Furthermore, the computer code developed for the present study was tested for accuracy using benchmark studies. These case studies are presented in this chapter.

Common Run Parameters for the case studies are given in tables below:

Table 2- Geometrical Parameters for case studies

Parameter	Symbol	Value
Length	L [m]	1.2
Diameter	D [m]	0.00254
Thickness	t [m]	0.000125

Table 3- Operational Parameters for case studies

Parameter	Symbol	Value
Inlet Mass Flow Rate	m_{dot} [kg/sec]	0.005
Inlet Temperature	T_i [K]	300
Exit Pressure	P_e [MPa]	3.1
Coefficient of Friction	C_f	0.99
Non-Uniform Heat Flux	Q_{dot} [kW/m^2]	22,000

Table 4- Physical Parameters for case studies

Parameter	Symbol	Value
Thermal Conductivity	k_t [W/m-K]	0.1554
Specific Heat	c_p [J/kg-K]	14065.0
Absolute Viscosity	μ [N-s/m^2]	1.76 x 10^{-5}

6.1 1-D Case Studies

6.1.1 Time Convergence Study for 1-D Model

A time convergence study was carried out for the present study which is second order accurate in time. Once the grid size is set, the time computational time convergence is determined by satisfying the diagonal dominance condition of the coefficient matrix. For the present code validation study, a non-dimensional computational time increment of 5 x 10^{-6} was considered. It was found that the time increment did not result in any significant changes in qualitative and quantitative results. To illustrate this point, a one-dimensional channel with a non-uniform heat flux distribution of 22,000 kW/m^2 along the axial length were compared for different time increment such as $\Delta t = 5x10^{-6}$, $\Delta t = 1x10^{-6}$ and $\Delta t = 5x10^{-7}$ for 41 x 41 mesh points with an inlet mass flow rate of 0.005 kg/s, inlet temperature of 300 K and outlet pressure of 3.1 MPa. The quantitative comparison is presented in Table 6 and the comparison of mean fluid temperature and axial velocity distributions is presented in Figure 9.

Table 5- Time Increment Study for 1D Unsteady State Case
[IN = 41 x 41, C_f = 0.1, turbulent, constant properties]

				Results			
Run No.	Time Increment, DT [s]	Mach Number, Ma	Reynolds Number, Re ($x10^5$)	Inlet Pressure, P_i [MPa]	Mean Outlet Fluid Temperature, T_e [K]	Outlet Velocity, u_e [m/s]	Pressure Difference, ΔP [MPa]
1D-H2-I	5×10^{-6}	0.157	3.18	5.90	2354.58	3038.88	2.80
	1×10^{-6}	0.156	3.18	5.91	2349.73	3037.67	2.81
	5×10^{-7}	0.156	3.18	5.91	2349.15	3037.45	2.81

Table 6- Fluid Temperature distribution along the axial length of the 1-D models for $\Delta t = 5 \times 10^{-6}$ sec, $\Delta t = 1 \times 10^{-6}$ sec, $\Delta t = 5 \times 10^{-7}$ sec for Run 1D-H2-I

Axial Distance, x [m]	Fluid Temperature, T_f [K] ($\Delta t = 5 \times 10^{-6}$ sec)	Fluid Temperature, T_f [K] ($\Delta t = 1 \times 10^{-6}$ sec)	Fluid Temperature, T_f [K] ($\Delta t = 5 \times 10^{-7}$ sec)
0	300.00	300.00	300.00
0.1	424.287	423.932	423.880
0.2	627.748	627.053	626.959
0.3	804.590	803.670	803.585
0.4	997.140	995.825	995.675
0.5	1267.99	1266.21	1266.02
0.6	1472.75	1470.59	1470.34
0.7	1670.51	1667.99	1667.76
0.8	1909.62	1906.61	1906.34
0.9	2059.94	2056.48	2056.05
1.0	2175.51	2171.69	2171.34
1.1	2253.54	2248.79	2248.30
1.2	2216.63	2210.30	2209.75

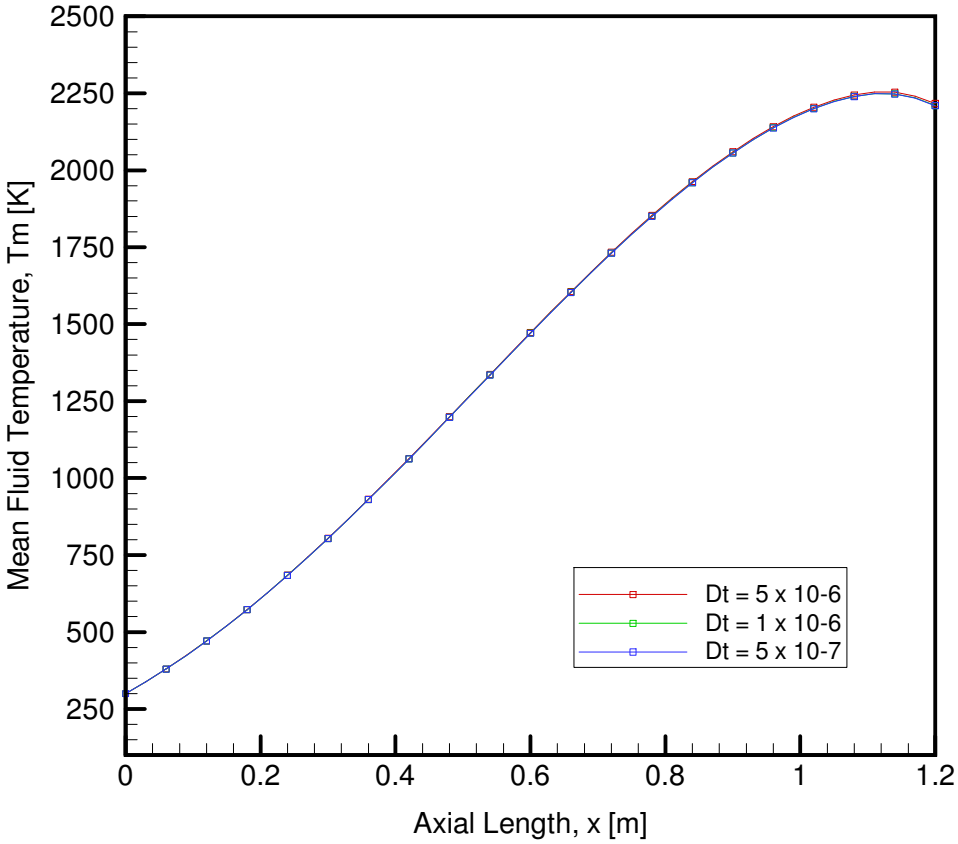

Figure 9 - Comparison of Mean Fluid Temperature distribution along the axial centerline of the 1-D models for $\Delta t = 5 \times 10^{-6}$ sec, $\Delta t = 1 \times 10^{-6}$ sec, $\Delta t = 5 \times 10^{-7}$ sec for Run 1D-H2-I

6.1.2 Grid Independence Study for 1-D Model

In order to validate the accuracy and convergence of the computer code, a grid independence study for the present study (Q_{max} = 22,000 kW/m2, m_{dot} = 0.005 kg/s, T_i = 300 K, P_e = 3.1 MPa) was also conducted. The grid size chosen for the present study was 41 x 41. To verify that the converged solutions were independent of the grid chosen two more studies were carried out with grid size of 31 x 31 and 51 x 51. Unsteady state results using uniform, orthogonal 31 x 31, 41 x 41 and 51 x 51 meshes were obtained using the present computer code. The comparison of distribution of the mean fluid temperature along the length of the channel is presented in Figure 10 and the quantitative comparison is presented in Table 8.

Table 7- Mesh Independence Study for 1-D Unsteady State Case
[$\Delta t = 5x10^{-6}$ - $1x10^{-6}$ sec, C_f = 0.1, turbulent, constant properties]

				Results			
Run No.	Number of Cells, IN	Mach Number, Ma	Reynolds Number, Re ($x10^5$)	Inlet Pressure, P_i [MPa]	Mean Outlet Fluid Temperature, T_e [K]	Outlet Velocity, u_e [m/s]	Pressure Difference, ΔP [MPa]
1D-H2-II	31	0.15	3.18	5.90	2356.29	3037.56	2.80
	41	0.15	3.18	5.90	2354.58	3038.88	2.80
	51	0.16	3.18	5.91	2349.66	3038.47	2.81

Table 8- Mean Fluid Temperature distribution along the axial length of the 1-D models for IN = 31x31, IN = 41x41, IN = 51x51 for Run 1D-H2-II

Axial Distance, x [m]	Fluid Temperature, T_f [K] (IN = 31x31)	Fluid Temperature, T_f [K] (IN = 41x41)	Fluid Temperature, T_f [K] (IN = 51x51)
0	300.00	300.00	300.00
0.1	409.276	424.287	433.288
0.2	609.365	627.748	594.168
0.3	764.005	804.590	828.461
0.4	1019.76	997.140	1035.63
0.5	1200.17	1267.99	1252.48
0.6	1473.61	1472.75	1470.56
0.7	1650.07	1670.51	1680.69
0.8	1892.14	1909.62	1873.30
0.9	2030.07	2059.94	2074.31
1.0	2186.22	2175.51	2190.01
1.1	2244.28	2253.54	2248.56
1.2	2219.09	2216.63	2209.83

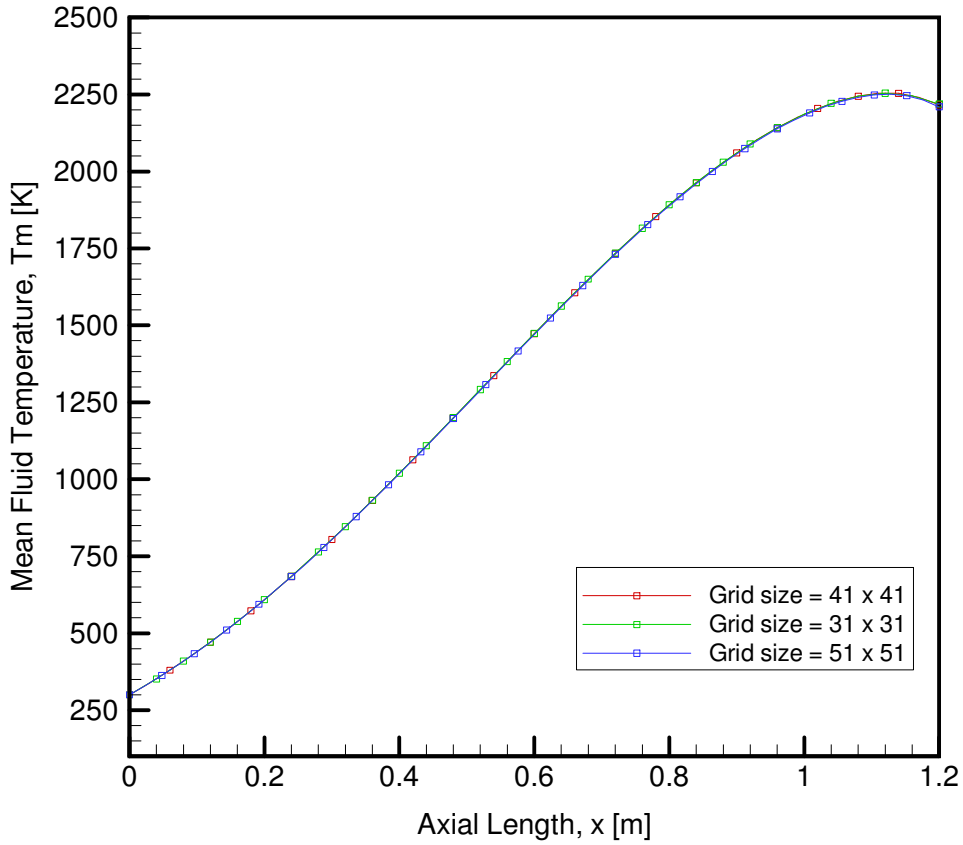

Figure 10 - Comparison of Mean Fluid Temperature Distribution along the axial centerline of the 1-D models for IN = 31x31, IN = 41x41, IN = 51x51 for Run 1D-H2-II

6.1.3 Coefficient of Friction Study for 1-D Model

In this study, a 41 x 4 1-D model is run with the similar initial and boundary conditions as that of the benchmark case but with different coefficient of friction. The effect in mean fluid temperature distribution due to the change in frictions is illustrated in Figure 11. A quantitative comparison of temperature distribution under different coefficient of frictions is shown in Table 10.

Table 9- Coefficient of Friction Study for 1-D Unsteady State Case
[IN = 41, $\Delta t = 5x10^{-6}$ sec, turbulent, constant properties]

				Results			
Run No.	Coefficient of Friction, C_f	Mach Number, Ma	Reynolds Number, Re ($x10^5$)	Inlet Pressure, P_i [MPa]	Mean Outlet Temperature, T_e [K]	Outlet Velocity, u_e [m/s]	Pressure Difference, ΔP [MPa]
1D-H2-III	0.10	0.16	3.18	5.803	1952.65	2523.27	2.703
	0.55	0.15	3.18	6.086	1937.23	2482.64	2.986
	0.99	0.14	3.18	6.54	1918.88	2421.14	3.44

Table 10- Pressure distribution along the axial length of the 1-D models for $C_f = 0.1$, $C_f = 0.55$, $C_f = 0.99$ for Run 1D-H2-III

Axial Distance, x [m]	Pressure, P [MPa] ($C_f = 0.10$)	Pressure, P [MPa] ($C_f = 0.55$)	Pressure, P [MPa] ($C_f = 0.99$)
0	5.905	6.591	7.079
0.1	5.820	6.505	6.992
0.2	5.670	6.350	6.831
0.3	5.533	6.206	6.681
0.4	5.375	6.037	6.503
0.5	5.132	5.772	6.219
0.6	4.927	5.543	5.970
0.7	4.704	5.287	5.689
0.8	4.380	4.903	5.260
0.9	4.119	4.580	4.892
1.0	3.842	4.221	4.474
1.1	3.442	3.657	3.799
1.2	3.1	3.1	3.1

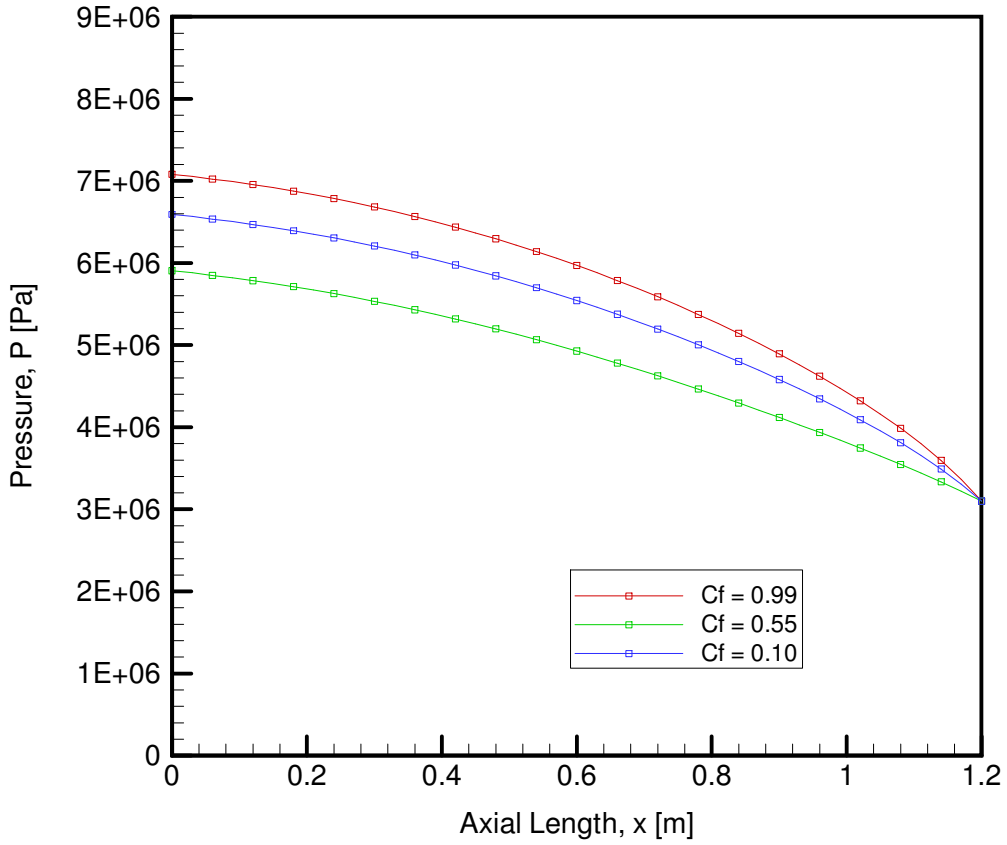

Figure 11- Comparison of Pressure distribution along the axial centerline for 1-D models with $C_f = 0.1$, $C_f = 0.55$, $C_f = 0.99$ for Run 1D-H2-III

6.1.4 Inlet Mass Flow Rate Study for 1-D Model

In this study, a one-dimensional mathematical model is used to study the effect of inlet mass flow rate. The model has a 41 x 41 mesh size and a time increment of 5 x 10^{-6} seconds. Comparison of the effects of different mass flow rate in temperature distribution is shown in Figure 12 and a quantitative comparison is presented in Table 12.

Table 11- Inlet Mass Flow Rate Study for 1-D Unsteady State Case
[IN = 41, $\Delta t = 5x10^{-6}$ sec, $C_f = 0.99$, turbulent, constant properties]

				Results			
Run No.	Mass Flow rate, m_{dot} [x10-3 kg/s]	Mach Number, Ma	Reynolds Number, Re ($x10^5$)	Inlet Pressure, P_i [MPa]	Mean Outlet Fluid Temperature, T_e [K]	Outlet Velocity, u_e [m/s]	Pressure Difference, ΔP [MPa]
1D-H2-IV	4.0	0.11	2.54	6.43	2812.14	2881.12	3.33
	5.0	0.13	3.18	7.08	2216.63	2846.33	3.98
	6.0	0.14	3.81	7.70	1897.69	2814.73	4.60

Table 12- Mean Fluid Temperature distribution along the axial length of the 1-D model for m_{dot} = 0.004 kg/s, m_{dot} = 0.005 kg/s, m_{dot} = 0.006 kg/s for Run 1D-H2-IV

Axial Distance, x [m]	Fluid Temperature, T_f [K] (m_{dot} = 0.004 kg/s)	Fluid Temperature, T_f [K] (m_{dot} = 0.005 kg/s)	Fluid Temperature, T_f [K] (m_{dot} = 0.006 kg/s)
0	300.00	300.00	300.00
0.1	455.842	424.287	403.288
0.2	711.501	627.748	572.177
0.3	933.840	804.590	718.902
0.4	1176.12	997.140	878.562
0.5	1517.42	1267.99	1102.91
0.6	1776.00	1472.75	1272.24
0.7	2026.48	1670.51	1435.41
0.8	2331.29	1909.62	1631.75
0.9	2525.52	2059.94	1753.88
1.0	2679.29	2175.51	1845.50
1.1	2800.61	2253.54	1897.53
1.2	2801.99	2216.63	1833.54

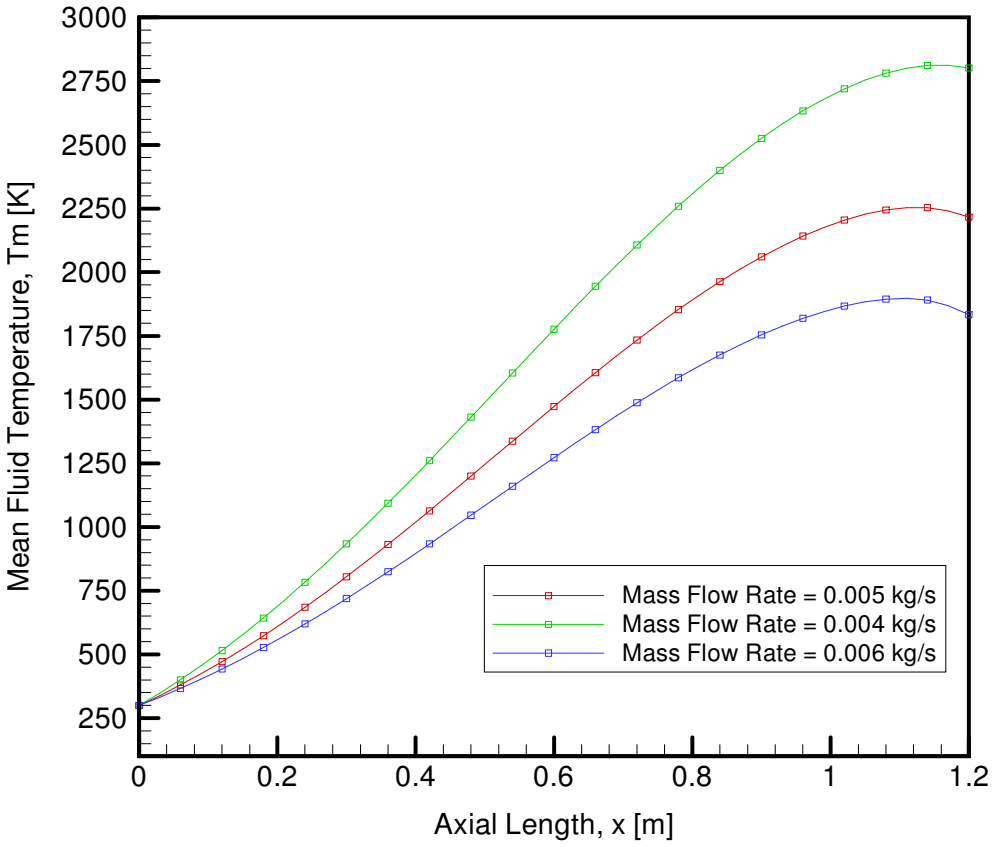

Figure 12- Comparison of Mean Fluid Temperature distribution along the axial centerline for 1-D model with m_{dot} = 0.004 kg/s, m_{dot} = 0.005 kg/s, m_{dot} = 0.006 kg/s for Run 1D-H2-IV

6.2 3-D Case Studies

6.2.1 Mesh Independence Study for 3-D CFD Models

A mesh independence study was carried out using a one domain and a two domain three-dimensional model, each with three different cell sizes and layers. A one domain case has five models with different number of cells. Table 3 compares the results between the one domain models with three different axial cell sizes of 1x 10^{-3}, 5x10^{-4} and 4x10^{-4} with five layers in radial direction. The mesh independence study has an inlet mass flow rate of 0.005 kg/s, inlet fluid temperature 300 K and a variable heat flux of 22,000 kJ/s-m^2. Also, the outlet pressure for the study is set to be 3.1 MPa. Similarly, Table 13 consists of 3-D one domain models with different axial cell sizes and constant numbers of layers (n_f) in radial direction. The geometrical, operational and physical parameters for this case study are similar to that of the previous case studies and are given in Table 2, Table 3 and Table 4 respectively.

Table 13- Mesh Independence (Cell Size) Study for 3-D One-Domain Steady State Case [n_f = 5, turbulent, constant properties]

					Results			
Run No.	Axial Cell Size, dx [m]	No. of Cells	Mach Number, Ma	Reynolds Number, Re (x10^5)	Inlet Pressure, P_i [MPa]	Outlet Centerline Fluid Temperature, T_e [K]	Outlet Velocity, u_e [m/s]	Pressure Difference, ΔP [MPa]
3D-H2-1DM-I	1x10^{-3}	200,400	0.113	3.18	8.197	1926.3	2912.11	5.097
	8x10^{-4}	217,000	0.113	3.18	8.198	1926.71	2910.71	5.098
	5x10^{-4}	348,000	0.11	3.18	8.30	1931.81	2921.21	5.20

Comparisons for pressure, velocity and temperature distribution between different models were carried out. The inlet pressures for all three models are very identical; however the values start to increase slightly as the axial size decreases. Similarly, the velocity distributions look very similar for different axial cell sizes. Finally, temperature distributions are compared between 3-D

one domain models with different axial cell sizes. A quantitative comparison is presented in Table 14 and a figurative comparison is shown in Figure 13.

Table 14- Fluid Temperature distribution along the axial centerline of the 3-D One-Domain models for dx = $1x10^{-3}$ m, dx = $8x10^{-3}$ m, dx = $5x10^{-4}$ m for Run 3D-H2-1DM-I

Axial Distance, x [m]	Fluid Temperature, T_f [K] (dx = $1x10^{-3}$ m)	Fluid Temperature, T_f [K] (dx = $8x10^{-4}$ m)	Fluid Temperature, T_f [K] (dx = $5x10^{-4}$ m)
0	299.221	299.221	299.231
0.1	313.464	313.602	314.329
0.2	376.583	376.911	379.197
0.3	471.436	472.043	478.36
0.4	602.752	603.683	618.893
0.5	790.515	791.75	819.636
0.6	1045.69	1047.13	1075.59
0.7	1313.24	1314.46	1334.11
0.8	1551.2	1552.18	1567.16
0.9	1750.77	1751.59	1764.15
1.0	1900.2	1900.9	1911.51
1.1	1980.54	1981.14	1990.02
1.2	1926.3	1926.71	1931.81

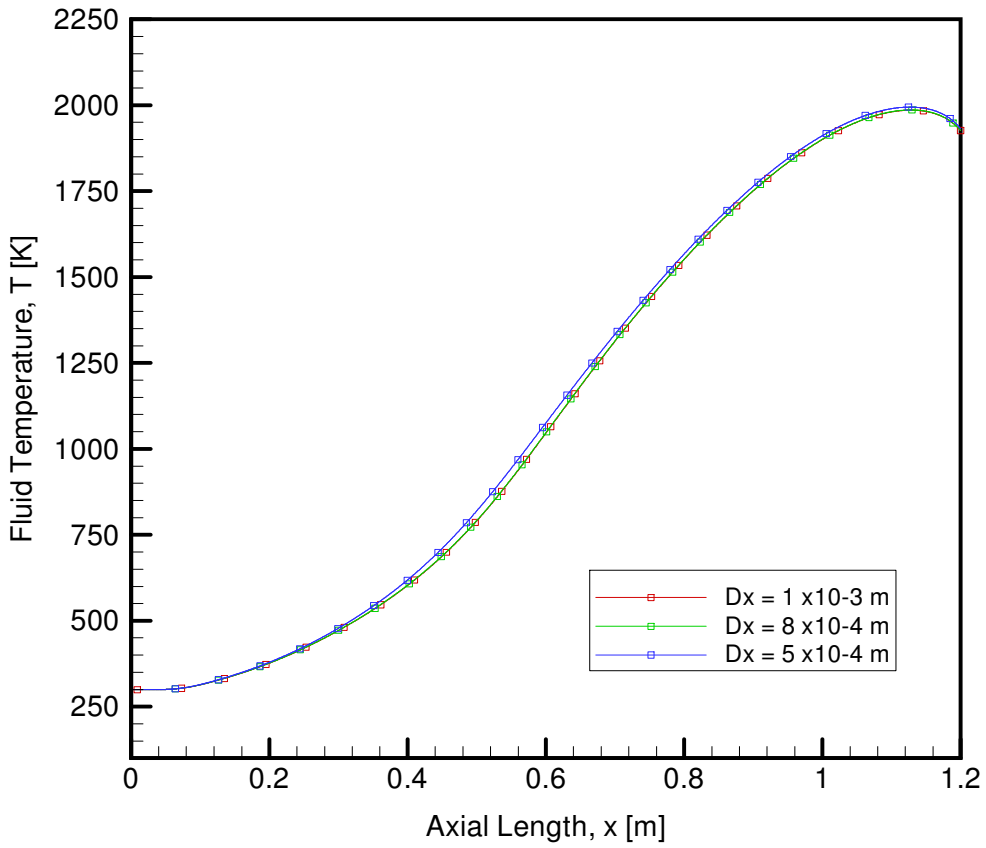

Figure 13- Comparison of Fluid Temperature distribution along the axial centerline of the 3-D One-Domain models for dx = $1x10^{-3}$ m, dx = $8x10^{-3}$ m, dx = $5x10^{-4}$ m for Run 3D-H2-1DM-I

Table 15 compares the outlet results between the one domain models with 3-D one domain models with different layers in radial direction. The mesh independence study has an inlet mass flow rate of 0.005 kg/s, inlet fluid temperature 300 K and a variable heat flux of 22,000 kJ/s-m^2. Also, the outlet pressure for the study is set to be 3.1 MPa. All three models have different layers in radial direction but have a constant axial cell size of $1x10^{-3}$ m.

Table 15- Mesh Independence (Fluid Layer) Study for 3D-1 Domain Steady State Case
[dx = $1x10^{-3}$ m, turbulent, constant properties]

					Results			
Run No.	No. of Layers, n_f	No. of Cells	Mach Number, Ma	Reynolds Number, Re ($x10^5$)	Inlet Pressure, P_i [MPa]	Outlet Centerline Fluid Temperature, T_e [K]	Outlet Velocity, u_e [m/s]	Pressure Difference, ΔP [MPa]
3D-H2-1DM-II	5	200,400	0.113	3.18	8.197	1926.3	2912.11	5.097
	10	320,400	0.114	3.18	8.095	1928.74	2904.1	4.995
	13	378,000	0.115	3.18	8.074	1929.3	2902.07	4.974

The inlet pressures for all three models are very identical; however the values start to increase slightly as the axial size decreases. The velocity distributions for different radial layers are similar. A model with five radial layers has the highest outlet velocity of 2912.11 m/s and the one with thirteen radial layers has an outlet velocity of 2902.07 m/s. Temperature distributions are also compared between 3-D one domain models with different number of layers in radial direction. The quantitative comparison is presented in Table 16 and a figurative comparison is shown in Figure 14.

Table 16- Fluid Temperature distribution along the axial centerline of the 3-D One-Domain models for $n_f = 5$, $n_f = 10$, $n_f = 13$ for Run 3D-H2-1DM-II

Axial Distance, x [m]	Fluid Temperature, T_f [K] ($n_f = 5$)	Fluid Temperature, T_f [K] ($n_f = 10$)	Fluid Temperature, T_f [K] ($n_f = 13$)
0	299.221	299.202	299.198
0.1	313.464	313.654	313.728
0.2	376.583	376.149	375.981
0.3	471.436	468.503	467.373
0.4	602.752	593.328	590
0.5	790.515	771.686	765.286
0.6	1045.69	1028.65	1022.59
0.7	1313.24	1308.23	1306.67
0.8	1551.2	1550.97	1551.23
0.9	1750.77	1751.56	1752.19
1.0	1900.2	1901.21	1901.92
1.1	1980.54	1981.58	1982.27
1.2	1926.3	1928.74	1929.3

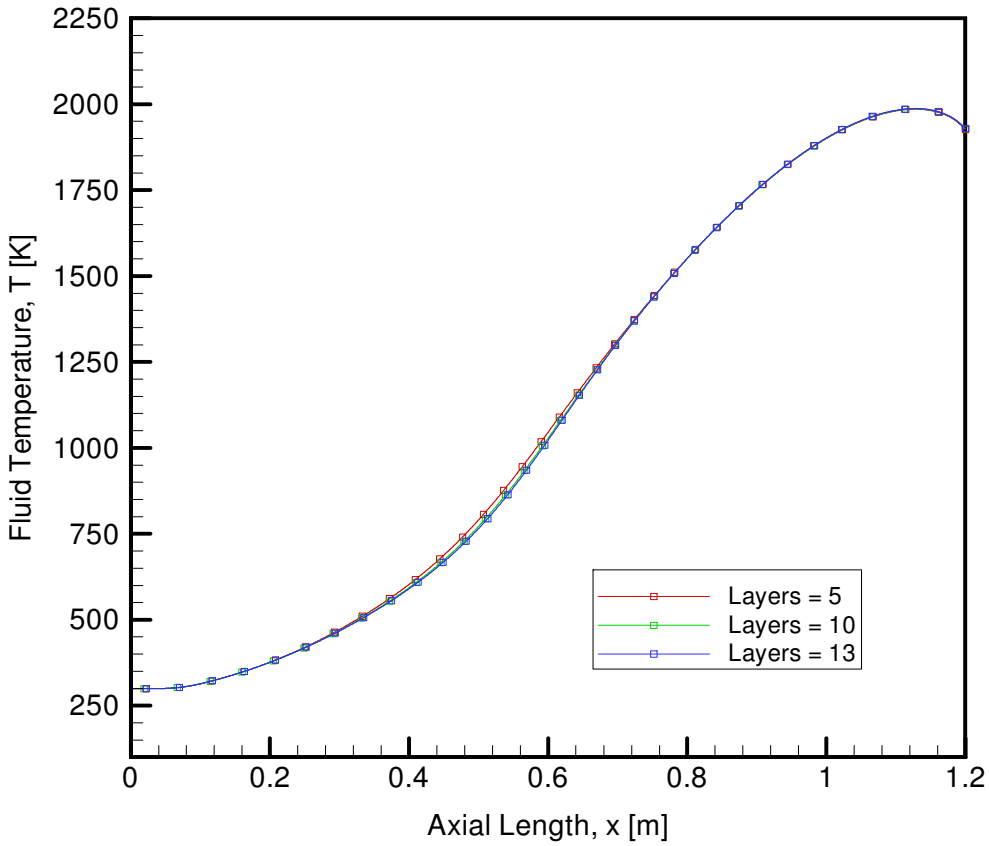

Figure 14- Comparison of Fluid Temperature distribution along the axial centerline of the 3-D One-Domain models for $n_f = 5$, $n_f = 10$, $n_f = 13$ for Run 3D-H2-1DM-II

A two domain case has five models with different number of cells. Table 17 compares the outlet results between the two domain models with three different cell sizes of 1x 10^{-3}, 2x10^{-3} and 5x10^{-3} with five layers in radial direction in the fluid domain and one layer in the solid domain. The mesh independence study has an inlet mass flow rate of 0.005 kg/s, inlet fluid temperature 300 K and a constant heat flux of 22,000 kJ/s-m^2. Also, the outlet pressure for the study is set to be 3.1 MPa. It was found that the change in cell size did not have any effect on the results

Table 17- Mesh Independence (Cell Size) Study for 3-D Two-Domain Steady State Case [n_f = 5, turbulent, constant properties]

					Results			
Run No.	Cell Size, dx [m]	No. of Cells	Mach Number, Ma	Reynolds Number, Re (x10^5)	Inlet Pressure, P_i [MPa]	Outlet Centerline Fluid Temperature, T_e [K]	Outlet Velocity, u_e [m/s]	Pressure Difference, ΔP [MPa]
3D-H2-2DM-I	5x10^{-3}	40,080	0.109	3.18	8.492	2073.52	3116.98	5.392
	2x10^{-3}	100,200	0.109	3.18	8.500	2072.04	3123.79	5.400
	1x10^{-3}	212,577	0.107	3.18	8.608	2076.79	3132.66	5.508

A comparison of pressure, velocity and temperature distribution between different models is presented in this section. The inlet pressures for all three models are very identical; however the values start to increase slightly as the axial size decreases. Similarly, the velocity distributions look very similar for different axial cell sizes. Finally, temperature distributions are compared between 3-D one domain models with different axial cell sizes. The quantitative comparison is presented in Table 18 and a figurative comparison is shown in Figure 15.

Table 18- Fluid Temperature distribution along the axial centerline of the 3-D Two-Domain models for dx = $5x10^{-3}$ m, dx = $2x10^{-3}$ m, dx = $1x10^{-3}$ m for Run 3D-H2-2DM-I

Axial Distance, x [m]	Fluid Temperature, T_f [K] (dx = $5x10^{-3}$ m)	Fluid Temperature, T_f [K] (dx = $2x10^{-3}$ m)	Fluid Temperature, T_f [K] (dx = $1x10^{-3}$ m)
0	299.274	299.275	299.284
0.1	314.956	314.957	315.918
0.2	382.736	382.494	385.422
0.3	480.594	480.159	488.472
0.4	610.728	609.808	631.237
0.5	799.359	797.698	842.398
0.6	1085.19	1084.07	1135.92
0.7	1405.46	1405.19	1434.1
0.8	1675.79	1675.73	1693.35
0.9	1896.01	1896.12	1909.87
1.0	2059.5	2059.88	2071.1
1.1	2145.27	2146.32	2155.62
1.2	2073.52	2072.04	2076.79

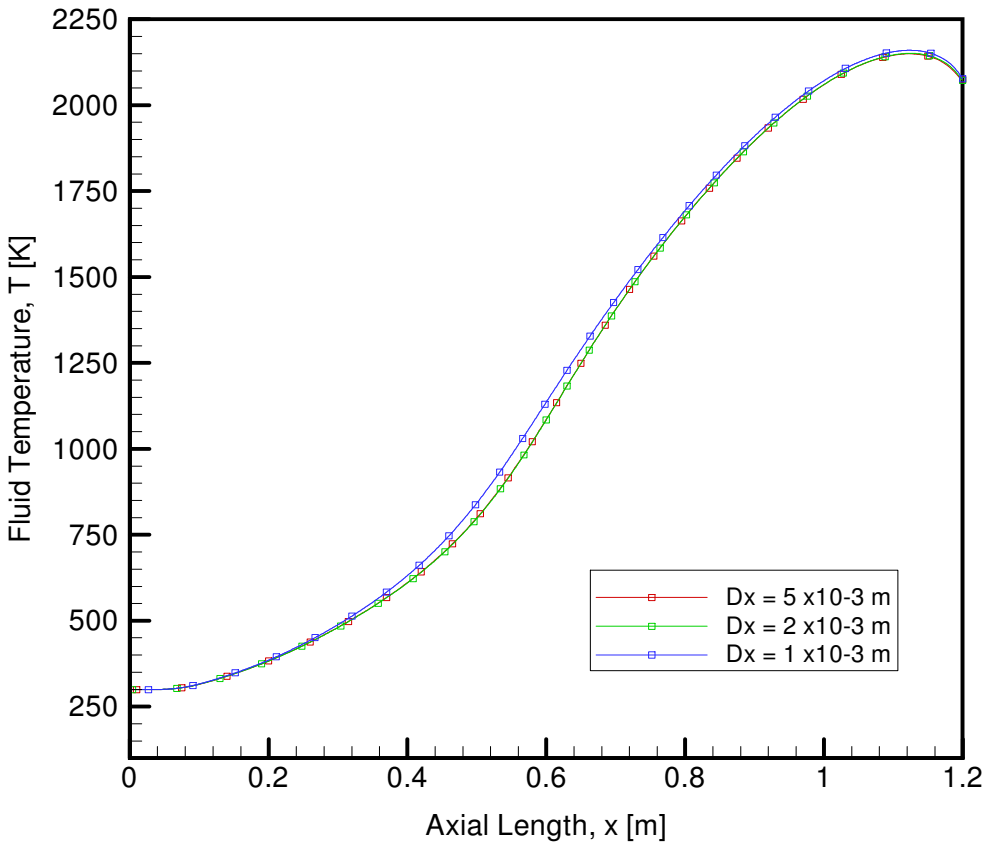

Figure 15- Comparison of Fluid Temperature distribution along the axial centerline of the 3-D Two-Domain models for dx = $5x10^{-3}$ m, dx = $2x10^{-3}$ m, dx = $1x10^{-3}$ m for Run 3D-H2-2DM-I

Table 19 consists of 3-D two domain models with different numbers of layers in radial direction. The results from this study also were similar with each other.

Table 19- Mesh Independence (Fluid Layer) Study for 3D-2 Domain Steady State Case [dx = $1x10^{-3}$ m, turbulent, constant properties]

					Results			
Run No.	No. of Layers, n_f	No. of Cells	Mach Number, Ma	Reynolds Number, Re ($x10^5$)	Inlet Pressure, P_i [MPa]	Outlet Centerline Fluid Temperature, T_e [K]	Outlet Velocity, u_e [m/s]	Pressure Difference, ΔP [MPa]
3D-H2-2DM-II	5	212,577	0.107	3.18	8.608	2076.79	3132.66	5.508
	10	319,200	0.1105	3.18	8.394	2074.79	3115.69	5.294
	13	386,400	0.1108	3.18	8.372	2076.85	3110.87	5.272

A comparison of pressure, velocity and temperature distribution between different models is presented in this section. The inlet pressures for all three models are identical and have very little deviation from each other. The velocity distributions look very similar for models with different number of layer. And, temperature distributions are compared between 3-D one domain models with different number of layers. A quantitative comparison is presented in Table 20 and a figurative comparison is shown in Figure 16.

Table 20- Fluid Temperature distribution along the axial centerline of the 3-D Two-Domain models for $n_f = 5$, $n_f = 10$, $n_f = 13$ for Run 3D-H2-2DM-II

Axial Distance, x [m]	Fluid Temperature, T_f [K] ($n_f = 5$)	Fluid Temperature, T_f [K] ($n_f = 10$)	Fluid Temperature, T_f [K] ($n_f = 13$)
0	299.284	299.257	299.253
0.1	315.918	315.304	315.518
0.2	385.422	382.23	382.444
0.3	488.472	477.097	476.393
0.4	631.237	598.859	595.36
0.5	842.398	773.695	766.38
0.6	1135.92	1050.35	1038.9
0.7	1434.1	1392.81	1389.34
0.8	1693.35	1675.61	1676.71
0.9	1909.87	1897.79	1899.35
1.0	2071.1	2061.75	2063.23
1.1	2155.62	2148.28	2149.58
1.2	2076.79	2074.79	2076.85

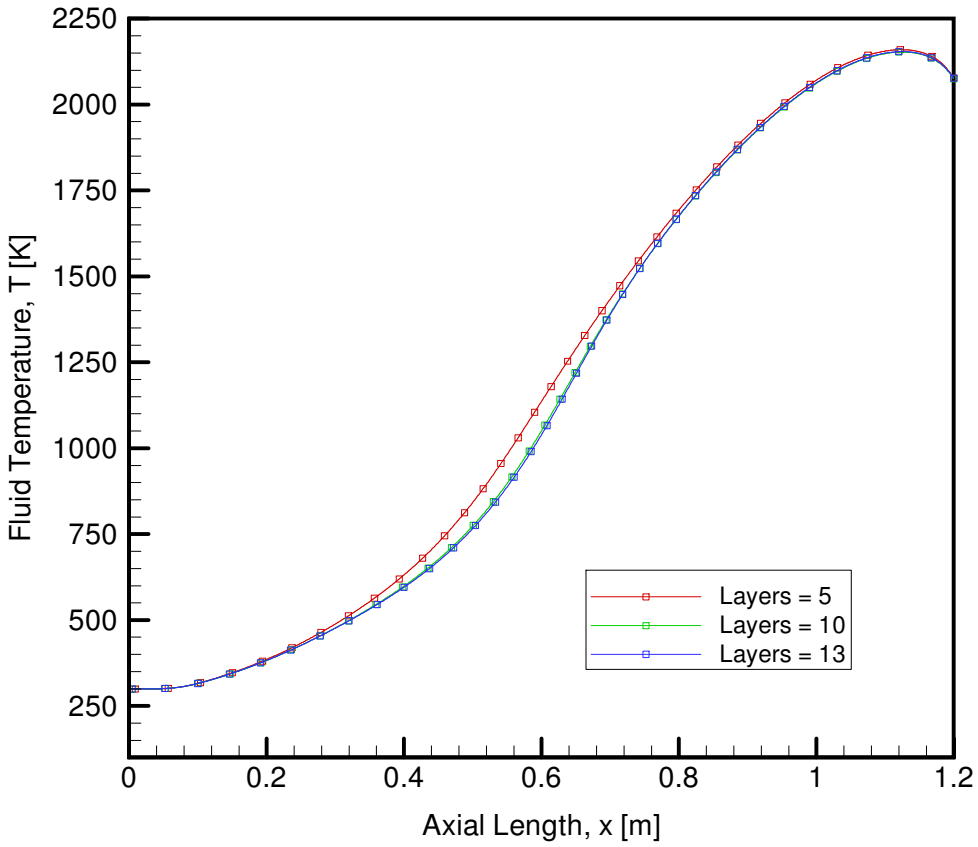

Figure 16- Comparison of Fluid Temperature distribution along the axial centerline of the 3-D Two-Domain models for $n_f = 5$, $n_f = 10$, $n_f = 13$ for Run 3D-H2-2DM-II

A two domain case in Table 21 has three models with different number of layers in the solid domain. The comparison between the two domain models with three different layers of 5, 8, and 10 with five layers in radial direction in the fluid domain is presented in the table below. The mesh independence study has an inlet mass flow rate of 0.005 kg/s, inlet fluid temperature 300 K and a constant heat flux of 22,000 kJ/s-m^2. Also, the outlet pressure for the study is set to be 3.1 MPa. It was found that the change in layers in the solid domain did not have any effect on the results.

Table 21 - Mesh Independence (Solid Layer) Study for 3-D Two-Domain Steady State Case [dx = $1x10^{-3}$ m, n_f = 5, turbulent, constant properties]

					Results			
Run No.	No. of Layers in solid, n_s	No. of Cells	Mach Number, Ma	Reynolds Number, Re ($x10^5$)	Inlet Pressure, P_i [MPa]	Outlet Centerline Fluid Temperature, T_e [K]	Outlet Velocity, u_e [m/s]	Pressure Difference, ΔP [MPa]
3D-H2-2DM-III	5	340,800	0.109	3.18	8.503	2071.73	3125.43	5.403
	8	403,200	0.109	3.18	8.503	2071.74	3125.44	5.403
	10	459,600	0.109	3.18	8.503	2071.74	3125.44	5.403

A comparison of pressure, velocity and temperature distribution between 3-D two domain models with different layers in the solid domain was conducted for this study. Quantitative and figurative comparison of temperature distribution is shown in Table22 and Figures 17.

Table 22- Fluid Temperature distribution along the axial centerline of the 3-D Two-Domain models for $n_s = 5$, $n_s = 8$, $n_s = 10$ for Run 3D-H2-2DM-III

Axial Distance, x [m]	Fluid Temperature, T_f [K] ($n_s = 5$)	Fluid Temperature, T_f [K] ($n_s = 8$)	Fluid Temperature, T_f [K] ($n_s = 10$)
0	299.275	299.275	299.275
0.1	314.915	314.911	314.911
0.2	382.44	382.431	382.431
0.3	480.044	480.032	480.031
0.4	609.732	609.712	609.709
0.5	797.588	797.556	797.551
0.6	1083.99	1083.96	1083.96
0.7	1405.15	1405.13	1405.14
0.8	1675.71	1675.71	1675.71
0.9	1896.15	1896.15	1896.15
1.0	2060.01	2060.01	2060.01
1.1	2146.65	2146.65	2146.65
1.2	2071.73	2071.74	2071.74

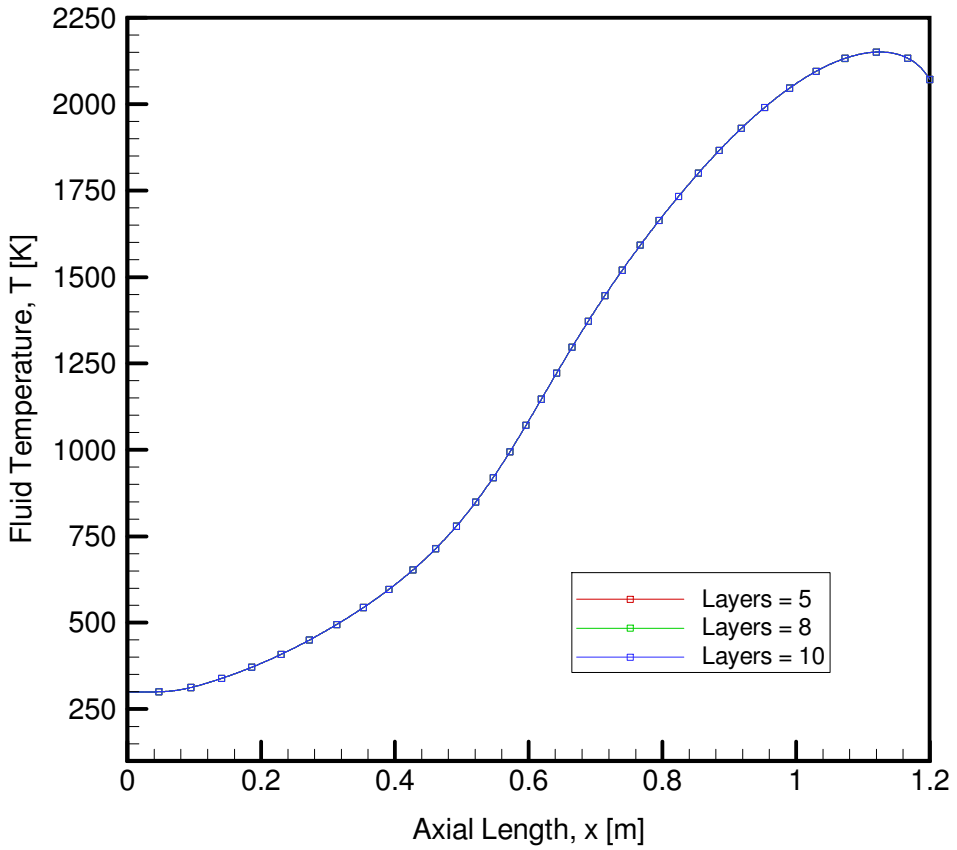

Figure 17- Comparison of Fluid Temperature distribution along the axial centerline of the 3-D Two-Domain models for $n_s = 5$, $n_s = 8$, $n_s = 10$ for Run 3D-H2-2DM-III

6.2.2 Physical Parameter Study for 3-D One-Domain Model

In this section, a 3-D one domain model is simulated to predict the pressure, temperature, and velocity distribution in the channel with a variable heat flux of 22000 kW/m^2; under constant and variable physical properties for gaseous hydrogen. The inlet fluid temperature and inlet mass flow rate is given to be 300 K and 0.005 kg/s respectively. The outlet pressure is set at 3.1 MPa. The values for constant physical properties are obtained from the default setting in Fluent and the values for variable physical properties are calculated using the polynomial relations as a function of temperature from the NIST [20].

Table 23 - Physical Parameter (c_p, k, and μ) Study for 3-D One-Domain Steady State Case [dx = 5x10^{-4} m, Mesh size = 348,000, n_f = 5, turbulent]

				Results			
Run No.	Parameters c_p, k, and μ	Mach Number, Ma	Reynolds Number, Re (x10^5)	Inlet Pressure, P_i [MPa]	Outlet Centerline Fluid Temperature, T_e [K]	Outlet Velocity, u_e [m/s]	Pressure Difference, ΔP [MPa]
3D-H2-1DM-VII	Constant	0.12	3.18	7.909	1791.97	2708.76	4.809
	Variable	0.11	3.18	8.30	1931.81	2921.21	5.20

Fluid temperature distribution shows a higher magnitude in case of variable properties compared to that of constant properties study. A quantitative comparison is shown in Table 24.

Table 24- Fluid Temperature distribution along the axial centerline of the 3-D One-Domain model for Constant and Variable properties for Run 3D-H2-1DM-VII

Axial Distance, x [m]	Fluid Temperature, T_f [K] (Constant Properties)	Fluid Temperature, T_f [K] (Variable Properties)	Fluid Temperature Difference, ΔT [K]	% Deviation
0	299.164	299.231	-0.067	0.0224
0.1	312.499	314.329	-1.83	0.5822
0.2	371.716	379.197	-7.481	1.9729
0.3	463.157	478.36	-15.203	3.1782
0.4	591.924	618.893	-26.969	4.3576
0.5	770.077	819.636	-49.559	6.0465
0.6	994.53	1075.59	-81.06	7.5363
0.7	1226.86	1334.11	-107.25	8.0391
0.8	1439.46	1567.16	-127.7	8.1485
0.9	1620.04	1764.15	-144.11	8.1688
1.0	1755.93	1911.51	-155.58	8.1391
1.1	1830.19	1990.02	-159.83	8.0316
1.2	1791.97	1931.81	-139.84	7.2388

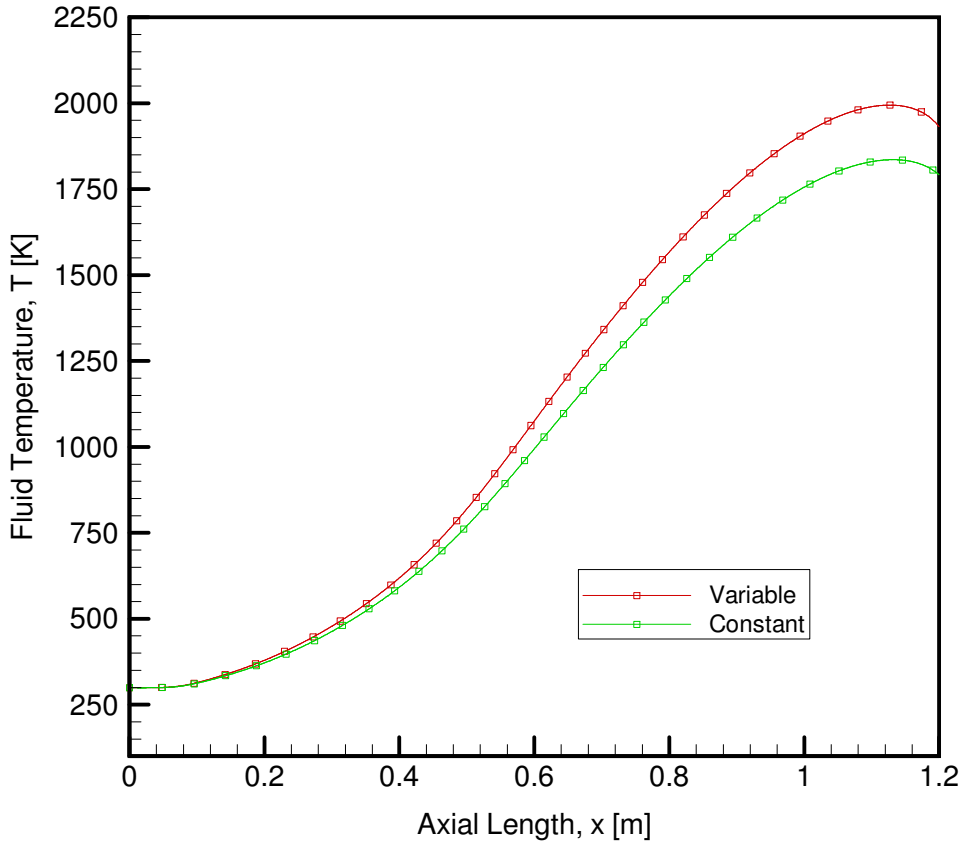

Figure 18- Comparison of Fluid Temperature distribution along the axial centerline of the 3-D One-Domain model for Constant and Variable properties for Run 3D-H2-1DM-VII

6.2.3 Fully Developed Flow Study for 3-D One-Domain Model

In this study, a 3-D one-domain model is used to differentiate between a developing and fully developed flow. Table 25 presents the heat input for developing and fully developed flow and the predicted thermodynamic parameters at the end of each run. A one domain model has gaseous hydrogen coming in at 300 K and 148 m/s. A constant heat flux of 15,000 W/m^2 is applied to the model. For a fully developed flow study, a flow in a 3-D one-domain model is run twice, where in the first leg of the run no heat flux (adiabatic) is applied to the model. During the second leg, profiles for temperature and velocity are retrieved from the outlet of the first leg run and given as the inlet conditions for the second leg run and a constant heat flux of 15,000 kW/m^2 is applied to the surface of the model. This procedure creates a fully developed flow in the channel even though the channel is not long enough to be fully developed. Whereas, the developing flow study simply consists of a flow with the similar initial conditions as that of the fully developed run but has just one leg with a constant heat flux of 15,000 kW/m^2. A quantitative comparison of axial velocity distribution along the axial length of the model is shown in Table 26.

Table 25- Developing and Fully Developed Flow Study for 3-D One-Domain Steady State Case [dx = 5x10^{-4} m, Mesh size: 348,000, n_f = 5, u_i = 148 m/s, turbulent, constant properties]

					Results			
Run No.	Flow Case	Heat Input, Q_{cst} [kJ/s-m^2]	Mach Number, Ma	Reynolds Number, Re (x10^5)	Inlet Pressure, P_i [MPa]	Outlet Centerline Fluid Temperature, T_e [K]	Outlet Velocity, u_e [m/s]	Pressure Difference, ΔP [MPa]
3D-H2-1DM-III	Fully Developed	0	0.28	3.18	3.361	299.606	185.092	0.261
		15,000	0.10	3.18	9.203	1547.55	2932.75	6.103
	Developing	15,000	0.11	3.18	8.238	1909.57	2955.85	5.138

Table 26- Axial Velocity distribution along the axial centerline of the 3-D One-Domain model for developing and fully developed flows for Run 3D-H2-1DM-III

Axial Distance, x [m]	Axial Velocity, u [m/s] (Developing Flow)	Axial Velocity, u [m/s] (Fully Developed Flow)	Axial Velocity Difference, Δu [m/s]	% Deviation
0	148.00	183.594	35.594	0.193873
0.1	245.927	263.868	17.941	0.067992
0.2	330.802	355.328	24.526	0.069024
0.3	447.439	457.331	9.892	0.02163
0.4	578.995	562.284	16.711	0.02972
0.5	705.456	673.736	31.72	0.047081
0.6	839.078	797.028	42.05	0.052758
0.7	990.475	936.289	54.186	0.057873
0.8	1166.18	1098.56	67.62	0.061553
0.9	1379.04	1296.25	82.79	0.063869
1.0	1654.93	1554.81	100.12	0.064394
1.1	2060.86	1942.71	118.15	0.060817
1.2	2955.85	2932.75	23.1	0.007877

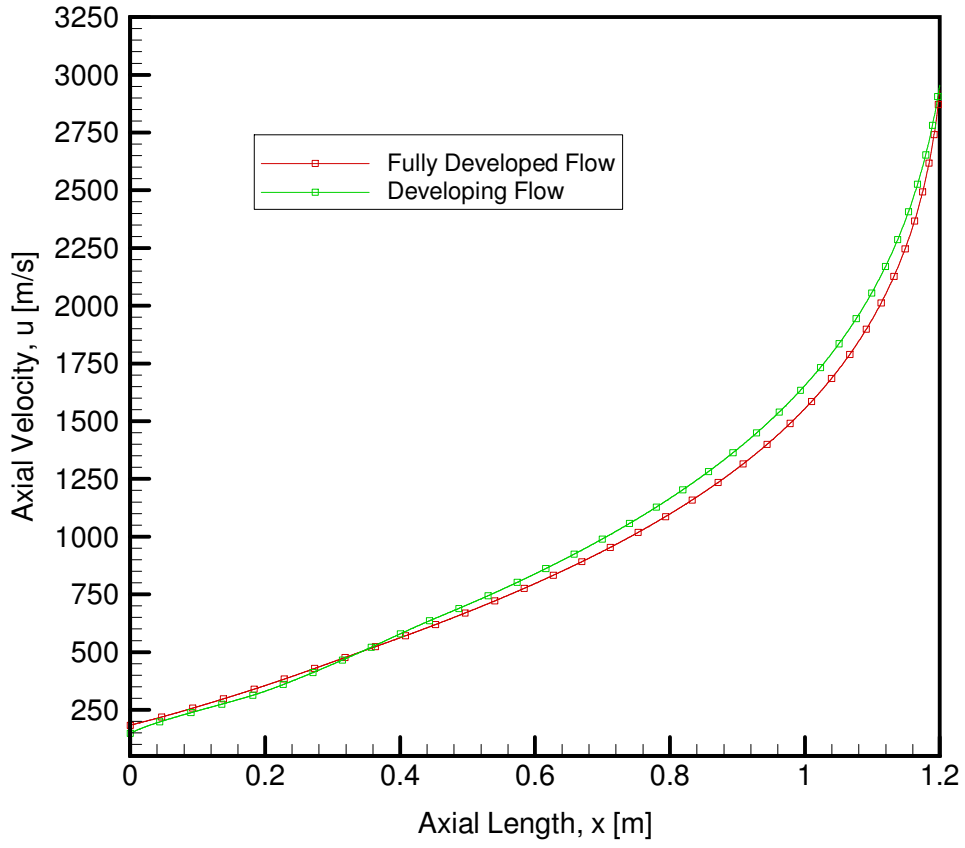

Figure 19- Comparison of Axial Velocity distribution along the axial centerline of the 3-D One-Domain model for developing and fully developed flows for Run 3D-H2-1DM-III

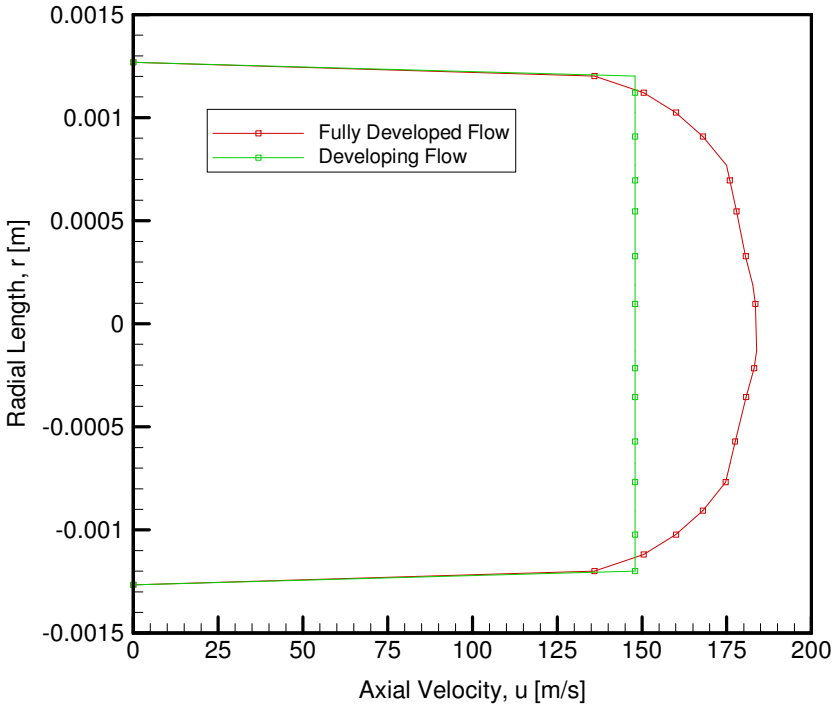

Figure 20- Comparison of Velocity Profile at the inlet of the 3-D One-Domain model for developing and fully developed flows

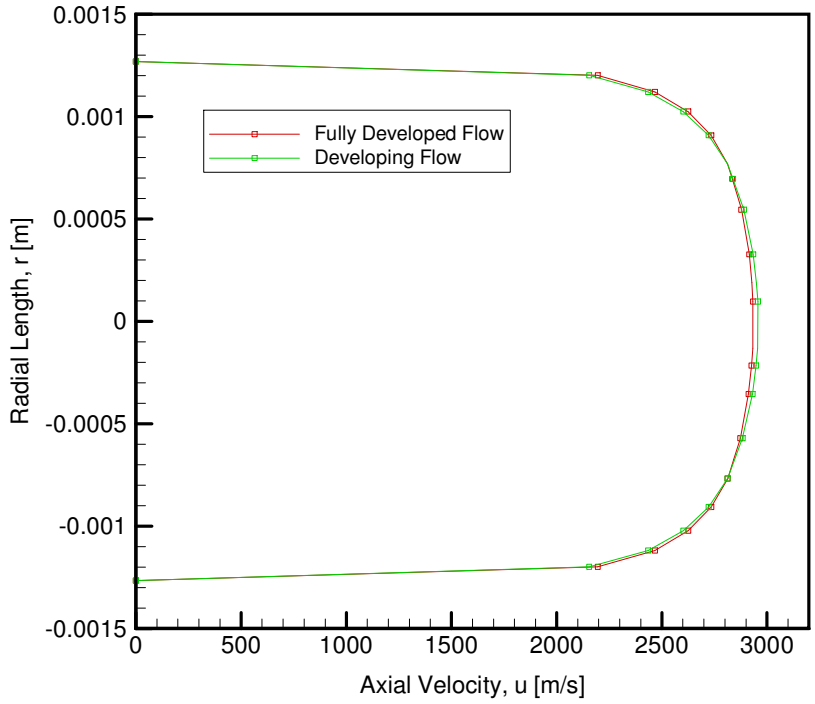

Figure 21- Comparison of Velocity Profile at the outlet of the 3-D One-Domain model for developing and fully developed flows

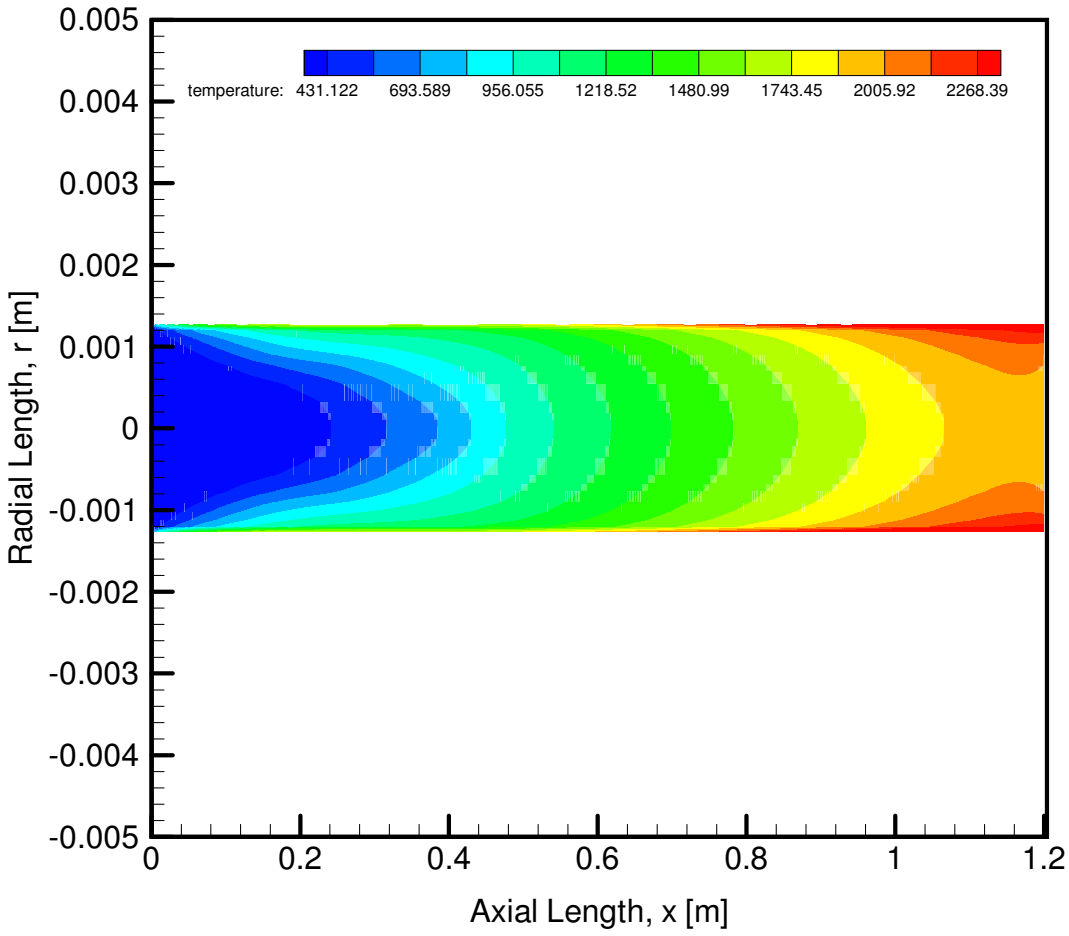

Figure 22- Fluid Temperature Contour plot along the axial length of the 3-D One-Domain model for developing flow

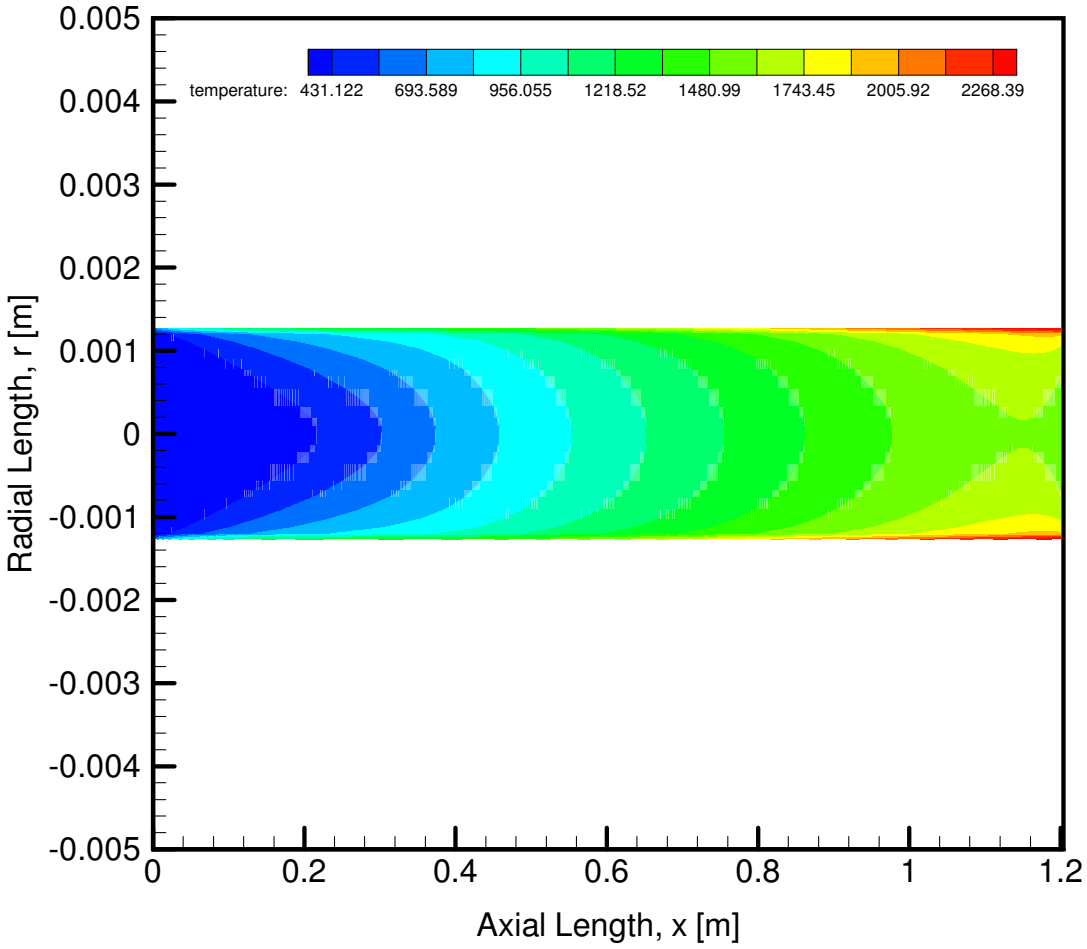

Figure 23- Fluid Temperature Contour plot along the axial length of the 3-D One-Domain model for developed flow

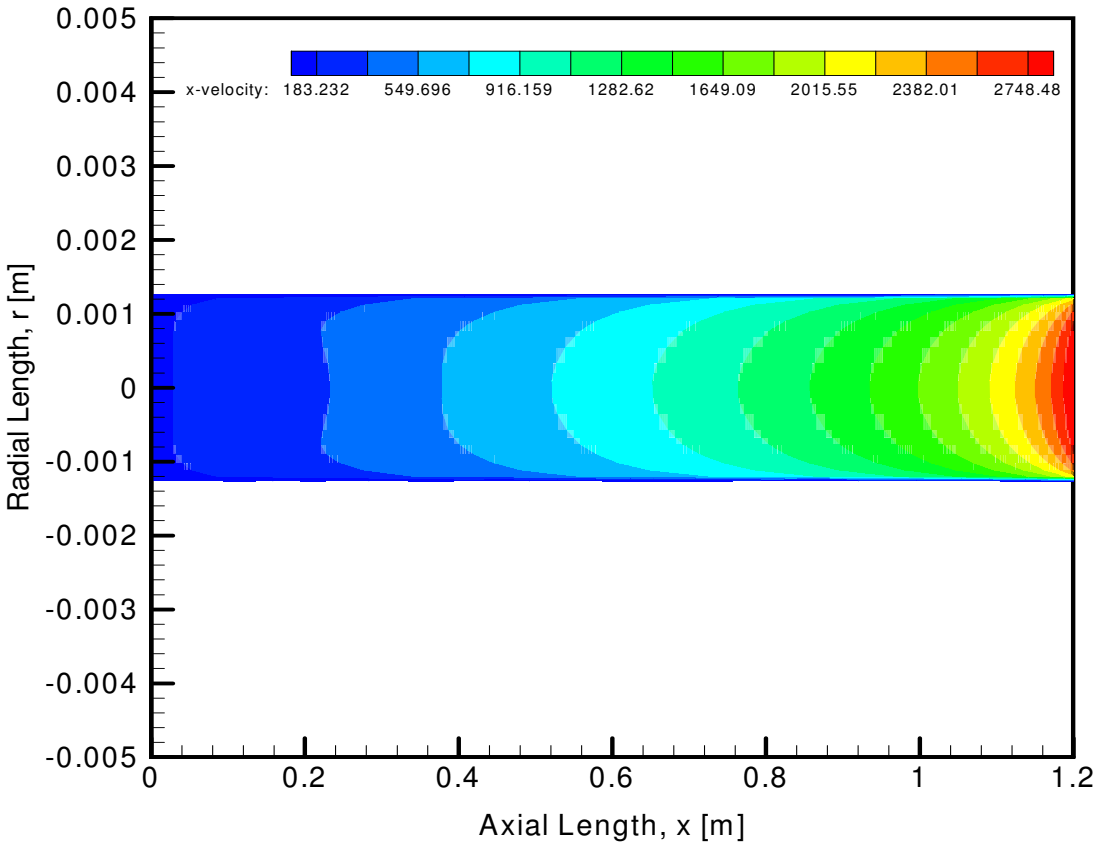

Figure 24- Axial Velocity Contour plot along the axial length of the 3-D One-Domain model for developing flow

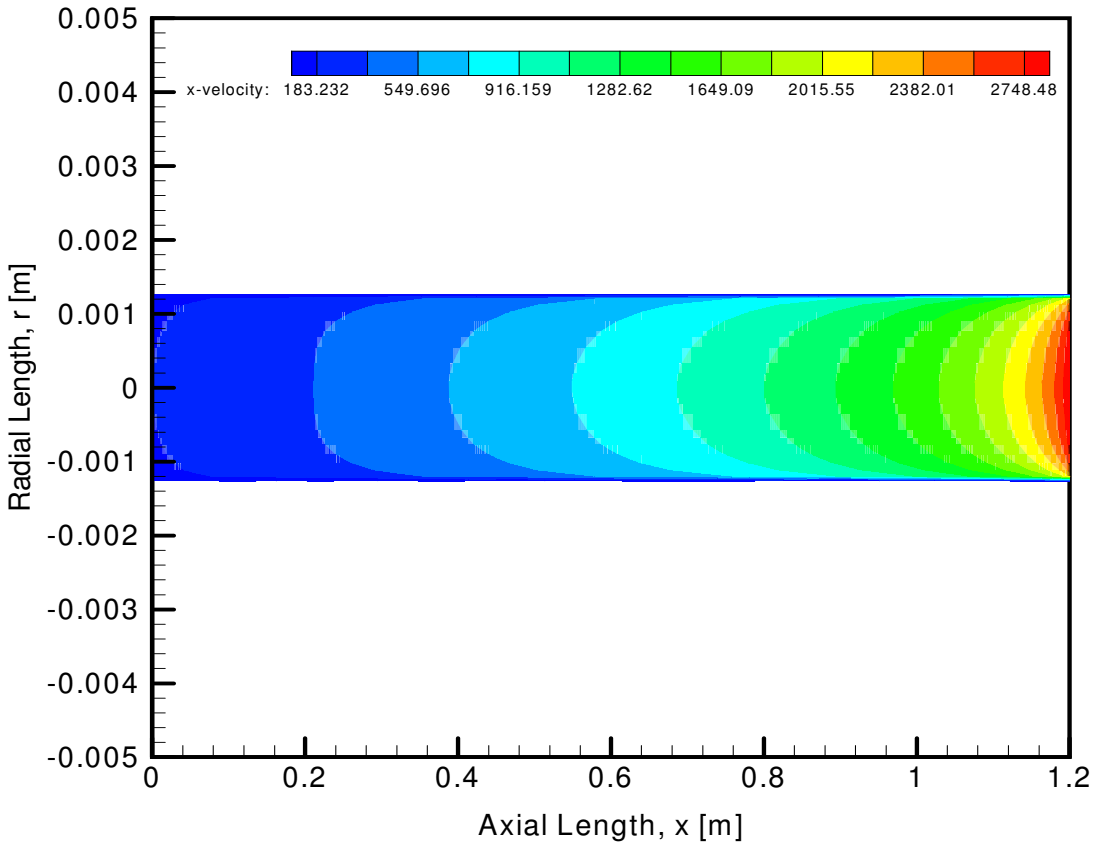

Figure 25- Axial Velocity Contour plot along the axial length of the 3-D One-Domain model for developed flow

6.2.4 Turbulence Model Study for 3-D One-Domain Model

In this study, a 3-D one domain model is used to study the effects of different turbulence models in the distribution of pressure, temperature and velocity of gaseous hydrogen flowing in the channel.

Table 27- Turbulence Model Study for 3-D One-Domain Steady State Case
[dx = $5x10^{-4}$ m, Mesh size = 348,000, nf = 5, turbulent, constant properties]

				Results			
Run No.	Turbulence Model	Mach Number, Ma	Reynolds Number, Re ($x10^5$)	Inlet Pressure, P_i [MPa]	Outlet Centerline Fluid Temperature, T_e [K]	Outlet Velocity, u_e [m/s]	Pressure Difference, ΔP [MPa]
3D-H2-1DM-VI	k-e	0.109	3.18	8.503	2071.73	3125.43	5.403
	Spalart-Allmaras	0.11	3.18	8.357	1937.03	2906.15	5.257
	k-omega	0.11	3.18	8.322	1920.42	2956.21	5.222

Table 28- Axial Velocity distribution along the axial centerline of the 3-D One-Domain model for Spalart-Allmaras, k-omega, k-epsilon for Run 3D-H2-1DM-VI

Axial Distance, x [m]	Axial Velocity, u [m/s] (Spalart-Allmaras)	Axial Velocity, u [m/s] (k-omega)	Axial Velocity, u [m/s] (k-epsilon)
0	146.372	146.969	147.362
0.1	193.119	197.657	195.325
0.2	249.17	254.299	252.544
0.3	339.801	345.145	343.887
0.4	462.477	467.763	467.13
0.5	614.662	622.93	621.946
0.6	792.794	809.638	803.191
0.7	994.443	1017.35	1005.99
0.8	1219.43	1245.22	1231.64
0.9	1471.77	1501.44	1484.61
1.0	1765.81	1800.46	1779.53
1.1	2149.31	2191.27	2164.7
1.2	2906.15	2956.21	2921.21

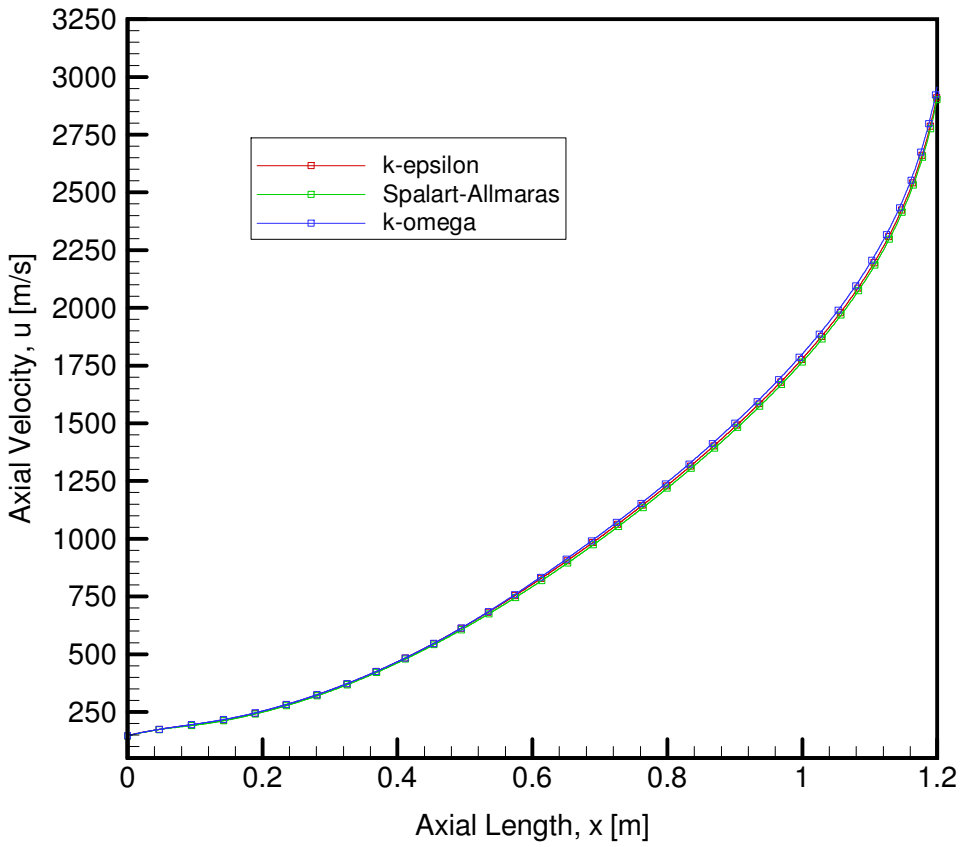

Figure 26- Comparison of Axial Velocity distribution along the axial centerline of the 3-D One-Domain model for Spalart-Allmaras, k-omega, k-epsilon for Run 3D-H2-1DM-VI

Table 29- Fluid Temperature distribution along the axial centerline of the 3-D One-Domain model for Spalart-Allmaras, k-omega, k-epsilon for Run 3D-H2-1DM-VI

Axial Distance, x [m]	Fluid Temperature, T_f [K] (Spalart-Allmaras)	Fluid Temperature, T_f [K] (k-omega)	Fluid Temperature, T_f [K] (k-epsilon)
0	299.241	299.235	299.231
0.1	315.422	311.064	314.329
0.2	387.58	372.039	379.197
0.3	505.719	464.015	478.36
0.4	672.936	586.809	618.893
0.5	883.648	757.086	819.636
0.6	1119.37	1003.16	1075.59
0.7	1358.29	1291.64	1334.11
0.8	1582.04	1542.86	1567.16
0.9	1774.21	1746.03	1764.15
1.0	1918.72	1897	1911.51
1.1	1995.76	1978.02	1990.02
1.2	1937.03	1920.42	1931.81

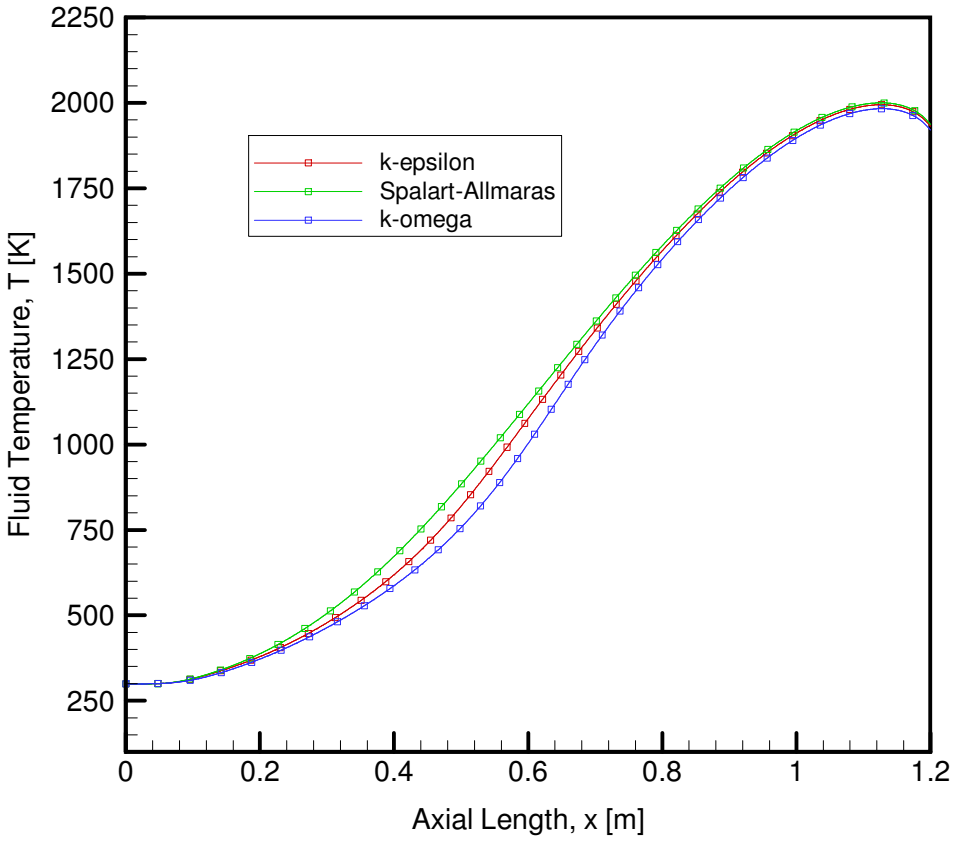

Figure 27- Comparison of Fluid Temperature distribution along the axial centerline of the 3-D One-Domain model for Spalart-Allmaras, k-omega, k-epsilon for Run 3D-H2-1DM-VI

6.2.5 Different Pipe Material Study for 3-D Two-Domain Model

In this study, a 3-D two-domain model is simulated with different pipe material. The outlet results are shown in Table 30. A quantitative comparison of temperature distribution is presented in Table 31.

Table 30- Different Pipe Material Study for 3-D Two-Domain Steady State Case
[dx = $1x10^{-3}$ m, Mesh size = 212,577, $n_f = 5$, $n_s = 1$, turbulent, variable properties]

				Results			
Run No.	Pipe Material	Mach Number, Ma	Reynolds Number, Re ($x10^5$)	Inlet Pressure, P_i [MPa]	Outlet Centerline Fluid Temperature, T_e [K]	Outlet Wall Temperature, T_w [K]	Outlet Velocity, u_e [m/s]
3D-H2-2DM-VII	Aluminum	0.107	3.18	8.608	2076.78	2450.66	3132.65
	Steel	0.107	3.18	8.608	2076.79	2450.67	3132.66

Table 31- Fluid Temperature distribution along the axial centerline of the 3-D Two-Domain models for Aluminum and Steel for Run 3D-H2-2DM-VII

Axial Distance, x [m]	Fluid Temperature, T_f [K] (Aluminum)	Fluid Temperature, T_f [K] (Steel)	Fluid Temperature Difference, ΔT [K]	% Deviation
0	299.284	299.284	0	0
0.1	315.919	315.918	0.001	3.16538E-06
0.2	385.417	385.422	0.005	1.29728E-05
0.3	488.444	488.472	0.028	5.73216E-05
0.4	631.156	631.237	0.081	0.000128319
0.5	842.248	842.398	0.15	0.000178063
0.6	1135.79	1135.92	0.13	0.000114445
0.7	1434.05	1434.1	0.05	3.48651E-05
0.8	1693.32	1693.35	0.03	1.77164E-05
0.9	1909.86	1909.87	0.01	5.23596E-06
1.0	2071.09	2071.1	0.01	4.82835E-06
1.1	2155.61	2155.62	0.01	4.63904E-06
1.2	2076.78	2076.79	0.01	4.81512E-06

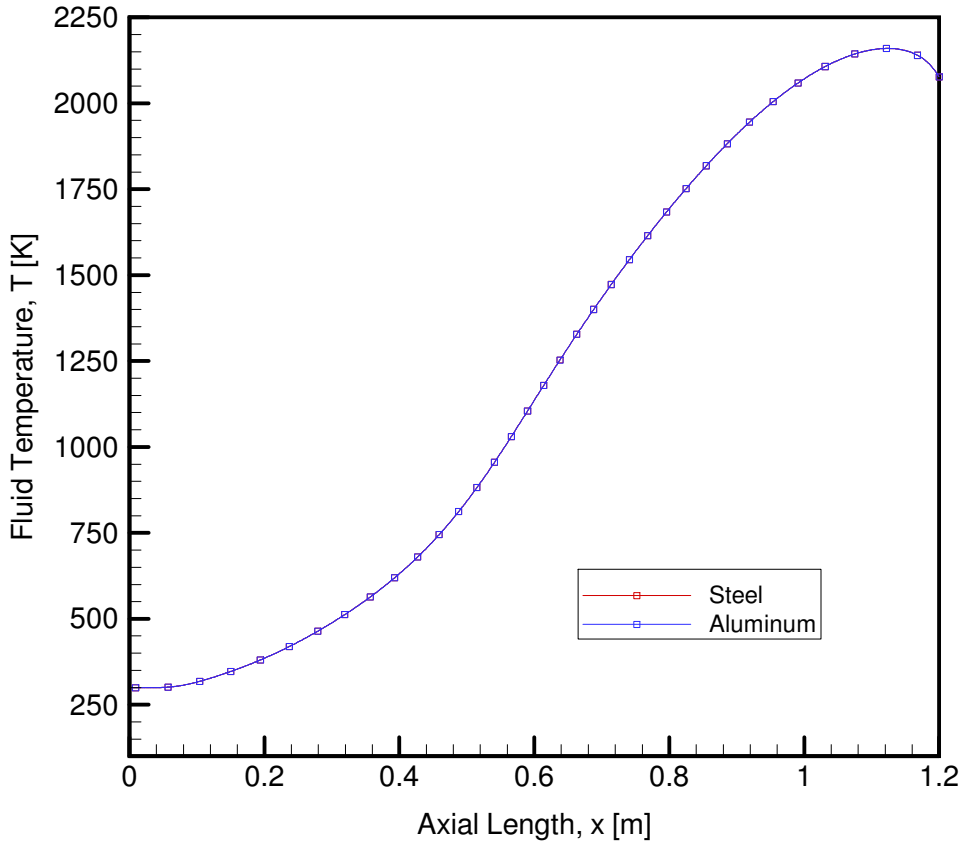

Figure 28- Comparison of Fluid Temperature distribution along the axial centerline of the 3-D Two-Domain models for Aluminum and Steel for Run 3D-H2-2DM-VII

6.3 Heat Flux Study

In this study, a 1-D model, 3-D one domain model, and 3-D two domain model were all subjected to different constant and variable heat fluxes. All the models had similar boundary and initial conditions. The inlet temperature of the gaseous hydrogen is 300 K, the inlet mass flow rate is 0.005 kg/s and the outlet pressure is set to 3.1 MPa. Pressure, velocity, and temperature distributions are compared between constant and variable heat flux cases for different magnitude of heat flux. Table 32 presents all the different heat fluxes used for this study.

A 1-D model with 41x41 mesh size and a time increment of $5x10^{-6}$ sec is used to study the effects of constant and variable heat flux in a 1-D model. The model is set to similar initial and boundary conditions as that of the 3-D one domain and 3-D two domain models with a coefficient of friction of 0.99. A quantitative comparison for temperature distribution between constant and variable heat fluxes is shown in Table 33

Table 32- Heat Flux Study for 1-D Unsteady State Case
[IN = 41, $\Delta t = 5x10^{-6}$ sec, $C_f = 0.99$, turbulent, constant properties]

					Results			
Run No.	Type	Heat Input, Q [kJ/s-m^2]	Mach Number, Ma	Reynolds Number, Re (x10^5)	Inlet Pressure, P_i [MPa]	Mean Outlet Fluid Temperature, T_e [K]	Outlet Velocity, u_e [m/s]	Pressure Difference, ΔP [MPa]
1D-H2-IV	Adiabatic	0	0.26	3.18	3.55	288.20	372.92	0.45
	Constant	1,600	0.23	3.18	3.96	486.37	629.31	0.86
		3,000	0.21	3.18	4.29	653.75	845.73	1.19
		7,000	0.18	3.18	5.14	1107.57	1430.28	2.04
		14,300	0.14	3.18	6.45	1874.00	2396.06	3.35
		18,000	0.13	3.18	7.03	2255.68	2844.89	3.93
	Variable	18,000	0.14	3.18	6.55	1913.41	2449.96	3.45
		20,000	0.136	3.18	6.82	2083.66	2650.72	3.72
		22,000	0.13	3.18	7.08	2253.74	2846.60	3.98

Table 33- Mean Fluid Temperature distribution along the axial length of the 1-D model for Q_{cst} = 14,299 kW/m^2 and Q_{max} = 22,000 kW/m^2 for Run 1D-H2-IV

Axial Distance, x [m]	Mean Fluid Temperature, T_m [K] Q_{cst} = 14,299.422 kW/m^2	Mean Fluid Temperature, T_m [K] Q_{max} = 22,000 kW/m^2	Fluid Temperature Difference, ΔT [K]	% Deviation
0	300.00	300.00	0	0
0.1	444.529	424.287	20.242	0.047708
0.2	635.998	627.748	8.25	0.013142
0.3	777.652	804.590	26.938	0.03348
0.4	917.299	997.140	79.841	0.08007
0.5	1099.55	1267.99	168.44	0.13284
0.6	1232.51	1472.75	240.24	0.163123
0.7	1361.33	1670.51	309.18	0.185081
0.8	1524.50	1909.62	385.12	0.201674
0.9	1637.88	2059.94	422.06	0.204889
1.0	1739.74	2175.51	435.77	0.200307
1.1	1844.63	2253.54	408.91	0.181452
1.2	1874.00	2216.63	342.63	0.154572

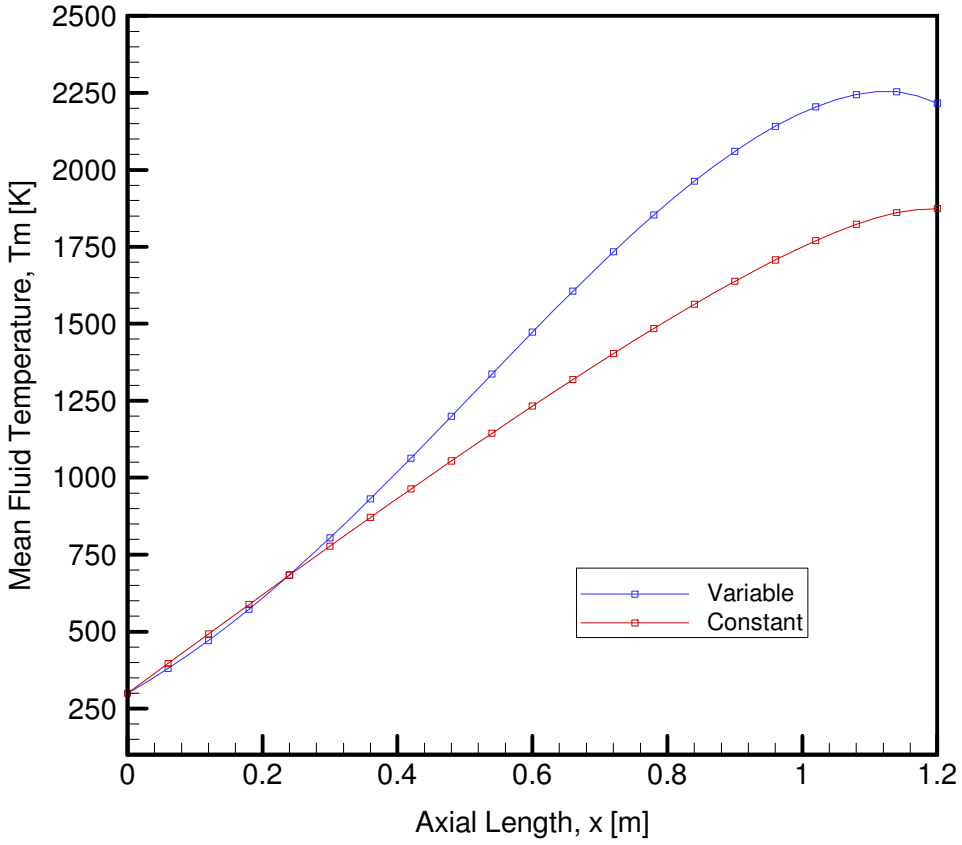

Figure 29- Comparison of Mean Fluid Temperature distribution along the axial length of the 1-D model for Q_{cst} = 14,299 kW/m^2 and Q_{max} = 22,000 kW/m^2 for Run 1D-H2-IV

Also, a 3-D one domain model with a mesh size of 348,000 cells and axial cell size of $5x10^{-4}$ m is used to study the effects of constant and variable heat flux in a 3-D one domain model. The model is set to similar initial and boundary conditions as that of the 1-D and 3-D two domain models. Table 34 lists all the heat fluxes used for this particular study. A quantitative comparison for temperature distribution between constant and variable heat fluxes is shown in Table 35.

Table 34- Heat Flux Study for 3-D One-Domain Steady State Case
[dx = $5x10^{-4}$ m, Mesh size = 348,000, n_f = 5, turbulent, variable properties]

					Results			
Run No.	Type	Heat Input, Q [kJ/s-m^2]	Mach Number, Ma	Reynolds Number, Re ($x10^5$)	Inlet Pressure, P_i [MPa]	Outlet Centerline Fluid Temperature, T_e [K]	Outlet Velocity, u_e [m/s]	Pressure Difference, ΔP [MPa]
3D-H2-1DM-III	Adiabatic	0	0.21	3.18	4.32	294	438	1.22
	Constant	1,600	0.19	3.18	4.89	490	745	1.79
		3,000	0.17	3.18	5.32	650	1000	2.22
		7,000	0.14	3.18	6.49	1100	1700	3.39
		14,299	0.11	3.18	8.12	1831	2850	5.02
		18,000	0.10	3.18	9.0	2195	3400	5.90
		22,000	0.095	3.18	9.7	2550	3900	6.6
	Variable	18,000	0.12	3.18	7.70	1650	2550	4.60
		20,000	0.115	3.18	8.0	1800	2740	4.90
		22,000	0.111	3.18	8.30	1930	2950	5.20

Table 35 - Fluid Temperature distribution along the axial centerline of the 3-D One-Domain model for Q_{cst} = 14,299 kW/m^2 and Q_{max} = 22,000 kW/m^2 for Run 3D-H2-1DM-III

Axial Distance, x [m]	Fluid Temperature, T_f [K] (Constant Heat Flux) 14,299 kW/m^2	Fluid Temperature, T_f [K] (Variable Heat Flux) 22,000 kW/m^2	Fluid Temperature Difference, ΔT [K]	% Deviation
0	299.206	299.231	-0.025	8.35475E-05
0.1	323.741	314.329	9.412	0.029943149
0.2	379.145	379.197	-0.052	0.000137132
0.3	516.261	478.36	37.901	0.079231123
0.4	750.259	618.893	131.366	0.212259631
0.5	978.287	819.636	158.651	0.193562752
0.6	1142.68	1075.59	67.09	0.062375069
0.7	1295.75	1334.11	-38.36	0.028753251
0.8	1443.87	1567.16	-123.29	0.078670972
0.9	1585.78	1764.15	-178.37	0.101108182
1.0	1717.12	1911.51	-194.39	0.101694472
1.1	1824.89	1990.02	-165.13	0.082979066
1.2	1831.41	1931.81	-100.4	0.051971985

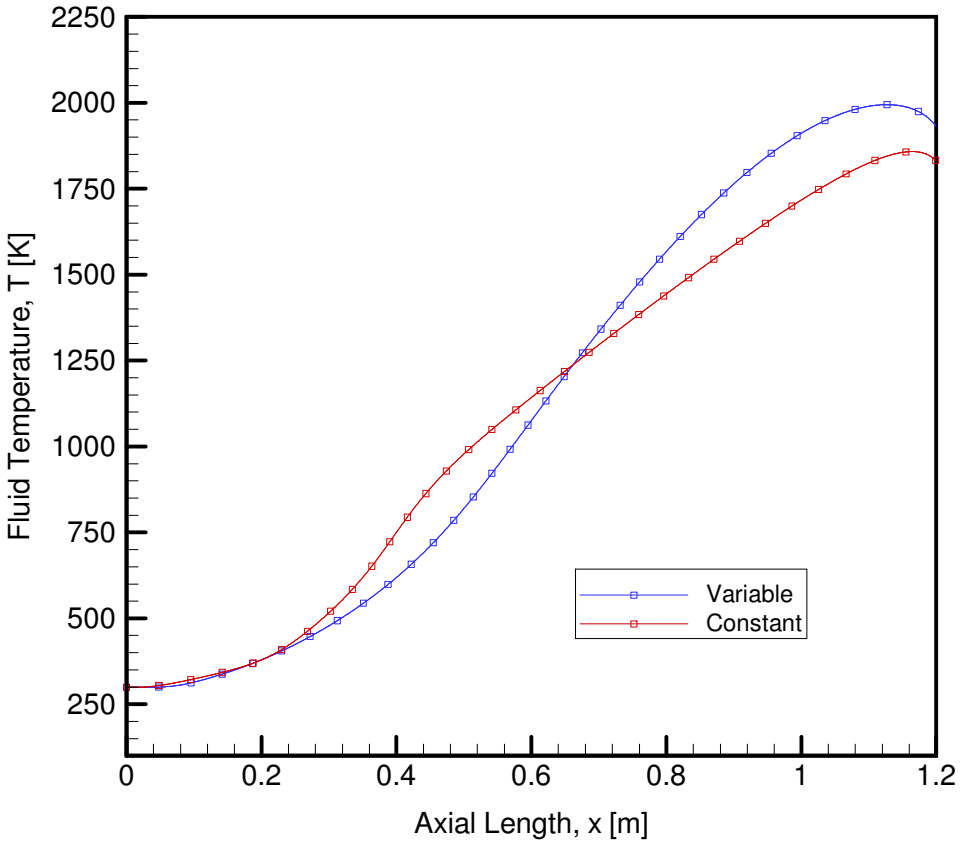

Figure 30- Comparison of Fluid Temperature distribution along the axial centerline of the 3-D One-Domain model for Q_{cst} = 14,299 kW/m^2 and Q_{max} = 22,000 kW/m^2 for Run 3D-H2-1DM-III

A 3-D two domain model with a mesh size of 212,577 cells and axial cell size of $1x10^{-3}$ m is used to study the effects of constant and variable heat flux in a 3-D two domain model. The model is set to similar initial and boundary conditions as that of the 1-D and 3-D one domain models. A comparison of outlet temperature, outlet velocity and inlet pressure between different heat fluxes is shown in Table 36.

Table 36- Heat Flux Study for 3-D Two-Domain Steady State Case
[dx = $1x10^{-3}$ m, Mesh size: 212,577, $n_f = 5$, $n_s = 1$, turbulent, variable properties]

					Results			
Run No.	Type	Heat Input, Q [kJ/s-m^2]	Mach Number, Ma	Reynolds Number, Re ($x10^5$)	Inlet Pressure, P_i [MPa]	Outlet Centerline Fluid Temperature, T_e [K]	Outlet Velocity, u_e [m/s]	Pressure Difference, ΔP [MPa]
3D-H2-2DM-III	Adiabatic	0	0.22	3.18	4.30	294	437	1.20
	Constant	1,600	0.19	3.18	4.89	505	760	1.79
		3,000	0.31	3.18	5.35	680	1005	2.25
		7,000	0.13	3.18	6.55	1170	1800	3.45
		14,299	0.11	3.18	8.41	1968	3057	5.31
		18,000	0.10	3.18	9.24	2350	3675	6.14
		22,000	0.092	3.18	10.1	2750	4225	7.0
	Variable	18,000	0.115	3.18	8.0	1795	2700	4.90
		20,000	0.112	3.18	8.25	1920	2900	5.15
		22,000	0.108	3.18	8.60	2075	3200	5.40

Similarly, for 3-D Two-domain model, the total heat input with a variable heat flux is 22000 kW/m^2 is 210662.637 W. To compare the difference in predicted results between the constant and variable heat flux, the model is run with a constant heat flux of 14299 kW/m^2, which is the average of 22.000 kW/m^2 variable heat flux. The quantitative comparison of temperature distribution is shown in Table 37.

Table 37- Fluid Temperature distribution along the axial centerline of the 3-D Two-Domain model for Q_{cst} = 14,299 kW/m^2 and Q_{max} = 22,000 kW/m^2 for Run 3D-H2-2DM-III

Axial Distance, x [m]	Fluid Temperature, T_f [K] (Constant Heat Flux) 14,299 kW/m^2	Fluid Temperature, T_f [K] (Variable Heat Flux) 22,000 kW/m^2	Fluid Temperature Difference, ΔT [K]	% Deviation
0	299.26	299.284	-0.024	0.008019
0.1	324.941	315.918	9.023	2.856121
0.2	383.712	385.422	-1.71	0.44367
0.3	543.773	488.472	55.301	11.32122
0.4	752.901	631.237	121.664	19.2739
0.5	1034.9	842.398	192.502	22.85167
0.6	1226.5	1135.92	90.58	7.974153
0.7	1395.73	1434.1	-38.37	2.675546
0.8	1558.71	1693.35	-134.64	7.951103
0.9	1714.7	1909.87	-195.17	10.21902
1.0	1858.8	2071.1	-212.3	10.25059
1.1	1975.99	2155.62	-179.63	8.333101
1.2	1967.62	2076.79	-109.17	5.25667

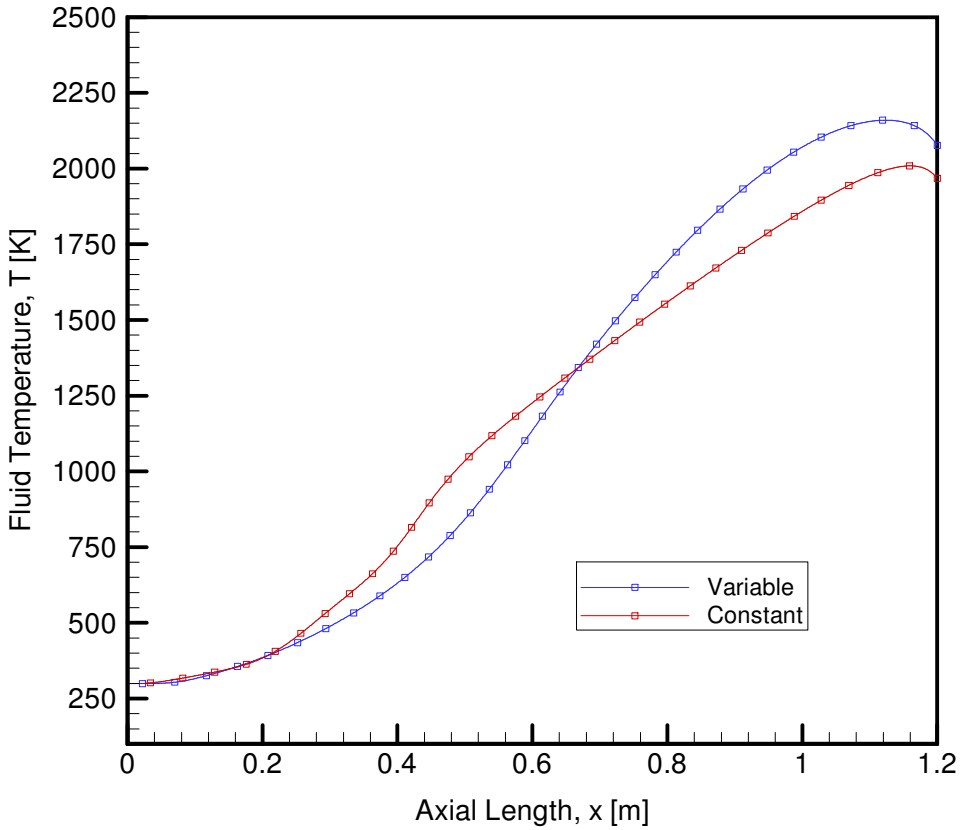

Figure 31- Comparison of Fluid Temperature distribution along the axial centerline of the 3-D Two-Domain model for Q_{cst} = 14,299 kW/m^2 and Q_{max} = 22,000 kW/m^2 for Run 3D-H2-2DM-III

Chapter 7

NTR Channel Flow Simulations – Results for Benchmark Case Study

In this study, a1-D mode and two 3-D commercial CFD models are simulated under same initial and boundary conditions. Gaseous hydrogen is the working fluid in the channel with an inlet temperature of 300 K and a set mass flow rate of 0.005 kg/s. The outlet pressure of the fluid is set to 3.1 MPa. The inner surface of the pipe is stationary with no slip conditions. For the CFD models, a coupled scheme is used for pressure-velocity coupling and second order upwind is set for spatial discretization of pressure, density, momentum, k, e, and energy.

7.1 1-D and 3-D Model Results

A variable heat flux is applied to the outer surface of the wall that is given by a sine function with the maximum magnitude of 22,000 kJ/s-m^2 and the distribution is shown in Figure 32. The minimum heat flux on the wall is 1408 kJ/s-m^2. Therefore, the average heat flux applied to the wall is 14299.422 kJ/s-m^2.

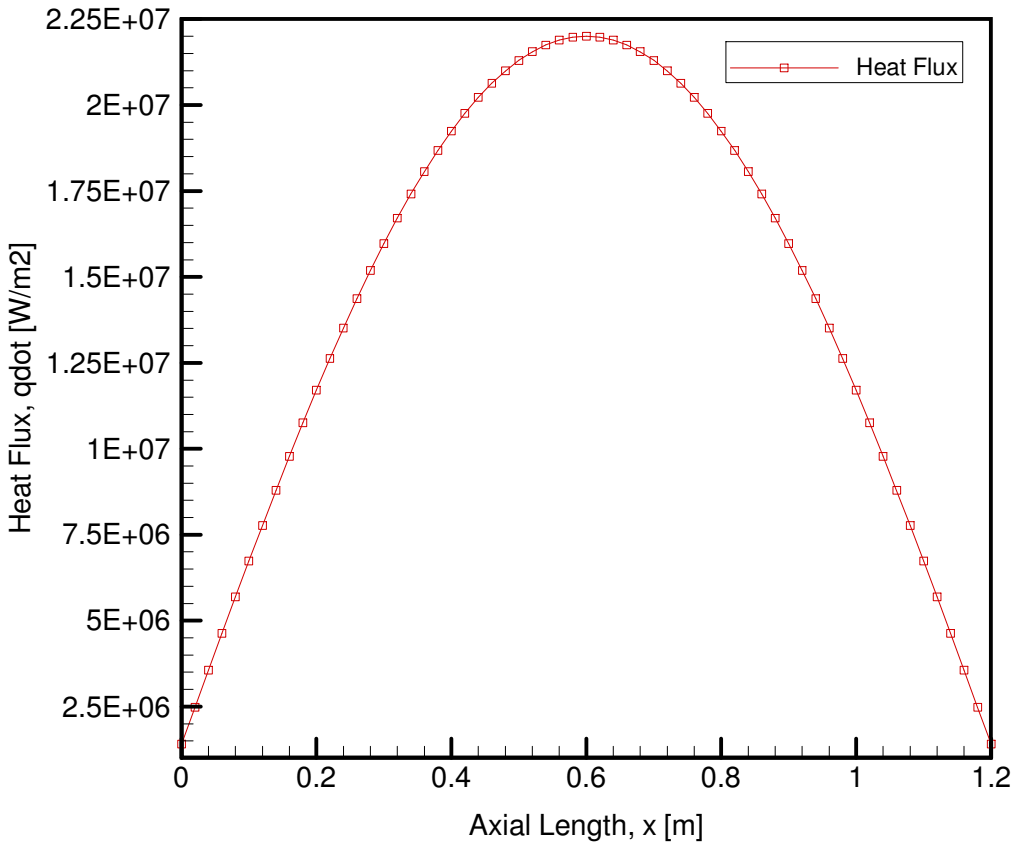

Figure 32- Non-uniform Heat Flux distribution along the length of the cooling channel

7.1.1 1-Dimensional Model Study

A one-dimensional computer model has a 41 x 41 mesh size with a time increment of 5 x 10^{-6} seconds. This computer numerical model is used to simulate the unsteady flow with similar run parameters as that of the experimental study so as to replicate the results. A heat flux distribution similar to Figure is applied to the 1-D computer model to achieve the results similar to that of the experiment. The run parameters for this study are presented in Table 38.

Table 38- Benchmark Run Parameters for 1-D Model
[compressible, unsteady, viscous, turbulent, constant properties]

			Run Parameters			
Run Model	Time Increment, Δt [s]	Mesh Size, IN	Inlet Mass Flow Rate, m_{dot} [kg/s]	Inlet Fluid Temperature, T_i [K]	Exit Pressure, P_e [MPa]	Heat Flux, Q_{max} [kW/m^2]
1D-H2-I.2	5 x10^{-6}	41x41	0.005	300	3.1	22,000

In this study, the outlet pressure of the fluid in the channel is set to 3.1 MPa and the inlet pressure is predicted through simulation of the model with the boundary and initial conditions shown in Table 1. The inlet pressure is predicted to be 7.079 MPa and decreases along the length of the pipe to its set value of 3.1 MPa at the outlet of the pipe. The pressure distribution along the channel is shown in Figure 33.

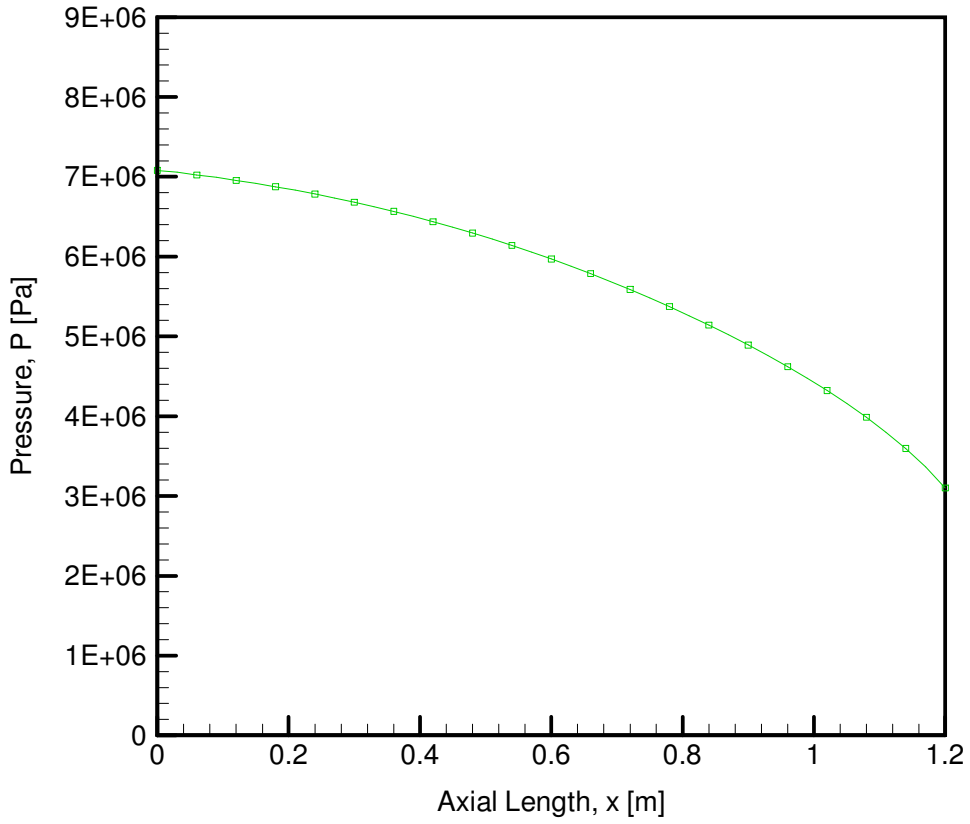

Figure 33- Pressure distribution along the axial length of the 1-D model for Run 1D-H2-I.2

Also, the density of the gaseous hydrogen decreases from its initial value of 5.805 kg/m^3 at the inlet to 0.345 kg/m^3 at the outlet of the channel. Density and pressure are directly proportional to each other through ideal gas relation; therefore increase in pressure causes density to increase as well. The distribution of density along the length of the channel is shown in Figure 34.

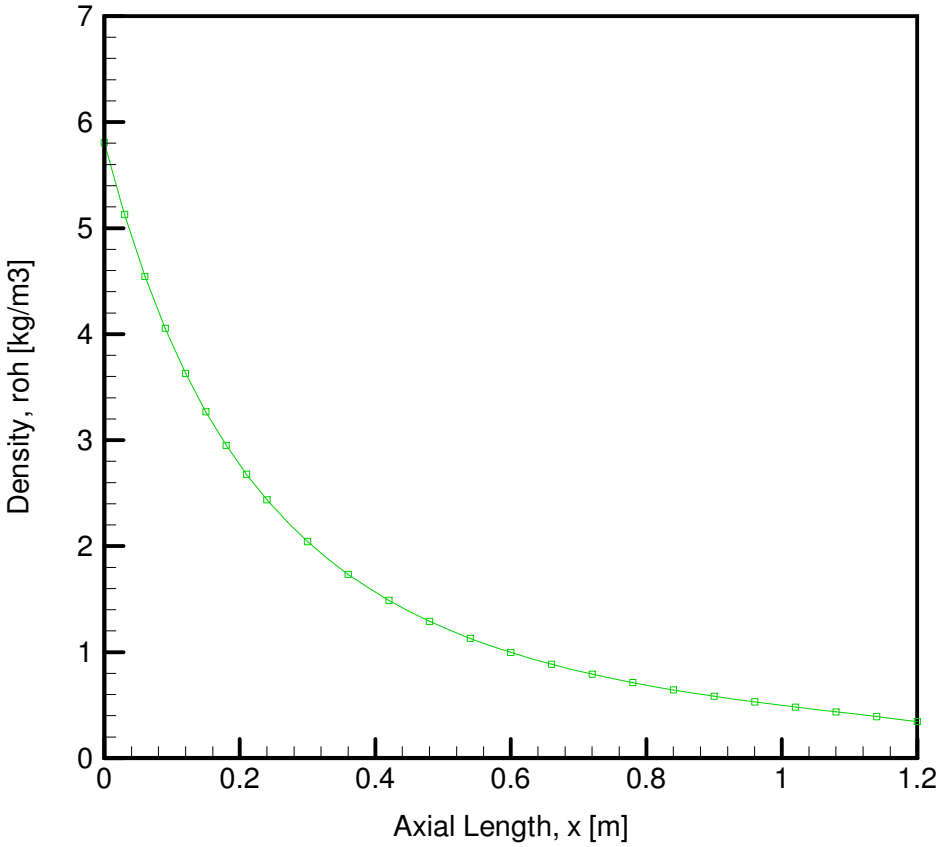

Figure 34- Density distribution along the axial length of the 1-D model for Run 1D-H2-I.2

High heat flux also results in high axial velocity of the fluid in the channel. The axial velocity increases from 169.971 m/s to 2846.333 m/s. The distribution of the axial velocity of the fluid along the length of the channel is shown in Figure 35.

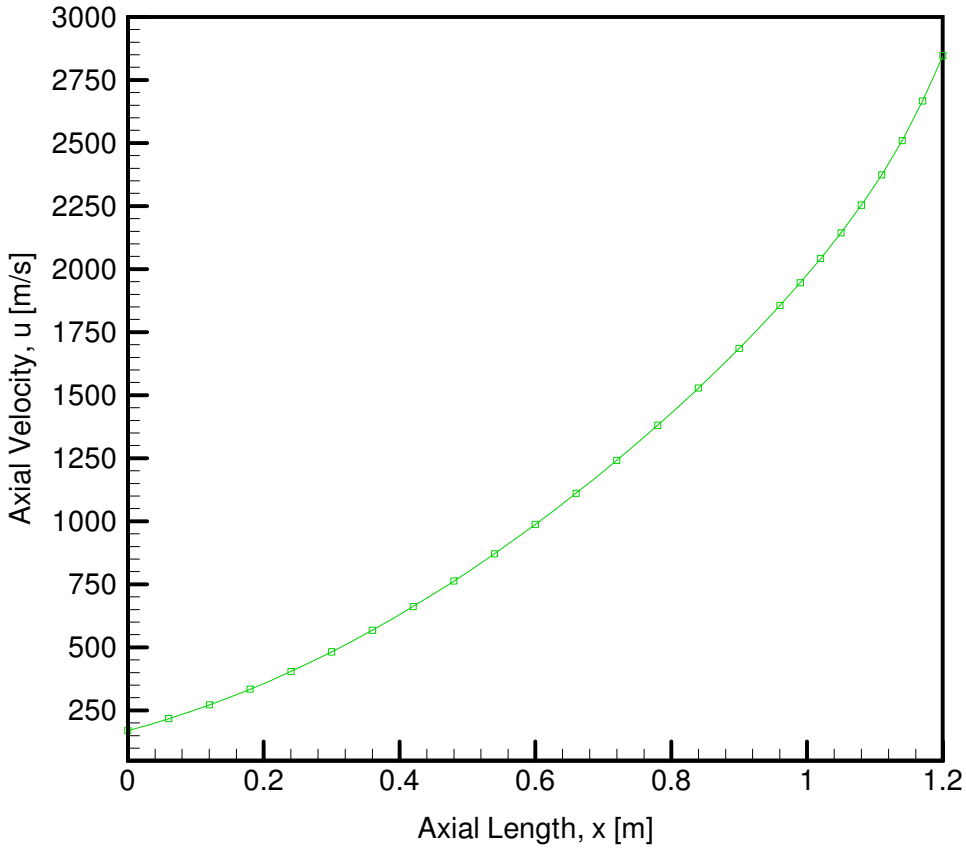

Figure 35- Axial Velocity distribution along the axial length of the 1-D model for Run 1D-H2-I.2

The 1-D model has an inlet fluid temperature of 300 K. With the non-uniform heat flux applied at the surface of the channel, the temperature of the fluid gradually increases along the length of the pipe. The maximum mean temperature of the fluid is 2253.54 K and the mean temperature of the fluid at the outlet is 2216.63 K. The mean fluid temperature distribution is shown in Figure 36.

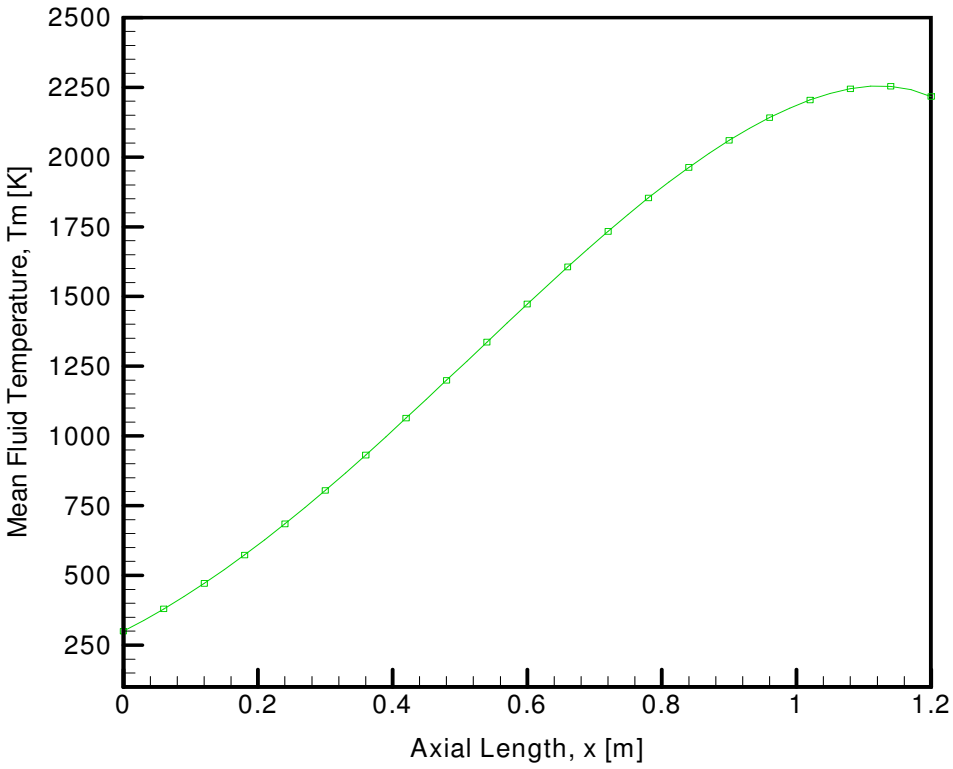

Figure 36- Mean Fluid Temperature distribution along the axial length of the 1-D model for Run 1D-H2-I.2

7.1.2 3-D One-Domain Model Study

A three-dimensional, one domain model created has a similar geometrical parameter as that of the experiment. However, the model only has a fluid domain with 5 layers in radial direction. A mesh generated has a cell size of 5 x 10^{-4} meters and has 348,400 cells in total. A heat flux distribution similar to Figure 32 is applied to the 3-D one domain model to achieve the results similar to that of the experiment. The run parameters for this study are presented in Table 39.

Table 39- Benchmark Run Parameters for 3-D One-Domain Model
[steady, compressible, viscous, turbulent, constant properties]

			Run Parameters			
Run Model	Cell size, dx [m]	Mesh Size	Inlet Mass Flow Rate, m_{dot} [kg/s]	Inlet Fluid Temperature, T_i [K]	Exit Pressure, P_e [MPa]	Heat Flux, Q_{max} [kW/m^2]
3D-H2-1DM-I.3	5x10^{-4}	348,400	0.005	300	3.1	22,000

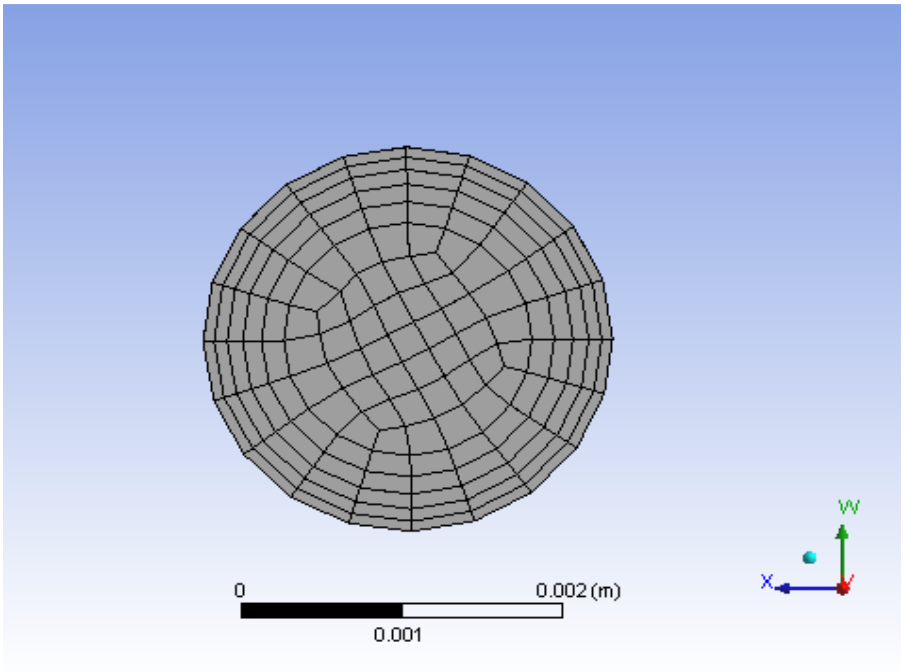

Figure 37- Cross-sectional view of the 3-D One-Domain mesh

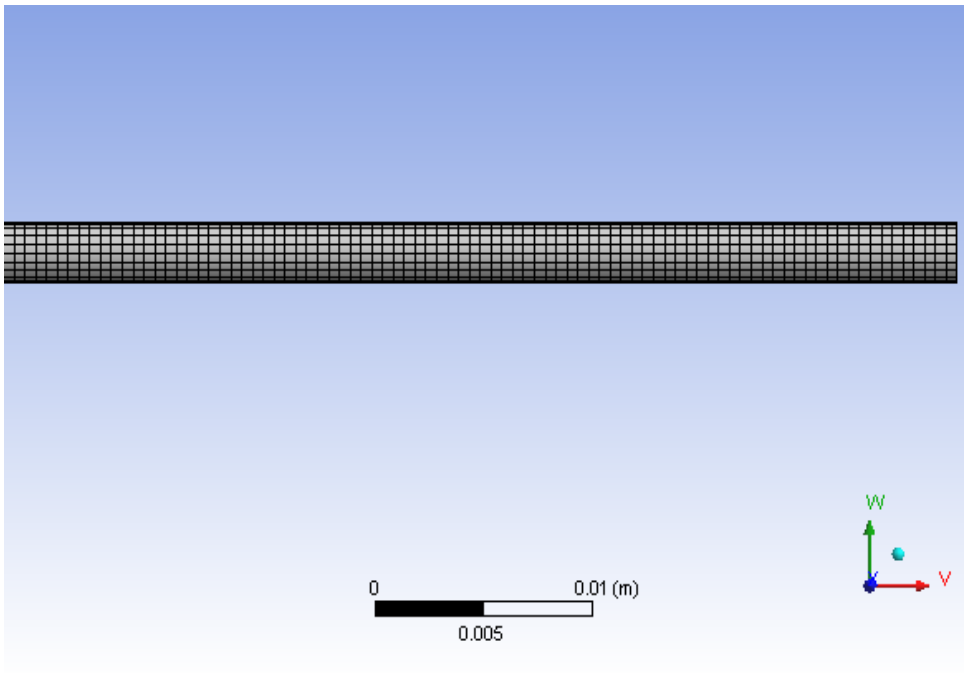

Figure 38- Axial View of the 3-D One-Domain mesh

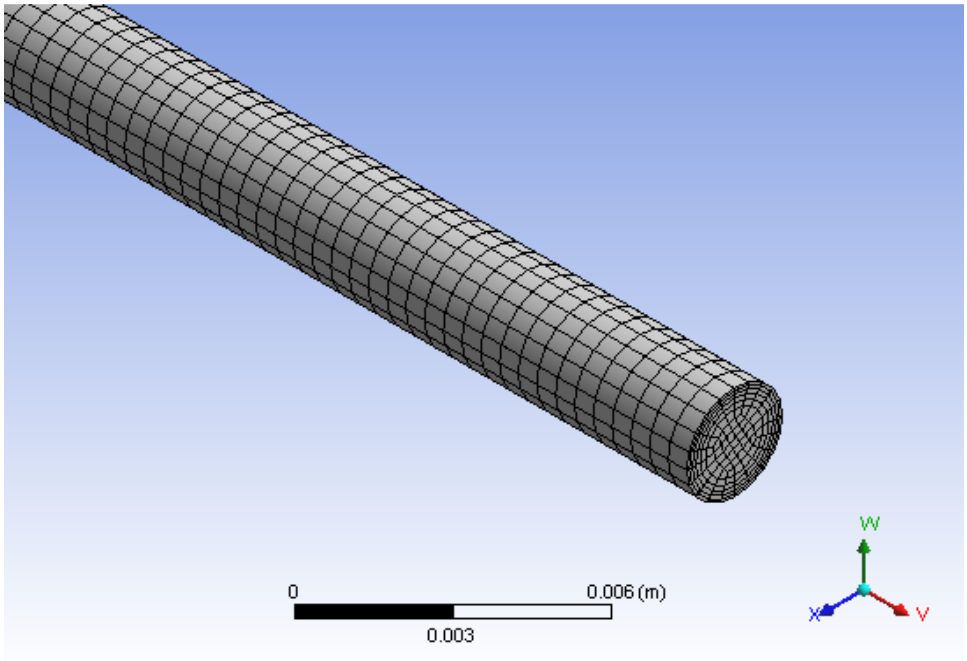

Figure 39- Isometric View of the 3-D Two-Domain mesh

In this case study, the outlet pressure of the fluid in the channel is set to 3.1 MPa and the inlet pressure is predicted through simulation of the model with the boundary and initial conditions presented in Table 38. The inlet pressure is predicted to be 8.298 MPa and it decreases along the length of the pipe to its set value of 3.1 MPa at the outlet of the pipe as shown in Figure 40.

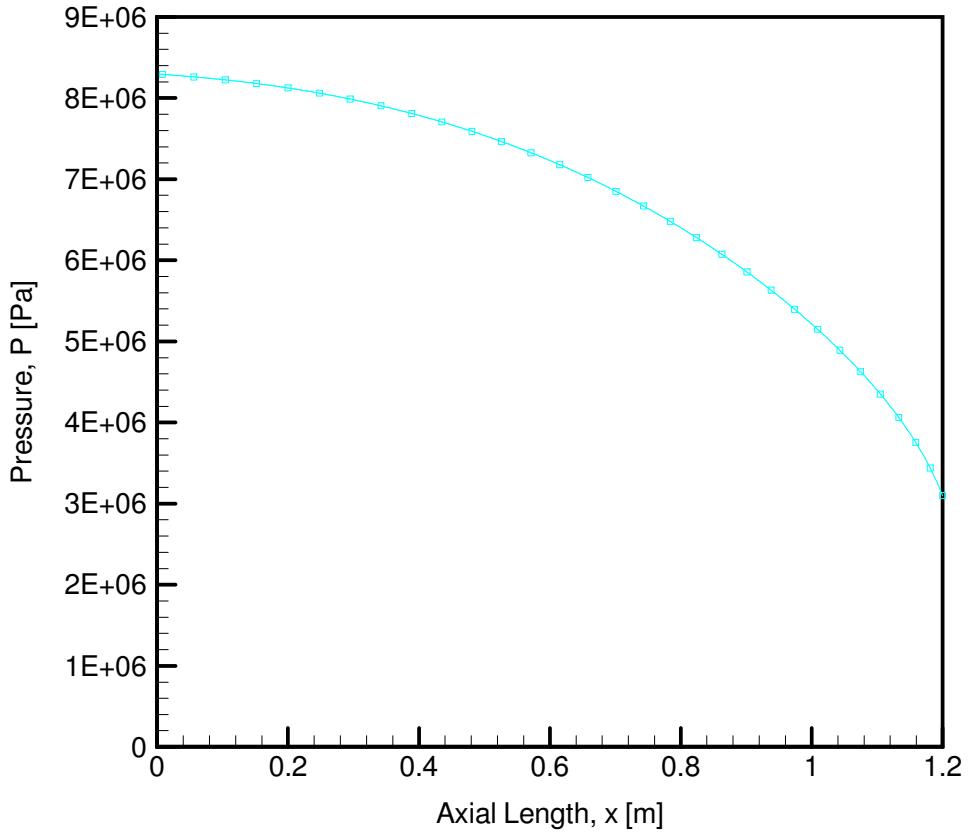

Figure 40- Pressure distribution along the axial centerline of the 3-D One-Domain model for Run 3D-H2-1DM-I.3

Also, the density of the gaseous hydrogen decreases from its initial value of 6.806 kg/m^3 at the inlet to 0.4027 kg/m^3 at the outlet of the channel. Density and pressure are directly proportional to each other through ideal gas relation; therefore increase in pressure causes

density to increase as well. The distribution of density along the length of the channel is shown in Figure 41.

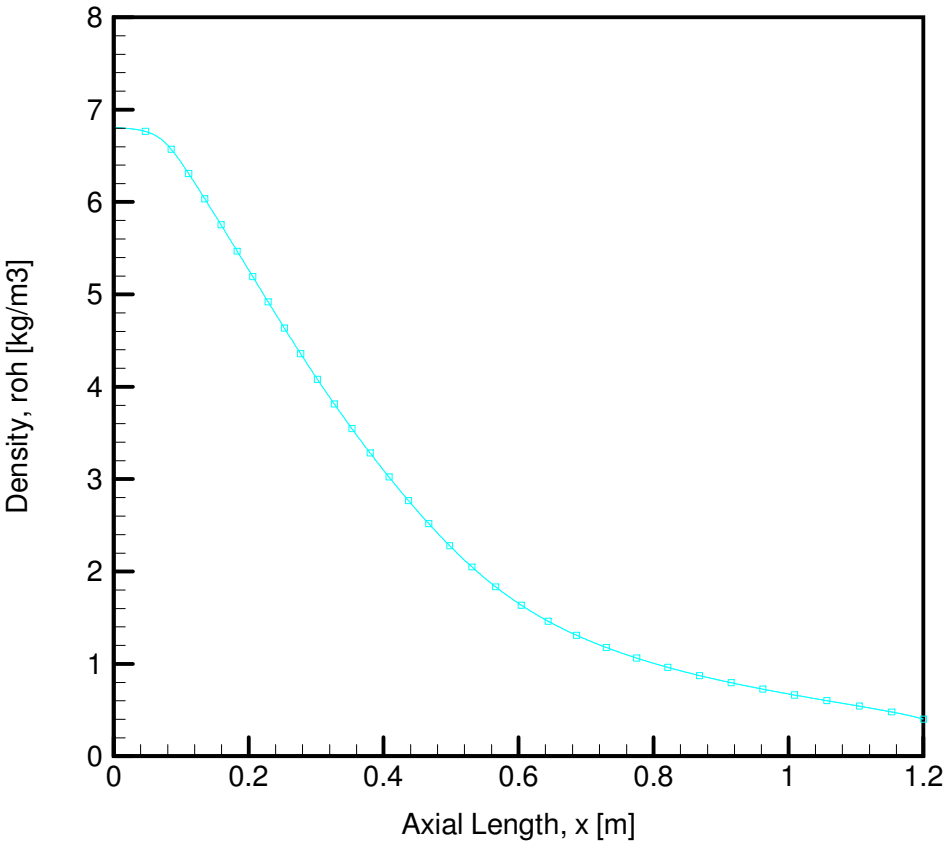

Figure 41- Density distribution along the axial centerline of the 3-D One-Domain model for Run 3D-H2-1DM-I.3

High heat flux also results in high axial velocity of the fluid in the channel. The axial velocity increases from 147.388 m/s to 2922.03 m/s. The distribution of the axial velocity of the fluid along the length of the channel is shown in Figure 42.

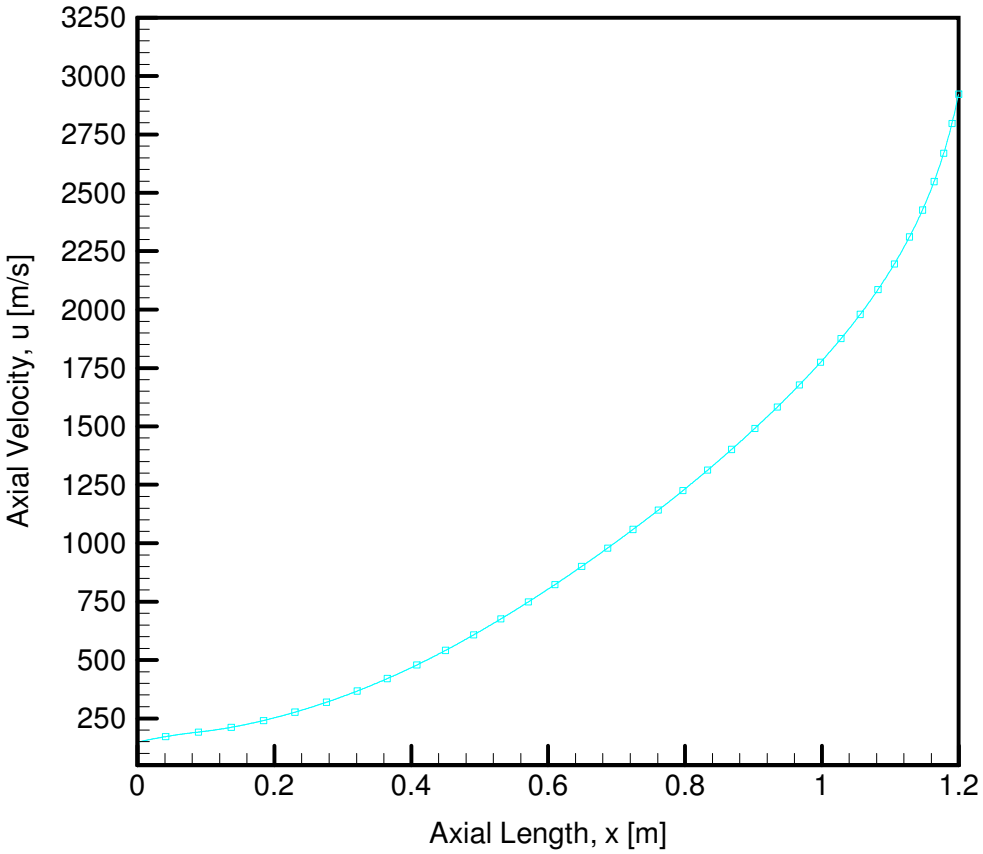

Figure 42- Velocity distribution along the axial centerline of the 3-D One-Domain model for Run 3D-H2-1DM-I.3

The 3-D, one-domain model has an inlet fluid temperature of 300 K. With the non-uniform heat flux applied at the surface of the channel, the temperature of the fluid gradually increases along the length of the pipe. The maximum temperature of the fluid at the centerline is 1993.88 K and the maximum mean fluid temperature is 2056.84 K. The centerline fluid temperature and the mean fluid temperature distributions are shown in Figure 43 and Figure 44 respectively.

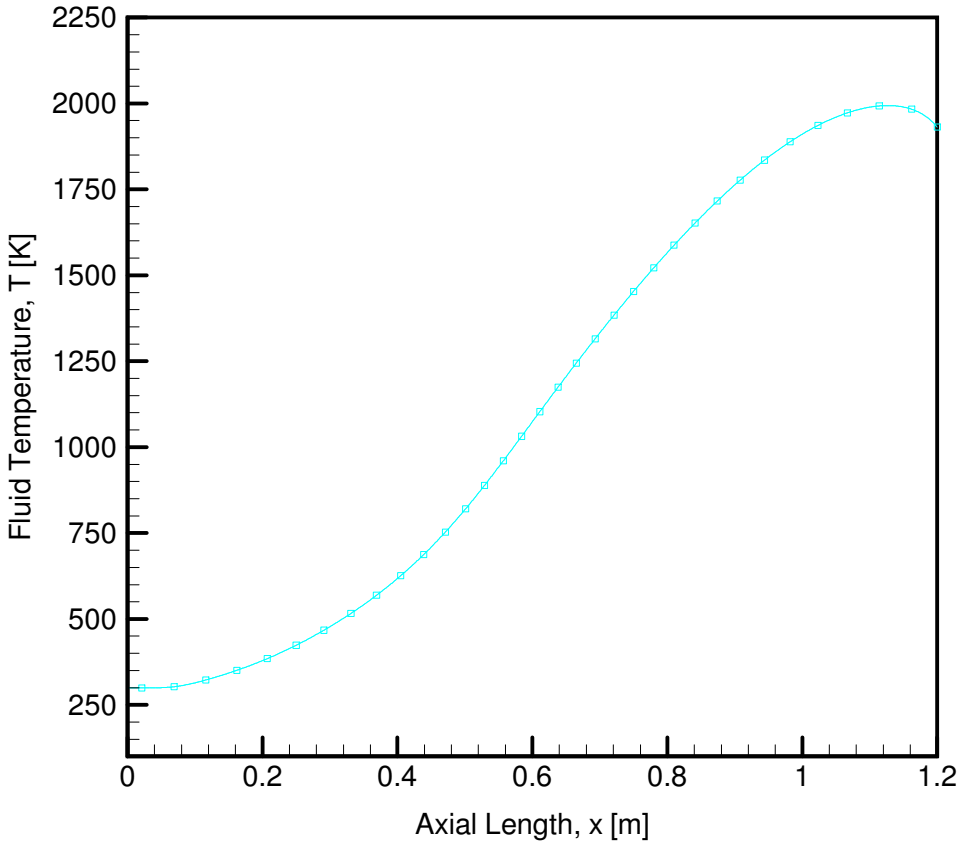

Figure 43- Fluid Temperature distribution along the axial centerline of the 3-D One-Domain model for Run 3D-H2-1DM-I.3

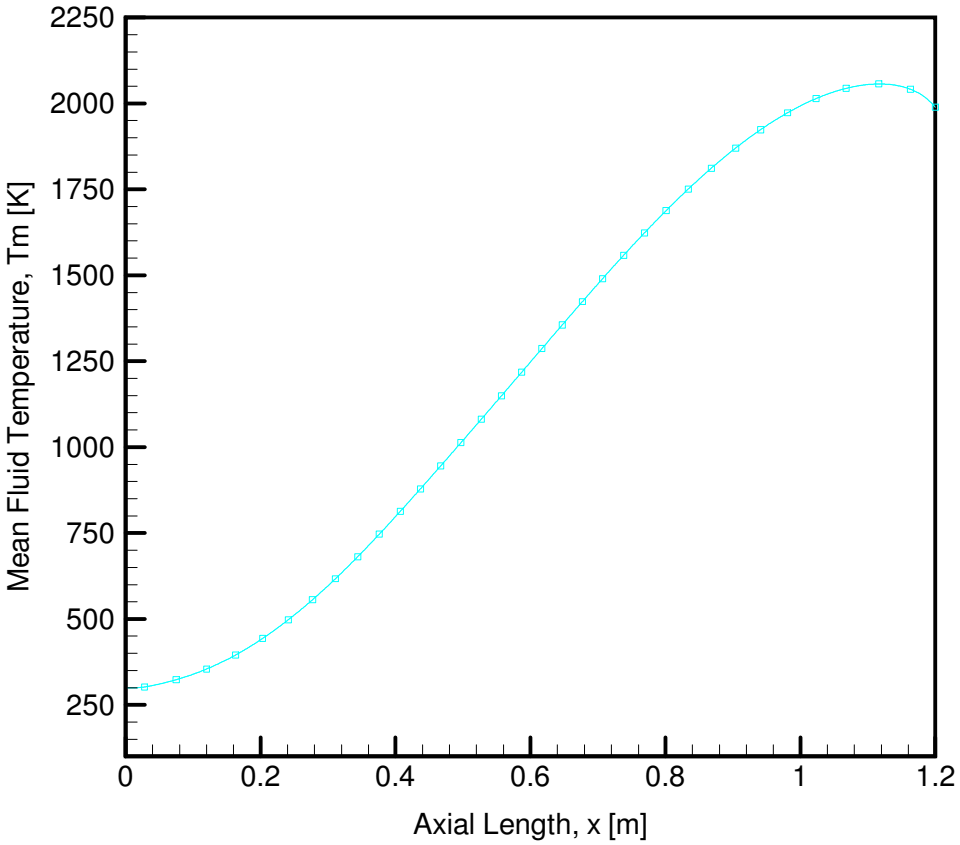

Figure 44- Mean Fluid Temperature distribution along the axial length of the 3-D One-Domain model for Run 3D-H2-1DM-I.3

7.1.3 3-D Two-Domain Model Study

The present study employs a three-dimensional, two domain model of a cylindrical pipe. It has a diameter of 0.00254 meters and thickness of 0.000125 meters. The solid domain of the metal is made of steel. The study conducted for the model uses a pressure-based and steady state time solver with a standard k-epsilon viscous model.

A three-dimensional model was created using a commercial CFD package to the exact geometrical details of the experimental model to replicate the effects of heat flux and mass flow

rate in it and compare the results. A mesh generated has a cell size of 1 x 10^{-3} meters and has 212,577 cells in total. The two-domain model has 5 layers in the fluid domain and one layer in the solid domain in radial direction.

Table 40- Benchmark Run Parameters for 3-D Two-Domain Model
[steady, compressible, viscous, turbulent, constant properties]

			Run Parameters			
Run Model	Cell size, dx [m]	Mesh Size	Inlet Mass Flow Rate, m_{dot} [kg/s]	Inlet Fluid Temperature, T_i [K]	Exit Pressure, P_e [MPa]	Heat Flux, Q_{max} [kW/m^2]
3D-H2-2DM-I.3	$1x10^{-3}$	212,577	0.005	300	3.1	22,000

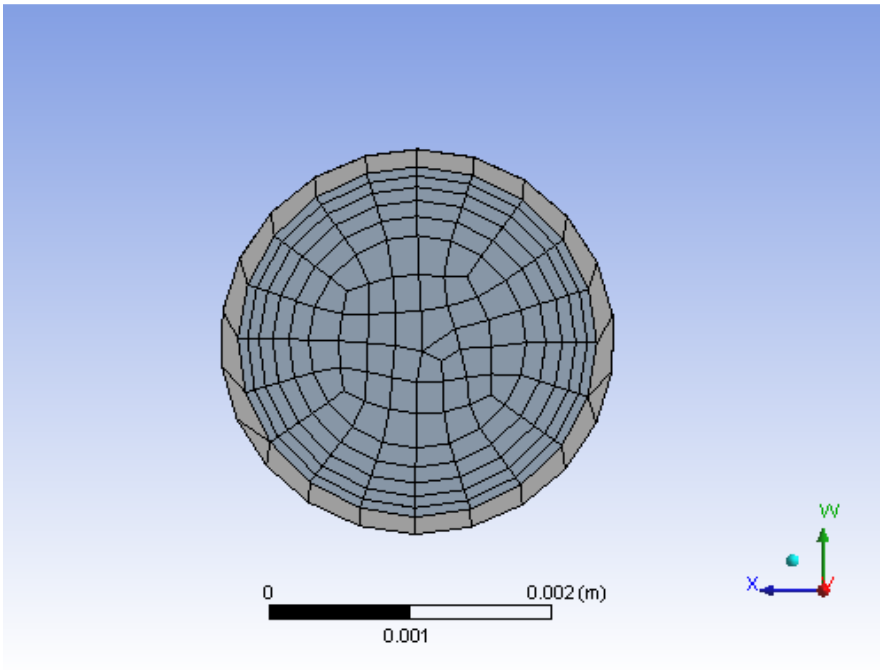

Figure 45- Cross-sectional view of the 3-D Two-Domain mesh

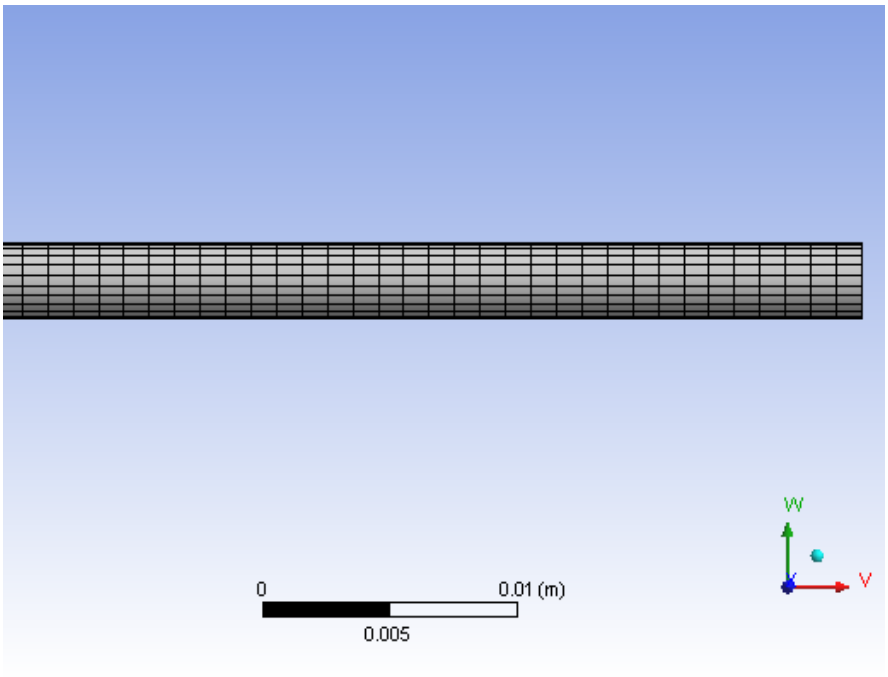

Figure 46- Axial View of the 3-D Two-Domain mesh

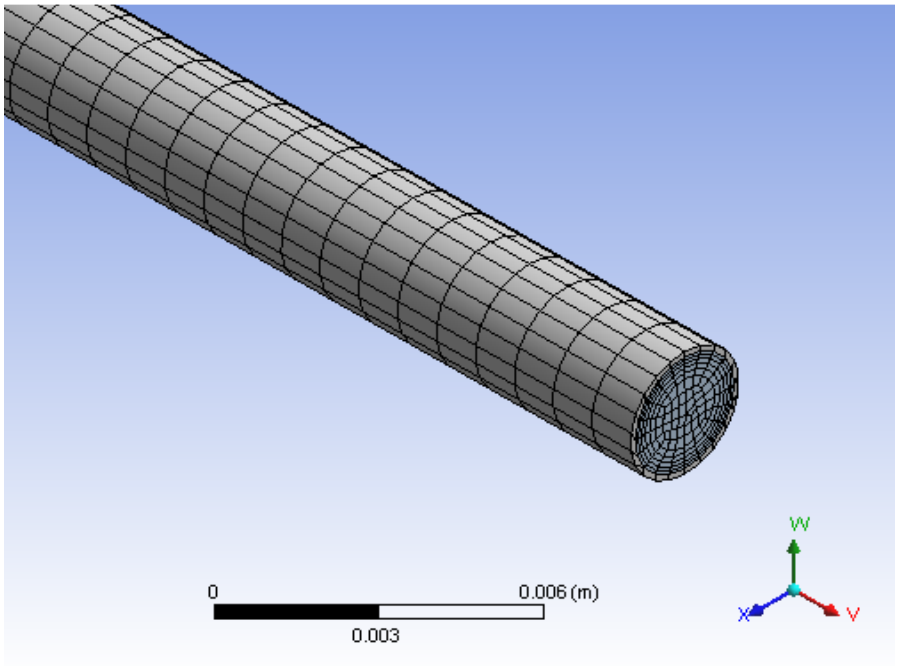

Figure 47- Isometric View of the 3-D Two-Domain mesh

The outlet pressure of the fluid in the channel is set to 3.1 MPa and the inlet pressure is predicted through simulation of the model with the boundary and initial conditions above. The inlet pressure is calculated to be 8.762 MPa and it decreases along the length of the pipe from its predicted value to 3.1 MPa at the outlet of the pipe as shown in Figure 48.

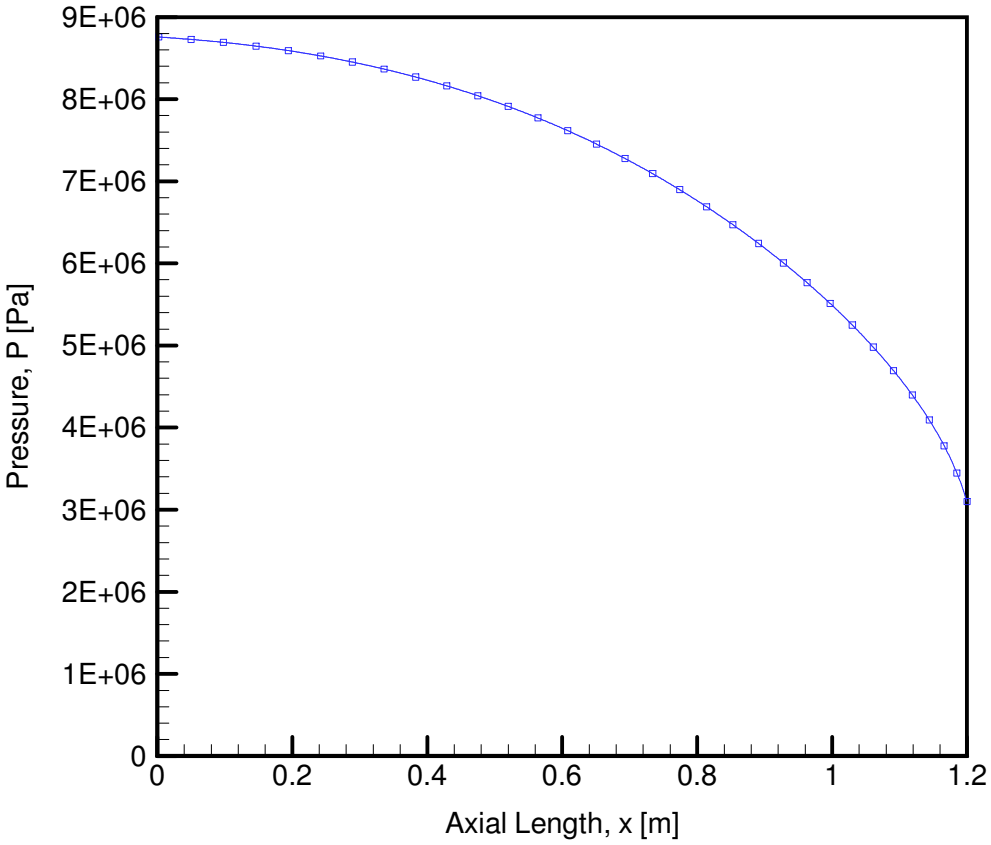

Figure 48- Pressure distribution along the axial centerline of the 3-D Two-Domain model for Run 3D-H2-2DM-I.3

Similarly, the density of the gaseous hydrogen also decreases from its initial value of 7.179 kg/m^3 at the inlet to 0.362 kg/m^3 at the outlet of the channel. Density and pressure are directly proportional to each other through ideal gas relation; therefore increase in pressure

causes density to increase as well. The distribution of density along the length of the channel is shown in Figure 49.

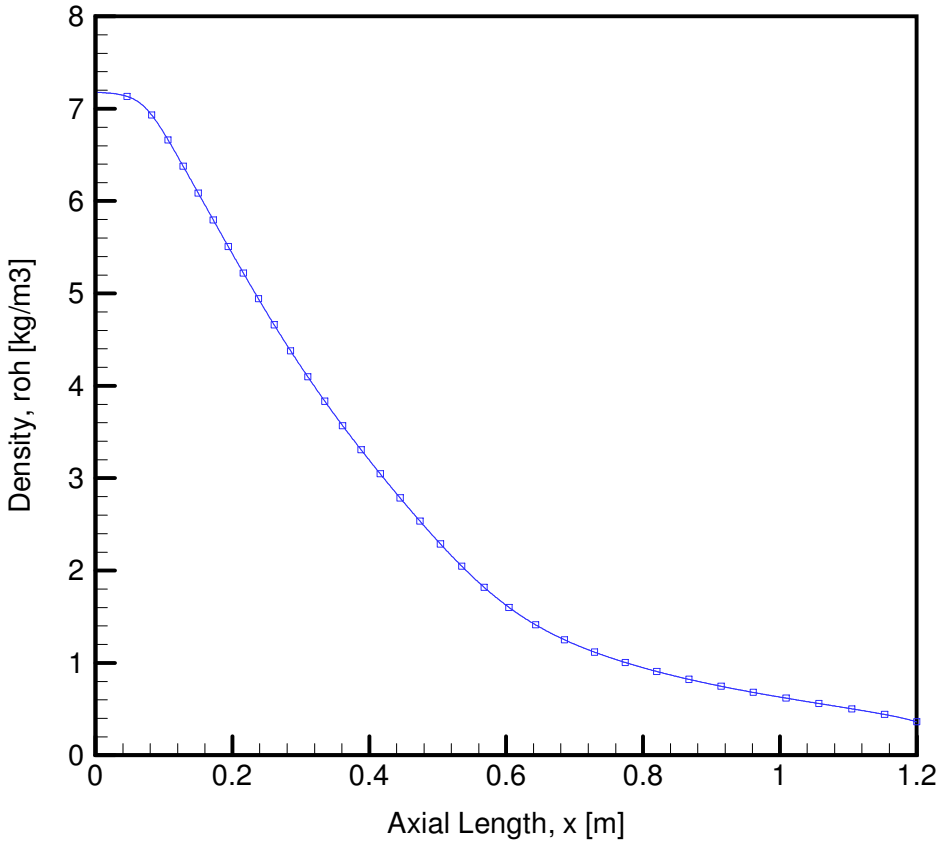

Figure 49- Density distribution along the axial centerline of the 3-D Two-Domain model for Run 3D-H2-2DM-I.3

High heat flux also results in high axial velocity of the fluid in the channel. The axial velocity increases from 139.74 m/s to 3239.25 m/s. The distribution of the axial velocity of the fluid along the length of the channel is shown in Figure 50.

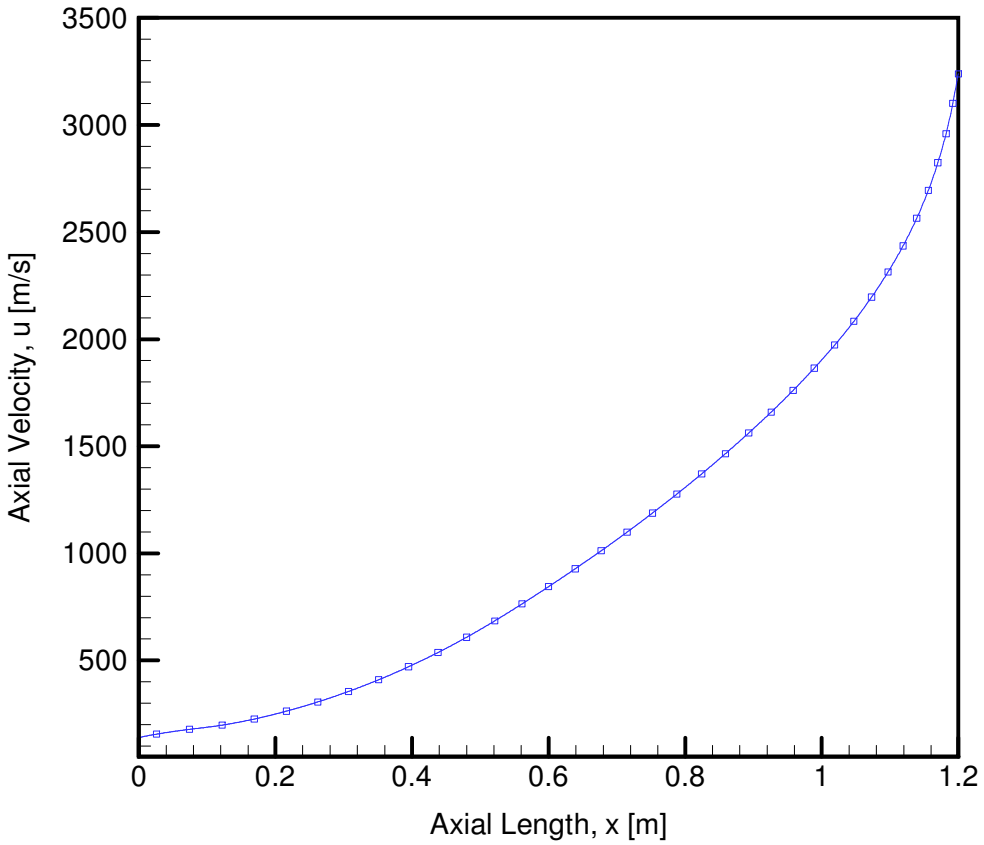

Figure 50- Velocity distribution along the axial centerline of the 3-D Two-Domain model for Run 3D-H2-2DM-I.3

The 3-D Two-Domain model has an inlet fluid temperature of 300 K. With the non-uniform heat flux applied at the surface of the channel, the temperature of the fluid gradually increases along the length of the pipe. The maximum mean fluid temperature is 2313.49 K at 1.1 meters and the mean temperature of the fluid at the outlet is 2213.71 K. The distribution of the mean fluid temperature of the fluid along the length of the channel is shown in Figure 51.

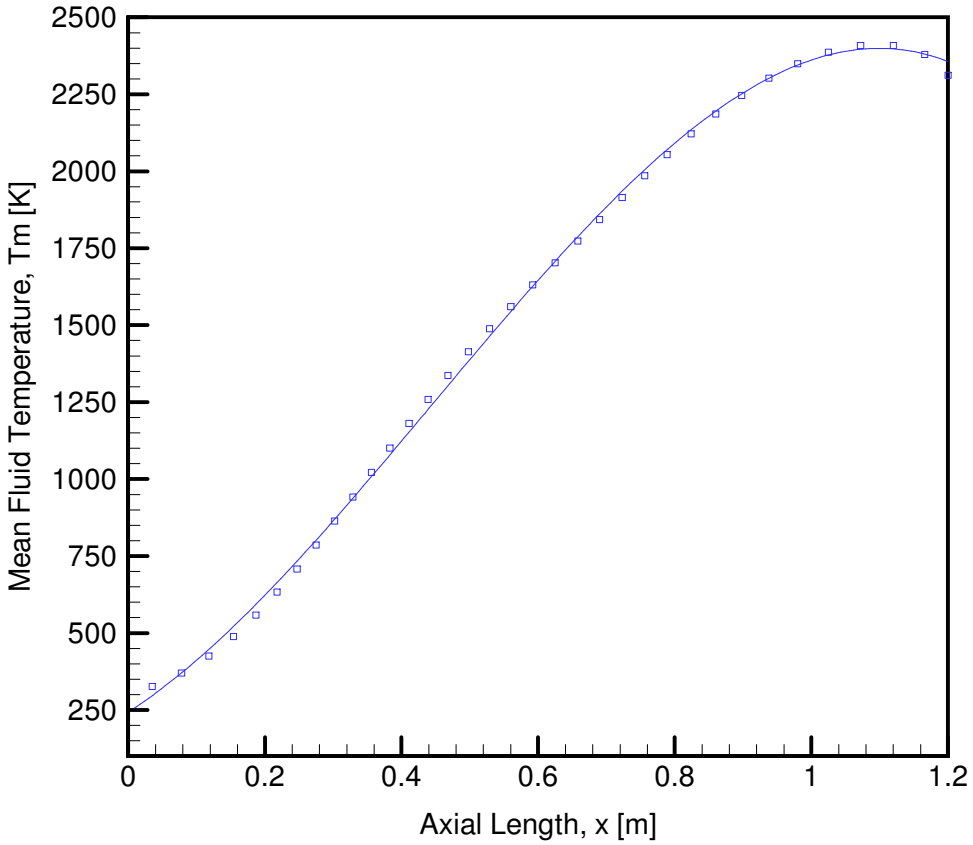

Figure 51- Temperature distribution along the axial centerline of the 3-D Two-Domain model for Run 3D-H2-2DM-I.3

The 3-D Two-Domain model has different temperature distribution between the inner wall and the outer wall of the cooling channel due to the thickness. The wall temperatures are much higher as compared to the temperature of the fluid flowing inside. The outer wall and the inner wall have a maximum temperature of 2653.06 K and 2525.01 K respectively. The outer wall and the inner wall temperature converge at the outlet of the cooling channel at around 2386 K. The comparison of wall temperature distribution between the inner and the outer wall is shown in Figure 52.

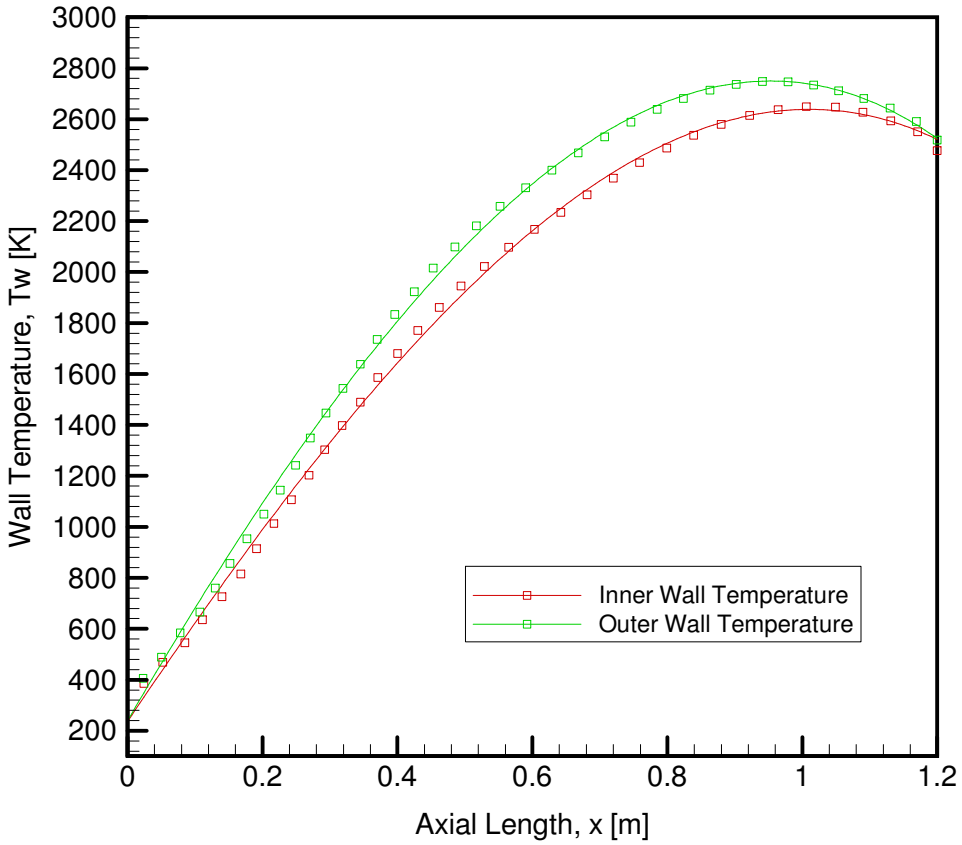

Figure 52- Temperature distribution along the axial length of the 3-D Two-Domain model for the inner and outer walls for Run 3D-H2-2DM-I.3

The temperature profile at the outlet of the pipe is shown in Figure 53. The outer-wall temperature of the pipe is 2424.90 K and the inner-wall temperature is 2386 K. The centerline temperature is 2075.96 K. Similarly, the velocity profile at the outlet of the pipe is shown in Figure 54. Since, the pipe has no moving boundary and no slip conditions the velocity at the interface is zero. The maximum velocity of the fluid at the outlet is at the centerline of the pipe and has a magnitude of 3135.67 m/s.

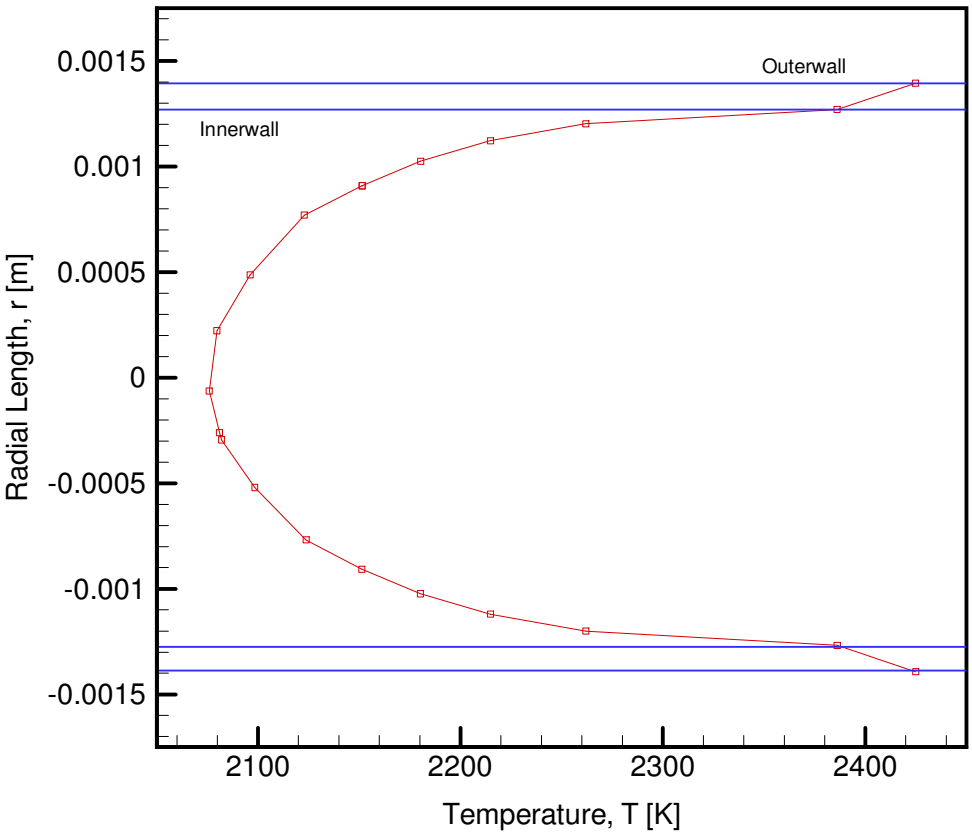

Figure 53- Fluid Temperature profile at the outlet of 3-D Two-Domain model for Run 3D-H2-2DM-I.3

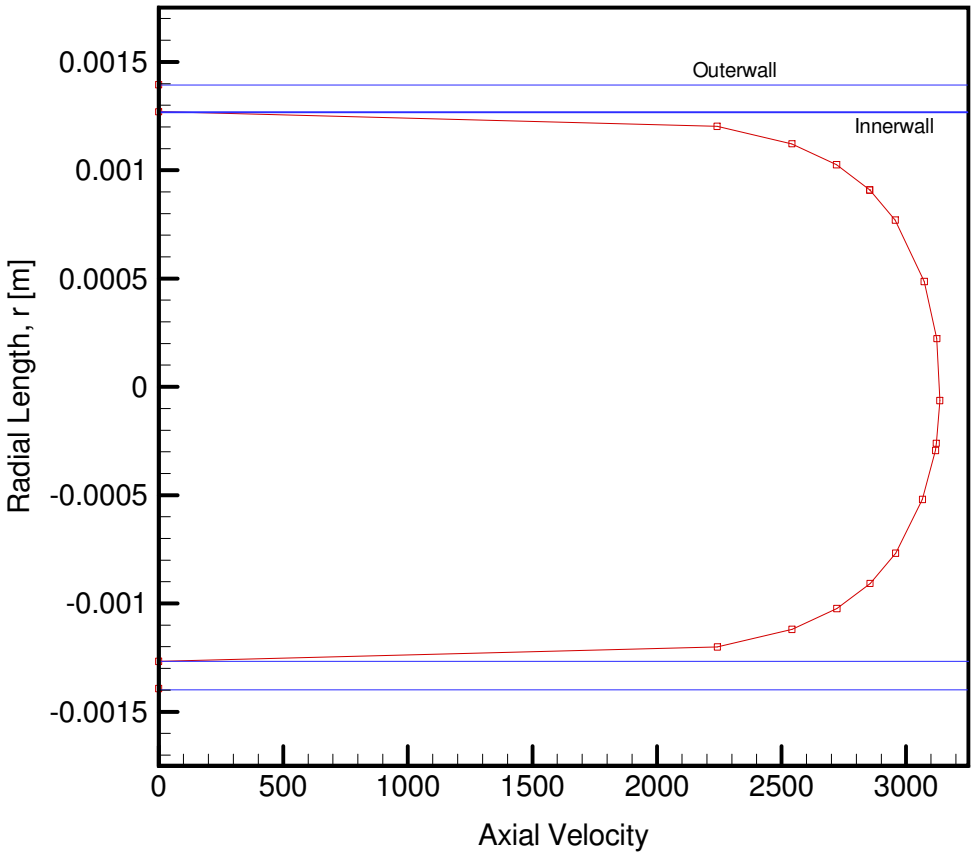

Figure 54- Axial Velocity profile at the outlet of 3-D Two-Domain model for Run 3D-H2-2DM-I.3

Also, temperature and velocity contours for the gaseous hydrogen gas flowing in the cooling channel are shown in Figure 55 and Figure 58 respectively.

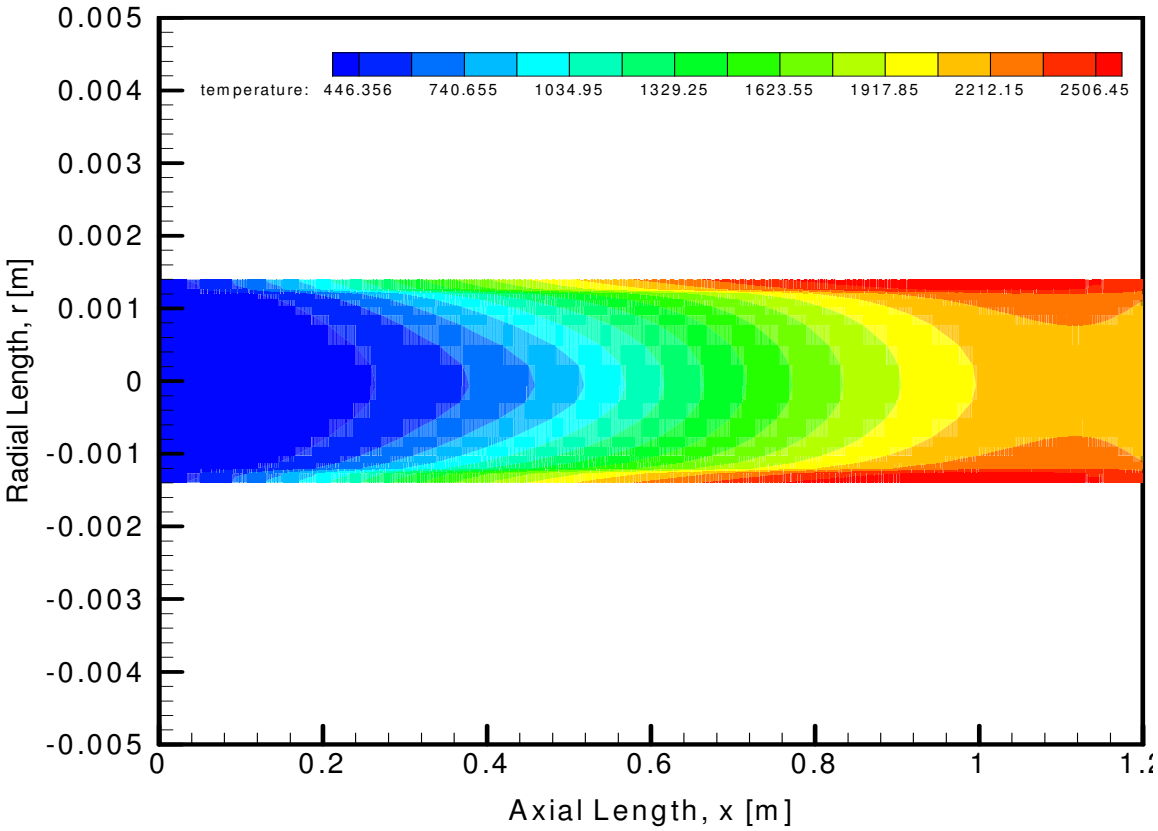

Figure 55- Fluid Temperature Contour for along the axial length of the 3-D Two-Domain model for Run 3D-H2-2DM-I.3

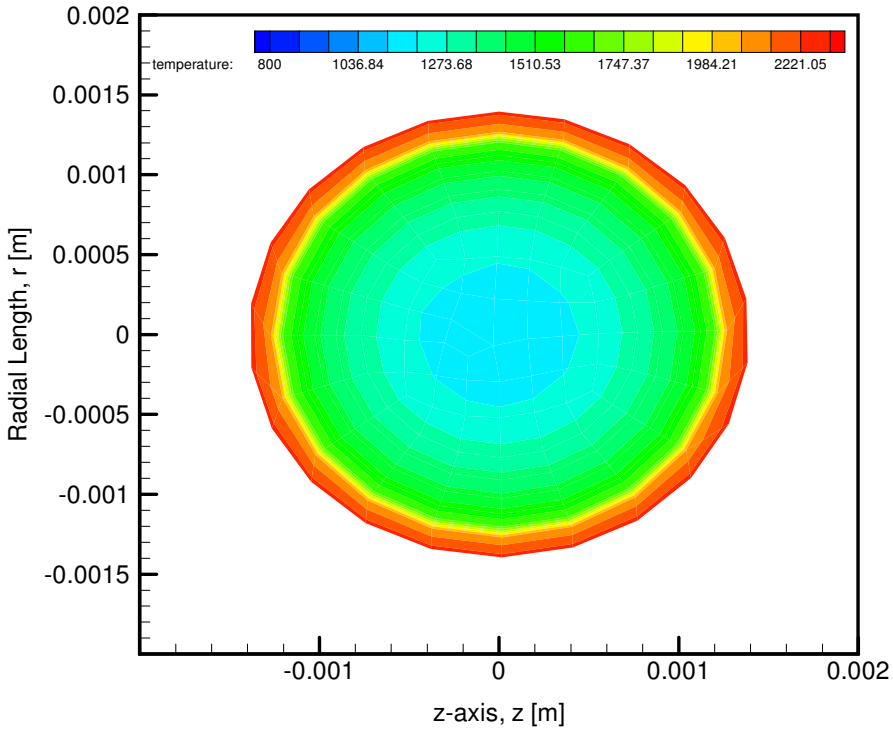

Figure 56 - Cross-sectional view of the Fluid Temperature Contour at the center of the 3-D Two-Domain model for Run 3D-H2-2DM-I.3

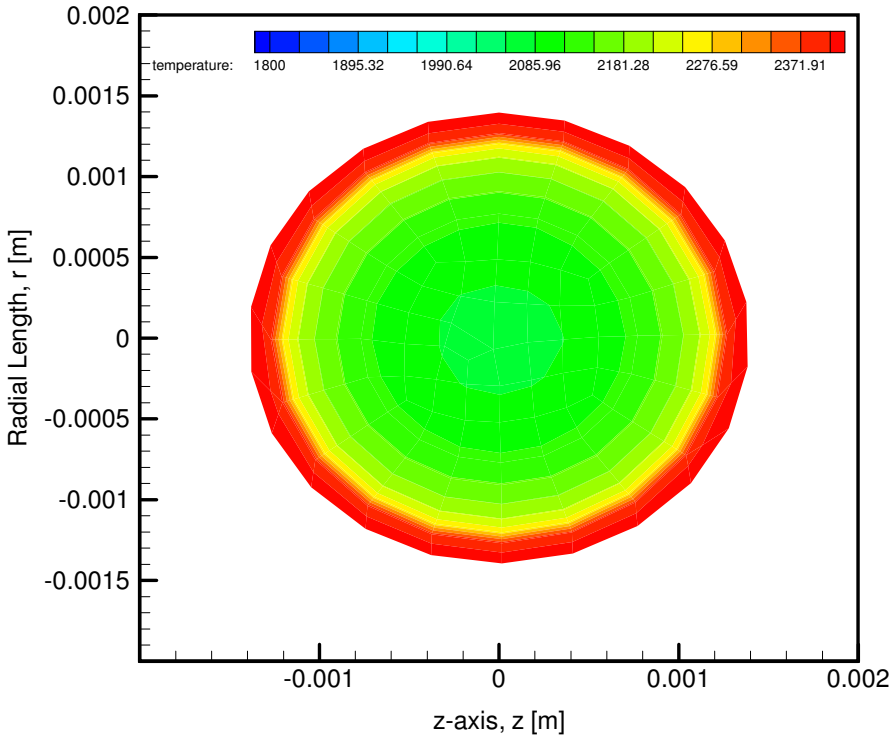

Figure 57- Cross-sectional view of the Fluid Temperature Contour at the exit of the 3-D Two-Domain model for Run 3D-H2-2DM-I.3

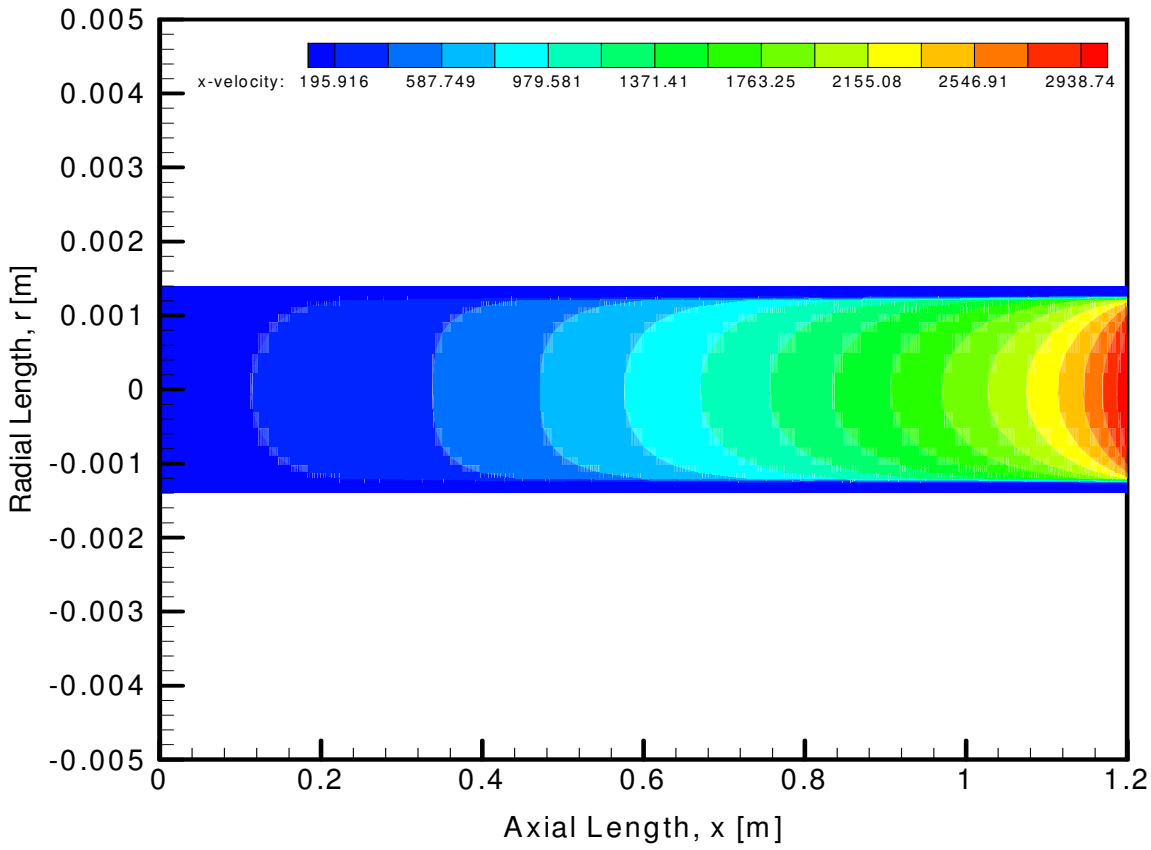

Figure 58- Axial Velocity Contour along the axial length of the 3-D Two-Domain model for Run 3D-H2-2DM-I.3

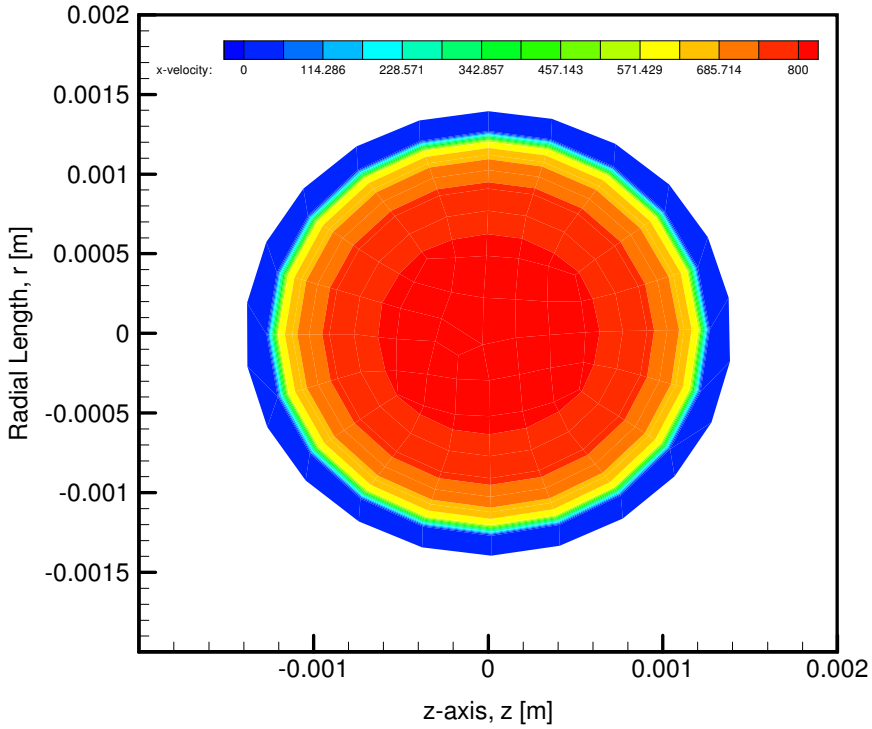

Figure 59- Cross-sectional view of the Axial Velocity Contour at the center of the 3-D Two-Domain model for Run 3D-H2-2DM-I.3

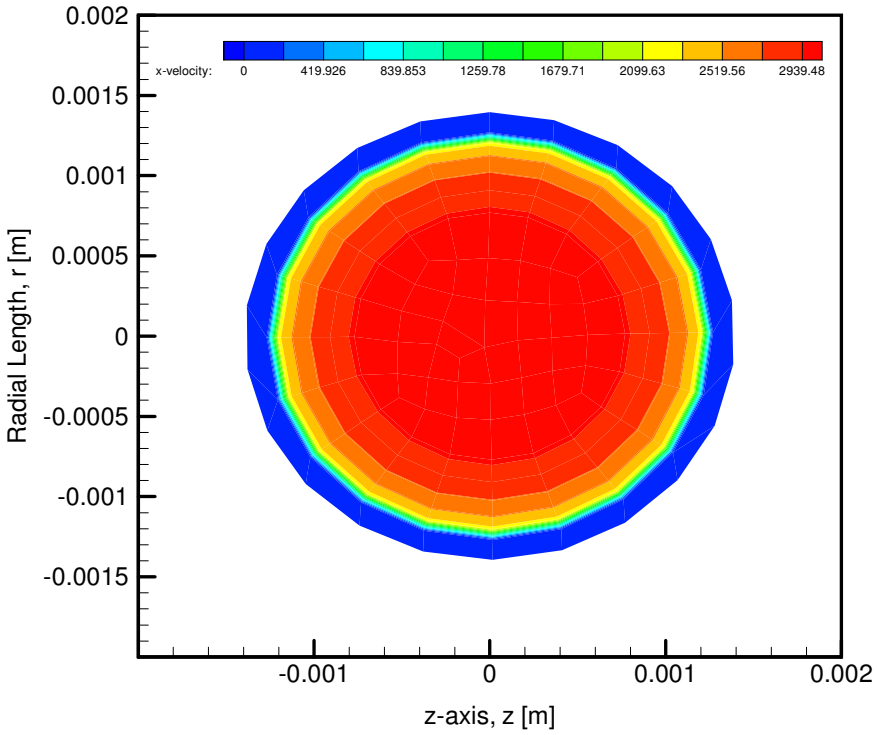

Figure 60- Cross-sectional view of the Axial Velocity Contour at the exit of the 3-D Two-Domain model for Run 3D-H2-2DM-I.3

7.2 Comparison of Results

7.2.1 Comparison of the 1-D Model with the 3-D One-Domain Model

Distributions of pressure, density, velocity and temperature for one-dimensional model and the 3-D one-domain model are conducted through Figure 61 through Figure 64. Both the models have similar initial conditions and same amount of non-uniform heat flux applied to them. In Figure 61, the inlet pressure for the 3-D one-domain model is 8.30 MPa which is higher compared to the one-dimensional model's inlet pressure of 7.08 MPa. The quantitative comparison of the pressure distribution is shown in Table 41.

Table 41- Pressure distribution along the axial length of the 1-Dimensional and 3-D One-Domain model for benchmark case

Axial Distance, x [m]	Pressure, P [MPa] One-Dimensional Model	Pressure, P [MPa] 3-D One-Domain Model	Pressure Difference, ∆P [MPa]	% Deviation
0	7.079	8.30	1.221	0.147108
0.1	6.99	8.22	1.23	0.149635
0.2	6.83	8.12	1.29	0.158867
0.3	6.68	7.98	1.3	0.162907
0.4	6.50	7.78	1.28	0.164524
0.5	6.21	7.54	1.33	0.176393
0.6	5.97	7.23	1.26	0.174274
0.7	5.68	6.85	1.17	0.170803
0.8	5.26	6.40	1.14	0.178125
0.9	4.89	5.86	0.97	0.165529
1.0	4.32	5.21	0.89	0.170825
1.1	3.79	4.40	0.61	0.138636
1.2	3.1	3.1	0	0

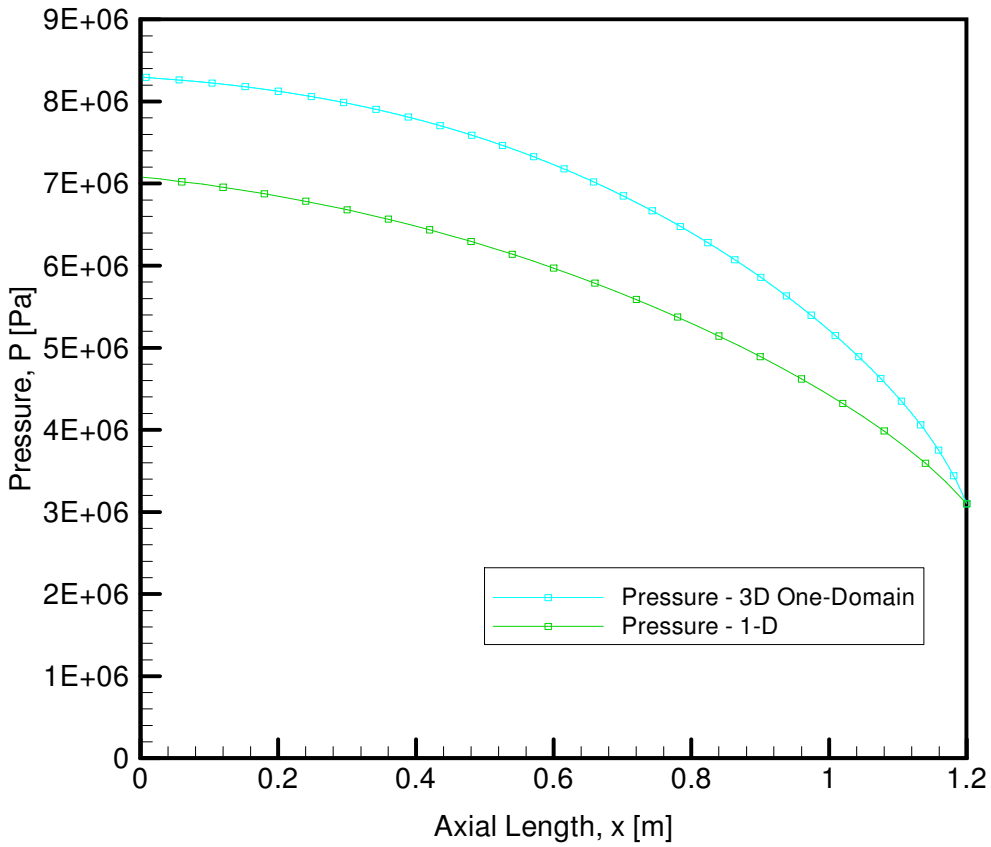

Figure 61- Comparison of Pressure distribution along the axial length of the 1-Dimensional and 3-D One-Domain model for benchmark case

Similarly, the density of the fluid is also higher in case of the 3D model compared to that of the one-dimensional model as shown in Figure 62. The 3-D one-domain model has an inlet density of 6.807 kg/m^3 whereas the one-dimensional model has 5.80 kg/m^3. The comparison of density distribution between the one-dimensional and the 3D model is given in Table 42.

Table 42- Density distribution along the axial length of the 1-Dimensional and 3-D One-Domain model for benchmark case

Axial Distance, x [m]	Density, ρ [kg/m^3] One-Dimensional Model	Density, ρ [kg/m^3] 3-D One-Domain Model	Density Difference, Δ ρ [kg/m^3]	% Deviation
0	5.805	6.807	1.002	0.147201
0.1	4.054	6.426	2.372	0.369125
0.2	2.677	5.260	2.583	0.491065
0.3	2.042	4.096	2.054	0.501465
0.4	1.604	3.091	1.487	0.481074
0.5	1.206	2.260	1.054	0.466372
0.6	0.997	1.653	0.656	0.396854
0.7	0.837	1.264	0.427	0.337816
0.8	0.677	1.006	0.329	0.327038
0.9	0.584	0.819	0.235	0.286935
1.0	0.506	0.674	0.168	0.249258
1.1	0.414	0.548	0.134	0.244526
1.2	0.345	0.402	0.057	0.141791

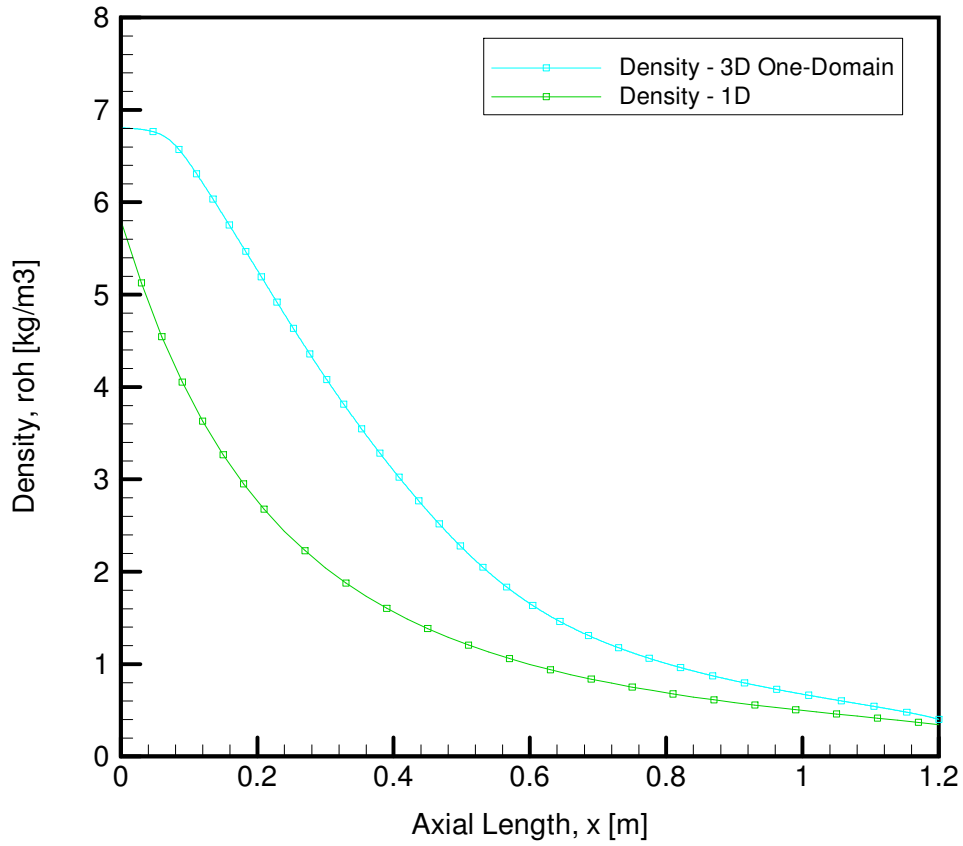

Figure 62- Comparison of Density distribution along the axial length of the 1-Dimensional and 3-D One-Domain model for benchmark case

The inlet axial velocity for both one-dimensional and the 3D model is 300 m/s. However, the 3-D one-domain model has an axial velocity 2921.21 m/s at the outlet and the one-dimensional model has an outlet axial velocity of 2846.60 m/s as shown in Figure 63. The quantitative comparison of velocity distribution between the one-dimensional and the 3D model is shown in Table 43.

Table 43- Axial Velocity distribution along the axial length of the 1-Dimensional and 3-D One-Domain model for benchmark case

Axial Distance, x [m]	Axial Velocity, u [m/s] One-Dimensional Model	Axial Velocity, u [m/s] 3-D One-Domain Model	Axial Velocity Difference, Δu [m/s]	% Deviation
0	169.97	147.36	22.61	0.153434
0.1	242.72	195.32	47.4	0.242679
0.2	367.74	252.54	115.2	0.456165
0.3	481.99	343.88	138.11	0.401623
0.4	613.72	467.13	146.59	0.31381
0.5	816.053	621.94	194.113	0.312109
0.6	987.33	803.19	184.14	0.229261
0.7	1175.24	1005.99	169.25	0.168242
0.8	1453.029	1231.64	221.389	0.179751
0.9	1685.29	1484.61	200.68	0.135174
1.0	1945.92	1779.53	166.39	0.093502
1.1	2373.92	2164.7	209.22	0.096651
1.2	2846.33	2921.21	74.88	0.025633

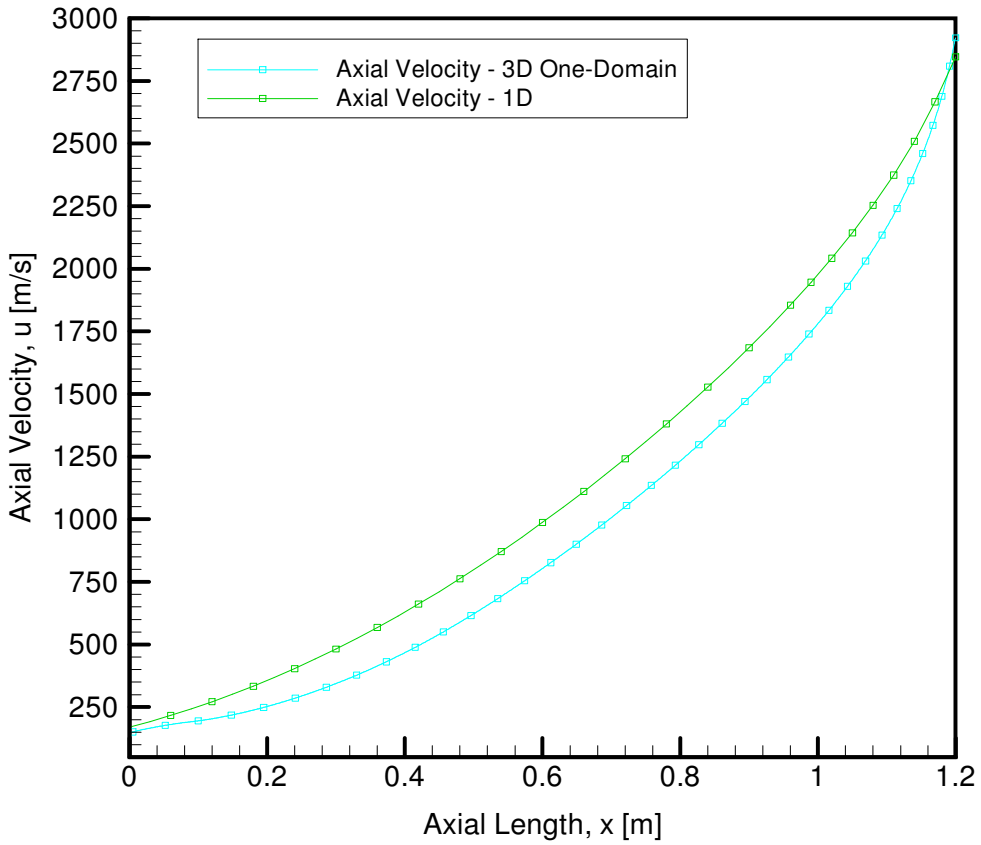

Figure 63- Comparison of the Axial Velocity distribution along the axial length of the 1-Dimensional and 3-D One-Domain model for benchmark case

Finally, the mean fluid temperature distribution between the one-dimensional model and the 3D model is shown in Figure 64. Both the models have an inlet fluid temperature of 300 K. With the non-uniform heat flux applied at the surface of the channel, the temperature of the fluid gradually increases along the length of the pipe. The maximum temperature of the fluid for one-dimensional and the 3-D one-domain model are 2253.74 K and 2056.84 K respectively. The mean fluid temperature at the outlet for the one-dimensional model is 2216.63 K and that for the base model is 1989.1 K. The quantitative values of temperature along the length of the channel for both one-dimensional and 3D model are shown in Table 44.

Table 44- Fluid Temperature distribution along the axial length of the 1-Dimensional and 3-D One-Domain model for benchmark case

Axial Distance, x [m]	Temperature, T_m [K] One-Dimensional Model	Temperature, T_m [K] 3-D One-Domain Model	Temperature Difference, ΔT [K]	% Deviation
0	300	299.23	0.77	0.002573
0.1	424.28	339.21	85.07	0.250789
0.2	627.74	439.40	188.34	0.42863
0.3	804.59	596.87	207.72	0.348015
0.4	997.14	797.92	199.22	0.249674
0.5	1267.99	1019.87	248.12	0.243286
0.6	1472.75	1247.82	224.93	0.180258
0.7	1670.51	1474.98	195.53	0.132565
0.8	1909.62	1686.11	223.51	0.13256
0.9	2059.94	1863.96	195.98	0.105142
1.0	2175.51	1992.95	182.56	0.091603
1.1	2253.41	2055.13	198.28	0.096481
1.2	2216.63	1989.1	227.53	0.114388

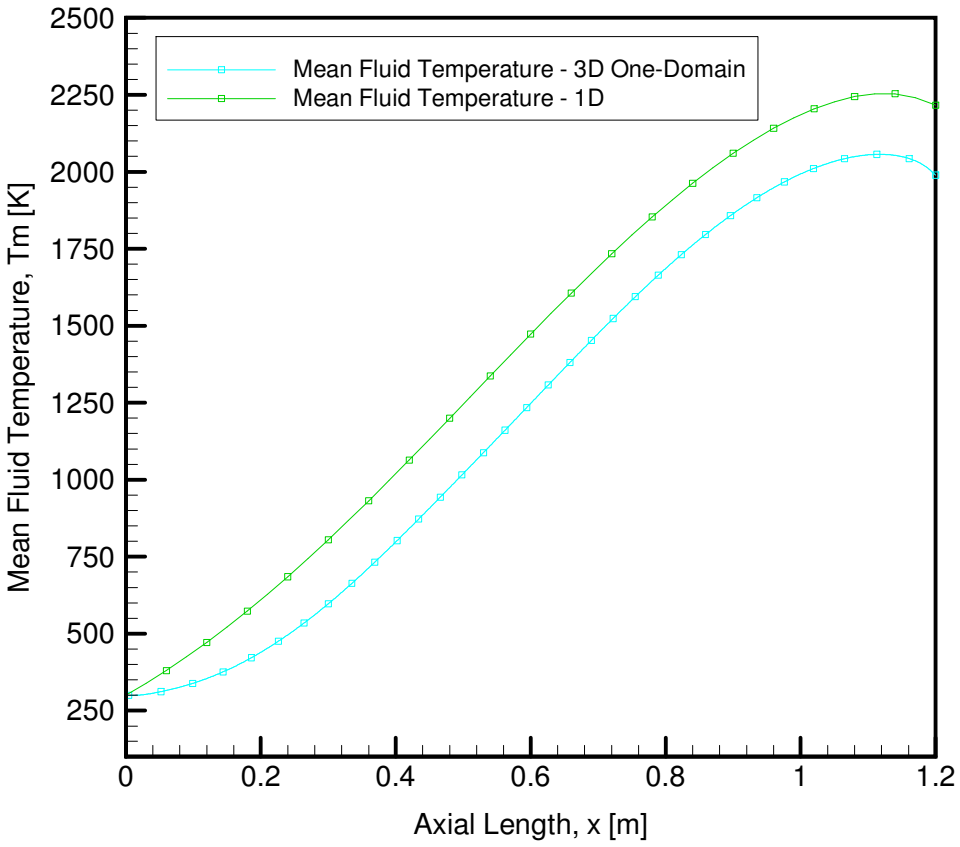

Figure 64- Comparison of the Mean Fluid Temperature distribution along the axial length of the 1-Dimensional and 3-D One-Domain model for benchmark case

7.2.2 Comparison of 3-D Two Domain Model to the Experimental Results

A comparative study between the experimental model and 3-D Two-Domain model is conducted in this study. The 3-D two-domain model is simulated with the benchmark initial and boundary conditions (Table 40) to achieve maximum accuracy with the experimental results. Mean fluid temperature and wall temperatures are compared between the two models. Temperatures at the outlet for both the models are shown in Table 45.

Table 45- Comparison of results between 3-D Two-Domain model and the Experiment

		Results			
Run No.	Models	Inlet Pressure, P_i [MPa]	Exit Wall Temperature, T_w [K]	Mean Outlet Fluid Temperature, T_e [K]	Outlet Velocity, u_e [m/s]
Experiment	-	-	2500	2450	-
3D-H2-2DM-I.3	Mesh size: 212,577	8.50	2425	2200	3150

Table 46 presents the quantitative distribution of mean fluid temperature along the axial length of the channel in the experimental and the base model. Both the models have almost identical inlet temperatures with the experimental value at 300 K and the base model value at 299.31 K. The mean fluid temperatures in both the model gradually increases along the length of the channel. Both the models reach their respective maximum temperature at 1.1 meters of the channel. At this point, the experimental model reaches 2425 K and the base model is at 2312.17 K. The mean fluid temperatures at the outlet for the experimental model and the base model are 2400 K and 2213.71 K respectively. The results are graphically shown in Figure 65.

Table 46- Mean Fluid Temperature along the axial length of the 3-D Two-Domain model and the experiment

Axial Distance, x [m]	Mean Fluid Temperature, T_m [K] 3-D Two-Domain Model	Mean Fluid Temperature, T_m [K] Experiment	Mean Fluid Temperature Difference, ΔT_m [K]	% Deviation
0	299.31	300	-0.69	0.23
0.1	345.24	390	-44.76	11.47692
0.2	460.88	490	-29.12	5.942857
0.3	645.62	700	-54.38	7.768571
0.4	884.18	950	-65.82	6.928421
0.5	1142.17	1250	-107.83	8.6264
0.6	1396.17	1450	-53.83	3.712414
0.7	1650.23	1750	-99.77	5.701143
0.8	1891.22	2000	-108.78	5.439
0.9	2094.95	2175	-80.05	3.68046
1.0	2242.47	2350	-107.53	4.575745
1.1	2312.17	2425	-112.83	4.652784
1.2	2213.71	2400	-186.29	7.762083

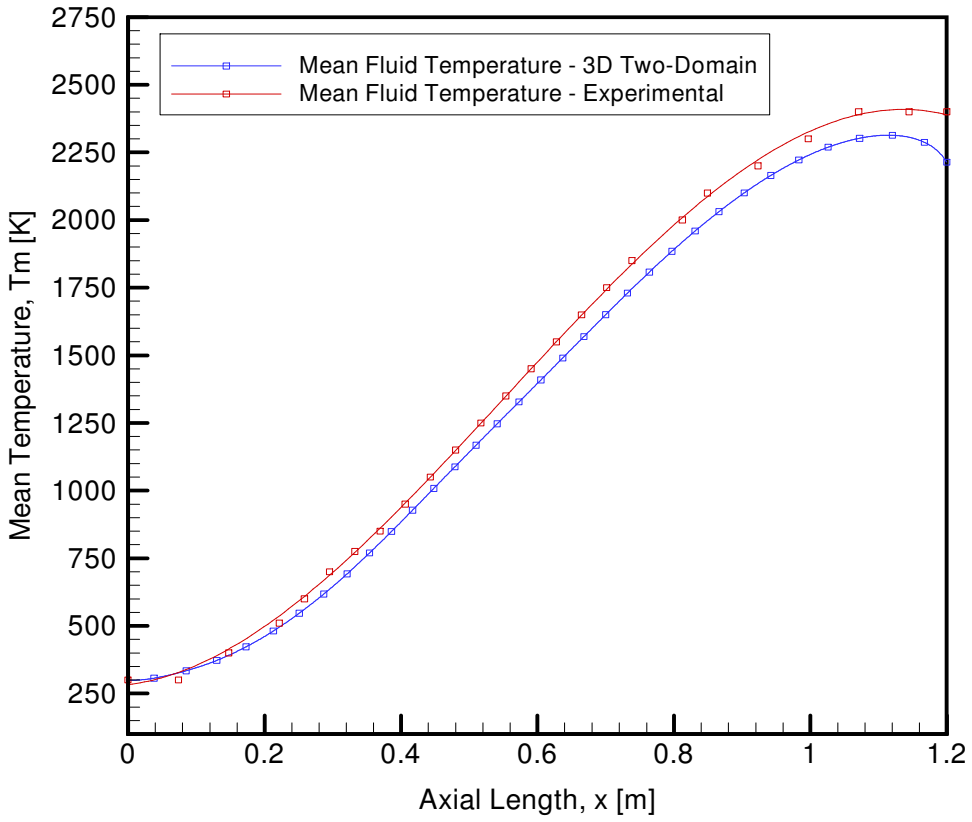

Figure 65- Comparison of the Mean Fluid Temperature along the axial length of the 3-D Two-Domain model and the experiment

The quantitative comparison of wall temperature along the axial length of the pipe for the experiment and the base model is presented in Table 47. The wall temperature of the experimental model at the inlet is 300 K whereas; the base model has a wall temperature of 324.55 K. The wall temperature for both the models reach maximum at 1.0 meter. The experimental mode has a maximum wall temperature of 2550 K and the base model has the maximum wall temperature of 2643.81 K. The wall temperature of experimental model at the outlet is 2400 K and that of the base model is 2476.6 K. The results are graphically compared in Figure 66.

Table 47- Wall Temperature along the axial length of the 3-D Two-Domain model and the experiment

Axial Distance, x [m]	Wall Temperature, T_w [K] 3-D Two-Domain Model	Wall Temperature, T_w [K] Experiment	Wall Temperature Difference, ΔT_w [K]	% Deviation
0	324.55	300	24.55	8.183333
0.1	596.9	600	-3.1	0.516667
0.2	944.71	800	144.71	18.08875
0.3	1329.09	1100	229.09	20.82636
0.4	1680.14	1450	230.14	15.87172
0.5	1958.36	1825	133.36	7.307397
0.6	2162.18	2000	162.18	8.109
0.7	2335.33	2250	85.33	3.792444
0.8	2488.9	2450	38.9	1.587755
0.9	2597.3	2500	97.3	3.892
1.0	2643.81	2550	93.81	3.678824
1.1	2619.78	2500	119.78	4.7912
1.2	2476.6	2400	76.6	3.191667

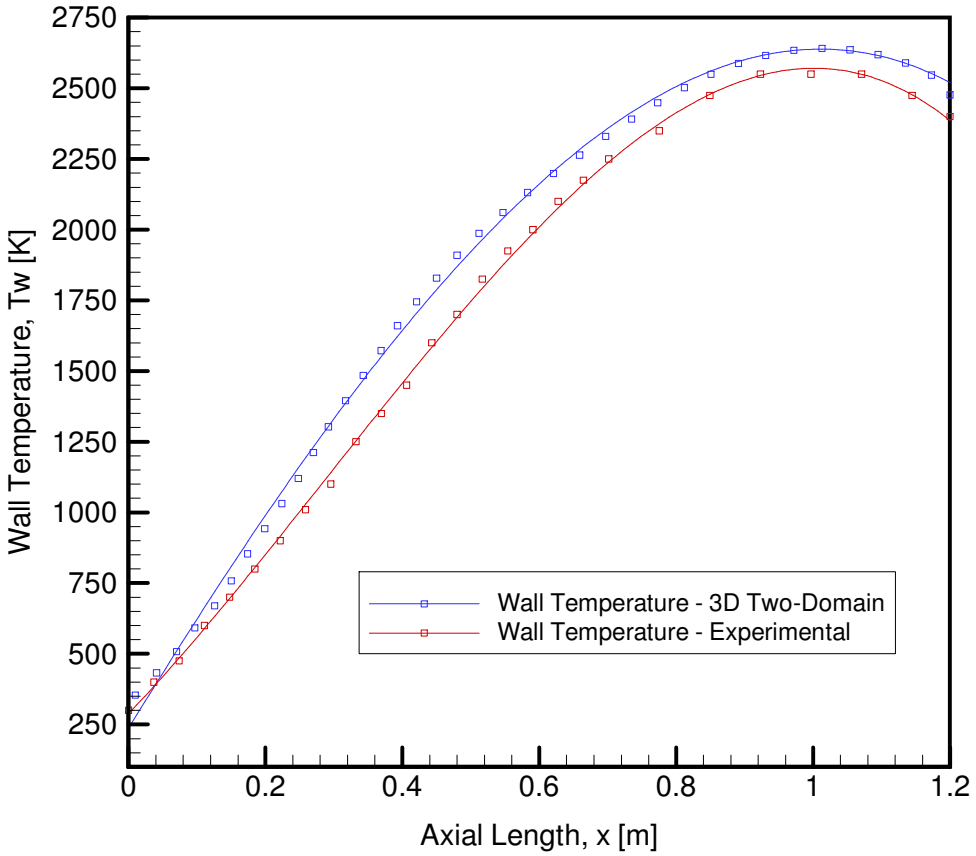

Figure 66- Comparison of the Wall Temperature along the axial length of the 3-D Two-Domain model and the experiment

7.2.3 Comparison of CFD Models with the Experiment

All the models are simultaneously run for the same initial and boundary conditions to simulate the results from the experimental model. The description of each model is shown in Table 48.

Table 48- Comparison of results between 1-D and 3-D Two-Domain models with the Experiment

		Results			
Run No.	Models	Inlet Pressure, P_i [MPa]	Outlet Wall Temperature, T_w [K]	Mean Outlet Fluid Temperature, T_e [K]	Outlet Velocity, u_e [m/s]
Experiment	-	-	2500	2400	-
1D-H2-IV.3	IN = 41 $\Delta t = 5 \times 10^{-6}$ s	7.08	-	2216.63	2847
3D-H2-2DM-I.3	Mesh size: 212,577	8.50	2425	2213.71	3150

Figure 67 shows the comparison of the results for the mean fluid temperature from all the models used in the present experiment with the experimental model. The mean fluid temperatures at the inlet for all the models are very identical with a deviation of. The temperature in all the models gradually increases along the length of the channel. At 1.1 meters, the experimental model has the highest mean fluid temperature of 2425 K. At the outlet, the experimental model has the highest mean fluid temperature of 2400 K and the 3-D two-domain (base) model and the one-dimensional model have quite identical mean fluid temperature at the outlet with 2213.71 K and 2216.63 K respectively. The quantitative comparison of mean fluid temperature distribution from the 1-D, 3-D One-Domain, 3-D Two-Domain, and the Experimental model is illustrated in Table 49.

Table 49- Mean Fluid Temperature distribution along the axial length of the 1-D model, 3-D Two-Domain model, and the experiment

Axial Distance, x [m]	Temperature, T_m [K] One-Dimensional Model	Temperature, T_m [K] 3-D Two-Domain Model	Temperature, T_m [K] Experiment
0	300	299.31	300
0.1	424.28	345.24	390
0.2	627.74	460.88	490
0.3	804.59	645.62	700
0.4	997.14	884.18	950
0.5	1267.99	1142.17	1250
0.6	1472.75	1396.17	1450
0.7	1670.51	1650.23	1750
0.8	1909.62	1891.22	2000
0.9	2059.94	2094.95	2175
1.0	2175.51	2242.47	2350
1.1	2253.41	2312.17	2425
1.2	2216.63	2213.71	2400

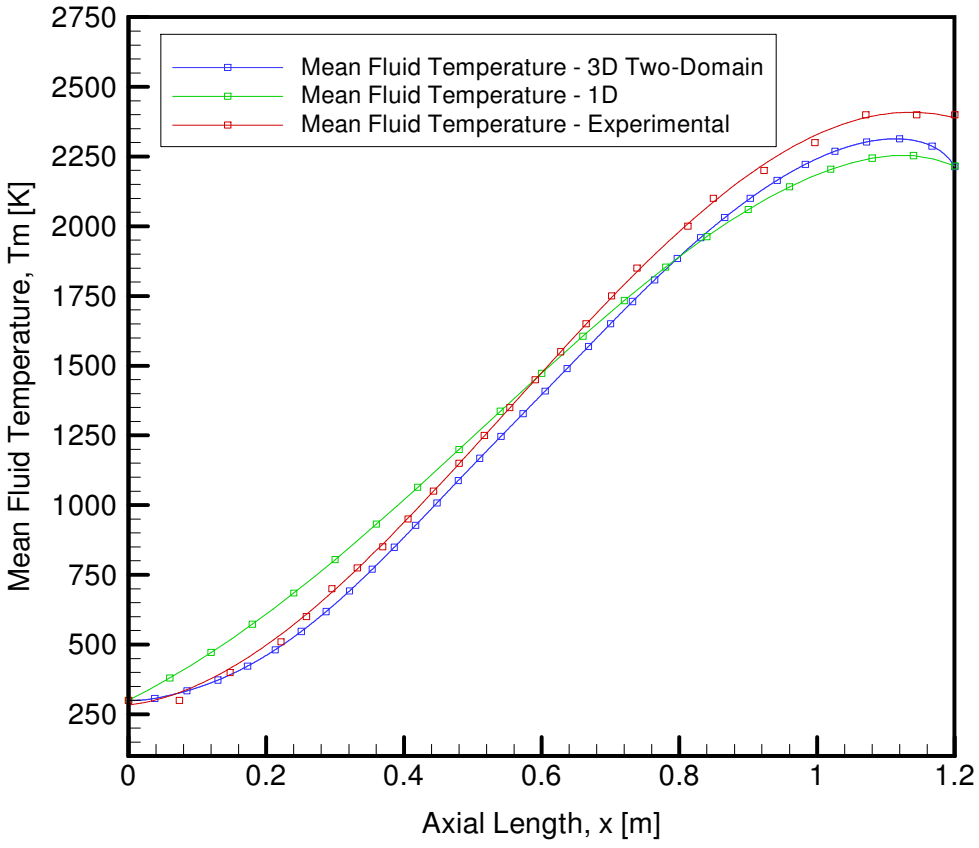

Figure 67- Comparison of the Mean Fluid Temperature distribution along the axial length of the 1-D model, 3-D Two-Domain model, and the experiment

Chapter 8

Parametric Study

In this study, a 3-D two-domain model with an axial cell size (dx) of 1 x 10^{-3} meters and 212,577 cells is chosen from the mesh independence study for the parametric study. The study focuses on the effects of boundary and initial conditions on the distributions on pressure, velocity and temperature along the channel.

8.1 Effects of Different Inlet Mass Flow Rate

In this study, a three-dimensional, two domain (base) model is used to study the effect of inlet mass flow rate. The model has a fluid domain with 5 layers in radial direction and a solid domain with one layer. A mesh generated has a cell size of 1 x 10^{-3} meters and has 212,577 cells in total. The variable parameter for this study is presented in Table 50.

Table 50- Inlet Mass Flow Rate study for 3-D Two-Domain model
[dx = 1x10^{-3} m, Mesh size = 212,577, n_f = 5, n_s = 1, turbulent, constant properties]

				Results			
Run No.	Mass Flow rate, m_{dot} [x10^{-3} kg/s]	Mach Number, Ma	Reynolds Number, Re (x10^5)	Inlet Pressure, P_i [MPa]	Mean Outlet Fluid Temperature, T_e [K]	Outlet Velocity, u_e [m/s]	Pressure Difference, ΔP [MPa]
3D-H2-2DM-V	4.0	0.097	2.54	7.62	2597.69	3145.17	4.50
	5.0	0.107	3.18	8.60	2076.79	3132.66	5.50
	6.0	0.12	3.81	9.35	1724.06	3099.28	6.25

In this study, as the mass flow rate of the gaseous hydrogen increases the inlet pressure increases as well. The inlet pressure for an inlet mass flow rate of 0.004 kg/s is 7.620 MPa whereas the inlet pressure for the mass flow rate of 0.005 kg/s is 8.609 MPa. As, the mass flow rate increases to 0.006 kg/s the pressure also goes up to 9.346 MPa. This is due to the fact that mass flow rate is directly proportional to the density of the fluid, and density is directly proportional to pressure. Therefore, increase in mass flow rate results in the increase in pressure.

In this case, the exit velocity of for the 3-D two-domain model decreases as mass flow rate increases. This is due to the fact that pressure and density are both increasing with the increase in mass flow rate. So, the increase in density results in the decrease in the exit velocity from 3145.17 m/s (for 0.004 kg/s) to 3099.28 m/s (for 0.006 kg/s). Similarly, the fluid temperature for the 3-D two-domain model decreases as mass flow rate increases. This is due to the fact that temperature is inversely proportional to pressure. Therefore, increase in mass flow rate results in the increase in density and pressure, which in turn decreases the temperature. From Table 51, the fluid temperature at the exit decreases from 2597.69 K (for 0.004 kg/s) to 1724.06 K (for 0.006 kg/s). Comparison between temperature distributions along the axial length with different mass flow rates is shown in Figure 68.

Table 51- Fluid Temperature distribution along the axial centerline of the 3-D Two-Domain model for m_{dot} = 0.004 kg/s, m_{dot} = 0.005 kg/s, m_{dot} = 0.006 kg/s for Run 3D-H2-2DM-V

Axial Distance, x [m]	Fluid Temperature, T_f [K] (m_{dot} = 0.004 kg/s)	Fluid Temperature, T_f [K] (m_{dot} = 0.005 kg/s)	Fluid Temperature, T_f [K] (m_{dot} = 0.006 kg/s)
0	299.423	299.284	299.135
0.1	318.856	315.918	312.375
0.2	396.694	385.422	371.533
0.3	496.83	488.472	461.644
0.4	622.345	631.237	586.778
0.5	844.483	842.398	760.563
0.6	1169.46	1135.92	987.614
0.7	1638.97	1434.1	1226.77
0.8	2026.38	1693.35	1442.86
0.9	2308.81	1909.87	1624.3
1.0	2517.46	2071.1	1758.86
1.1	2634.66	2155.62	1826.77
1.2	2597.69	2076.79	1724.06

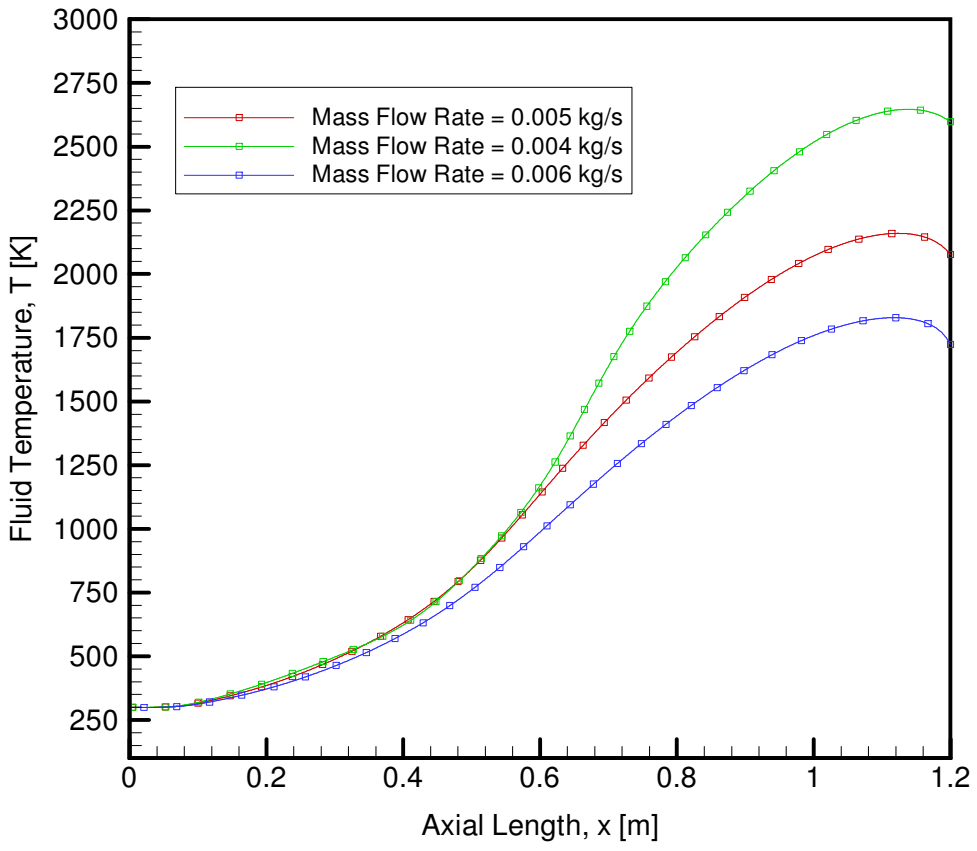

Figure 68- Comparison of Fluid Temperature distribution along the axial centerline of the 3-D Two-Domain model for m_{dot} = 0.004 kg/s, m_{dot} = 0.005 kg/s, m_{dot} = 0.006 kg/s for Run 3D-H2-2DM-V

8.2 Effects of Different Heat Flux

In this study, a three-dimensional, two domain (base) model is used to study the effect of variable heat flux. Predicted pressure, axial velocity and fluid temperature distribution are compared between different heat fluxes. The variable parameter for the study is shown in Table 52.

Table 52- Heat Flux study for 3-D Two-Domain model
[dx = $1x10^{-3}$ m, Mesh size = 212,577, n_f = 5, n_s = 1, turbulent, constant properties]

					Results			
Run No.	Type	Mach Number, Ma	Reynolds Number, Re ($x10^5$)	Heat Input, Q [kJ/s-m^2]	Inlet Pressure, P_i [MPa]	Outlet Centerline Fluid Temperature, T_e [K]	Outlet Velocity, u_e [m/s]	Pressure Difference, ΔP [MPa]
3D-H2-2DM-III.3	Variable	0.11	3.18	20,00	8.25	1920	2900	5.15
		0.107	3.18	22,000	8.60	2076	3132	5.50
		0.095	3.18	30,000	9.67	2642	4126	6.57

From the result tables, we can conclude that the increase in heat flux is directly proportional to the increase in the inlet pressure in the 3-D two-domain model. Initially, at 18000 kW/m^2, the inlet pressure of the fluid in the channel is 7.973 MPa. As the heat flux is increased to 20000 kW/m^2, the pressure goes up to 8.297 MPa and finally for 22,000 kW/m^2 the pressure is 8.609 MPa. Similarly, the fluid temperature increases with the increase in heat flux. Since, temperature is directly proportional to pressure through ideal gas relation, increase in pressure results in the increase of temperature. Therefore, as the heat flux increases from 18000 kW/m^2 to 22000 kW/m^2, temperature also increase from 1783.53 K to 2076.79. A quantitative comparison between the temperature distributions along the axial length of the model for different non-uniform heat fluxes is shown in Table 53.

Table 53- Fluid Temperature distribution along the axial centerline of the 3-D Two-Domain model for Q_{max} = 20,000 kJ/s-m^2, Q_{max} = 22,000 kJ/s-m^2, Q_{max} = 30,000 kJ/s-m^2 for Run 3D-H2-2DM-III.3

Axial Distance, x [m]	Fluid Temperature, T_f [K] (Q_{max} =22,000 kJ/s-m^2)	Fluid Temperature, T_f [K] (Q_{max} = 22,000 kJ/s-m^2)	Fluid Temperature, T_f [K] (Q_{max} = 30,000 kJ/s-m^2)
0	299.168	299.23	299.43
0.1	313.374	314.689	319.95
0.2	373.766	379.898	400.40
0.3	468.578	479.822	495.20
0.4	603.581	621.354	641.21
0.5	787.501	822.475	913.90
0.6	1009.15	1077.62	1241.71
0.7	1234.6	1335.33	1754.22
0.8	1442.16	1567.86	2187.05
0.9	1618.93	1764.44	2490.09
1.0	1751.66	1911.42	2708.87
1.1	1823.53	1989.59	2819.83
1.2	1783.53	1931.41	2641.28

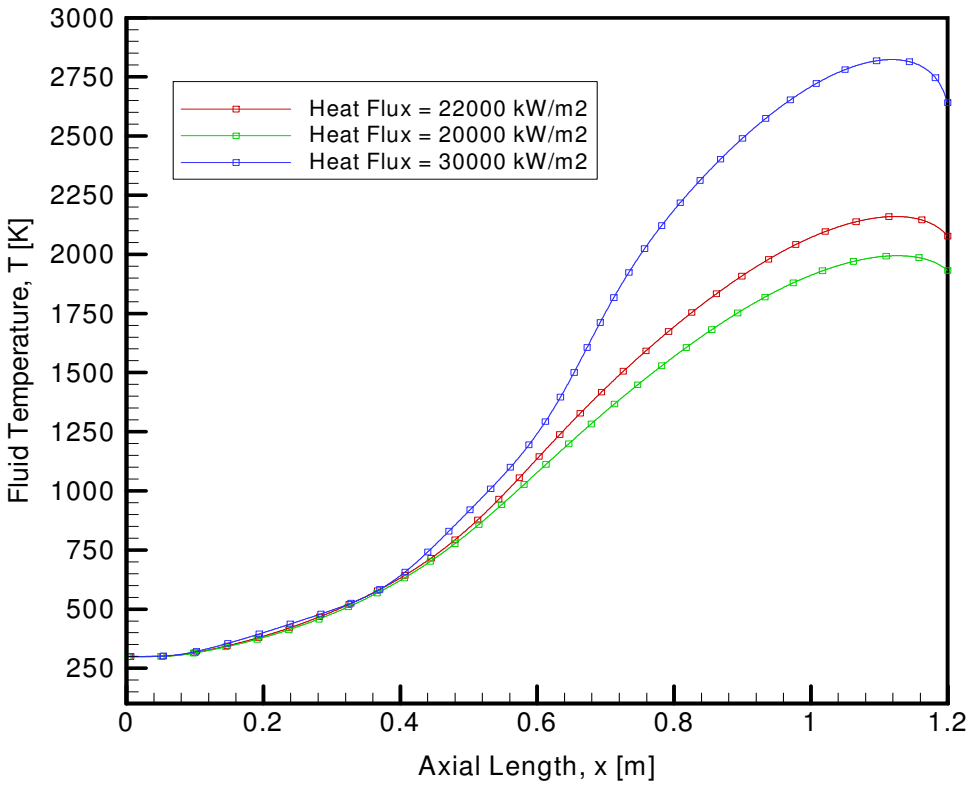

Figure 69- Comparison of Fluid Temperature distribution along the axial centerline of the 3-D Two-Domain model for Q_{max} = 20,000 kJ/s-m^2, Q_{max} = 22,000 kJ/s-m^2, Q_{max} = 30,000 kJ/s-m^2 for Run 3D-H2-2DM-III.3

8.3 Effects of Different Inlet Fluid Temperature

In this study, a three-dimensional, two domain (base) model is used to study the effect of different inlet fluid temperature. Predicted pressure, axial velocity and fluid temperature distribution are compared between different inlet fluid temperature runs studies. The variable parameter for the study is shown in Table 54 along with the predicted results at the outlet of the channel.

Table 54- Inlet Temperature study for 3-D Two-Domain model
[dx = $1x10^{-3}$ m, Mesh size = 212,577, $n_f = 5$, $n_s = 1$, turbulent, constant properties]

				Results			
Run No.	Inlet Temperature, T_i [K]	Mach Number, Ma	Reynolds Number, Re ($x10^5$)	Inlet Pressure, P_i [MPa]	Outlet Centerline Fluid Temperature, T_e [K]	Outlet Velocity, u_e [m/s]	Pressure Difference, ΔP [MPa]
3D-H2-2DM-VI	300	0.11	3.18	8.60	2076.79	3132.66	5.50
	400	0.12	3.18	8.83	2151.2	3241.35	5.73
	500	0.13	3.18	9.04	2225.13	3348.83	5.94

Pressure is directly proportional to temperature through ideal gas relation. Therefore, increase in temperature results in the increase in pressure. In this case, the inlet temperature increases from 300 K to 500 K, so through ideal gas relation the pressure also increases from 8.609 MPa to 9.047 MPa.

Increasing the inlet temperature of the flow increases the pressure of the flow at the inlet, which result in the increase of the temperature at the outlet. The flow with an inlet temperature of 300 K has an exit temperature of 2076.79 K, and the temperature gradually increases with the increase in inlet flow temperature. For a flow with an inlet temperature of 400 K, the exit temperature is 2151.2 K and for the flow with an inlet temperature of 500 K, the exit temperature

is 2225.13 K. Table 55 shows a quantitative distribution of fluid temperature along the axial length of the model. A figurative comparison is shown in Figure 70.

Table 55- Fluid Temperature distribution along the axial centerline of the 3-D Two-Domain model for T_i = 300 K, T_i = 400 K, T_i = 500 K for Run 3D-H2-2DM-VI

Axial Distance, x [m]	Fluid Temperature, T_f [K] (Inlet Fluid Temperature, T_i = 300 K)	Fluid Temperature, T_f [K] (Inlet Fluid Temperature, T_i = 400 K)	Fluid Temperature, T_f [K] (Inlet Fluid Temperature, T_i = 500 K)
0	299.284	398.793	498.205
0.1	315.918	416.394	516.249
0.2	385.422	491.628	594.32
0.3	488.472	611.413	721.043
0.4	631.237	781.552	898.414
0.5	842.398	1006.83	1123.17
0.6	1135.92	1271.39	1379.54
0.7	1434.1	1541.26	1642.42
0.8	1693.35	1791.61	1888.9
0.9	1909.87	2004.89	2099.7
1.0	2071.1	2163.7	2256.28
1.1	2155.62	2244.91	2334.28
1.2	2076.79	2151.2	2225.13

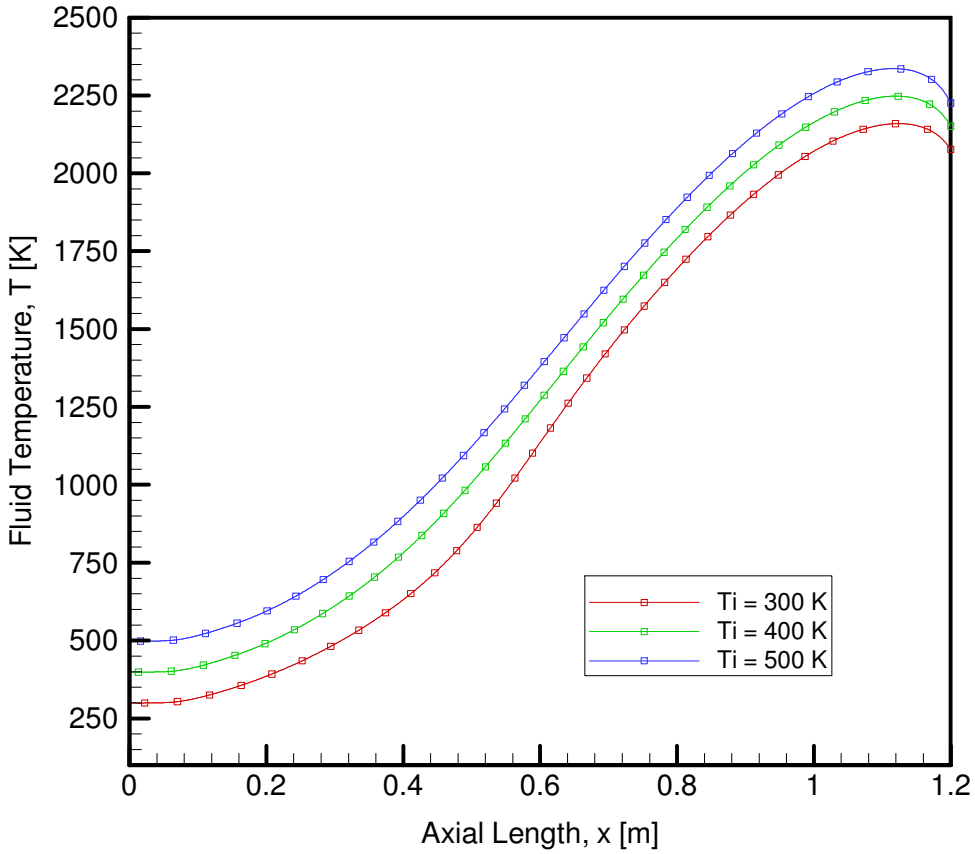

Figure 70- Comparison of the Fluid Temperature distribution along the axial centerline of the 3-D Two-Domain model for T_i = 300 K, T_i = 400 K, T_i = 500 K for Run 3D-H2-2DM-VI

Chapter 9

Results for Unsteady Flow Study Using in 1-D Model

A one-dimensional computer model has a 41 x 41 mesh size with a time increment of 5 x 10^{-6} seconds. This computer numerical model is used to simulate the unsteady flow with similar run parameters as that of the experimental study so as to replicate the results. The run parameters for this study are presented in Table 56.

Table 56- Benchmark Run Parameters for 1-D Model
[unsteady, compressible, viscous, turbulent, constant properties]

			Run Parameters			
Run Model	Time Increment, Δt [s]	Mesh Size, IN	Inlet Mass Flow Rate, m_{dot} [kg/s]	Inlet Fluid Temperature, T_i [K]	Exit Pressure, P_e [MPa]	Heat Flux, Q_{max} [kW/m^2]
1D-H2-I.2	5 x10^{-6}	41x41	0.005	300	3.1	22,000

A variable heat flux is applied to the outer surface of the wall that is given by a sine function with the maximum magnitude of 22000 kJ/s-m^2 and the distribution is shown in Figure . The minimum heat flux in the heat flux distribution is 1408 kJ/s-m^2. Therefore, the mean heat flux for this distribution is 14299.422 kJ/s-m^2.

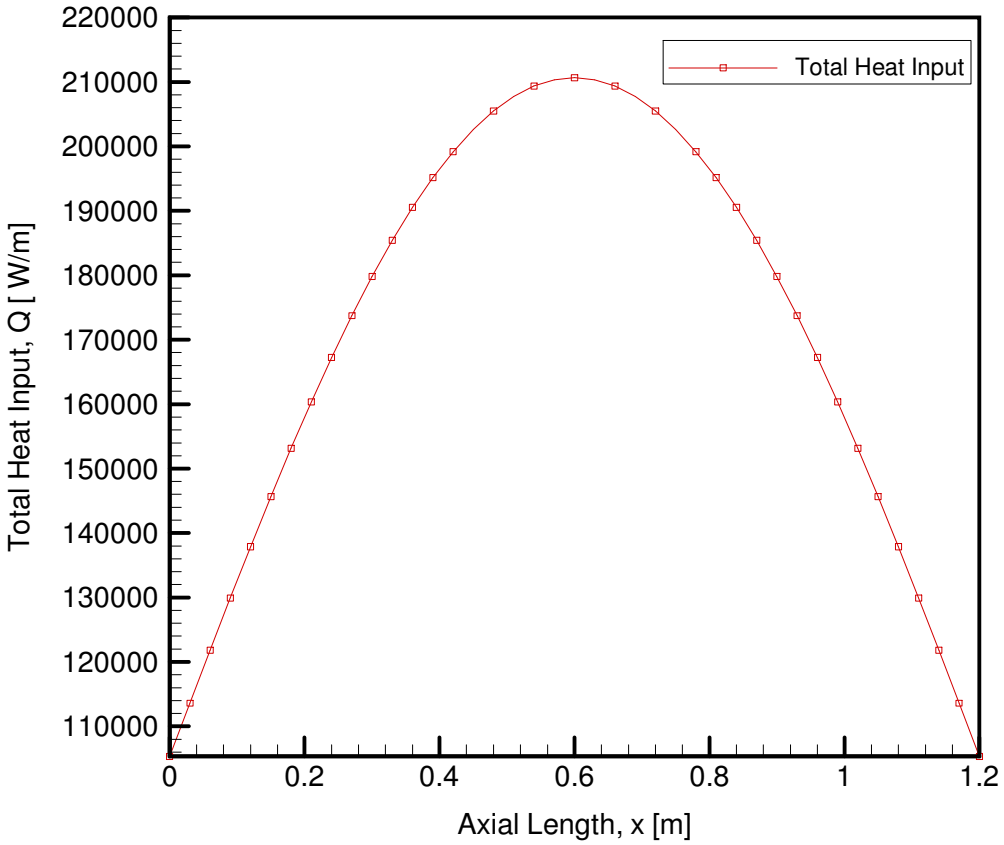

Figure 71– Non-Uniform Heat Input distribution along the axial length of the 1-D model for Run 1D-H2-I.2

In this study, initially the flow is static and the pressure in the channel is constant at 3.1 MPa similar to the exit of the channel. A constant mass flow of 0.005 kg/s is then introduced at the inlet with constant temperature of 300 K which acts as a driving factor for the flow.

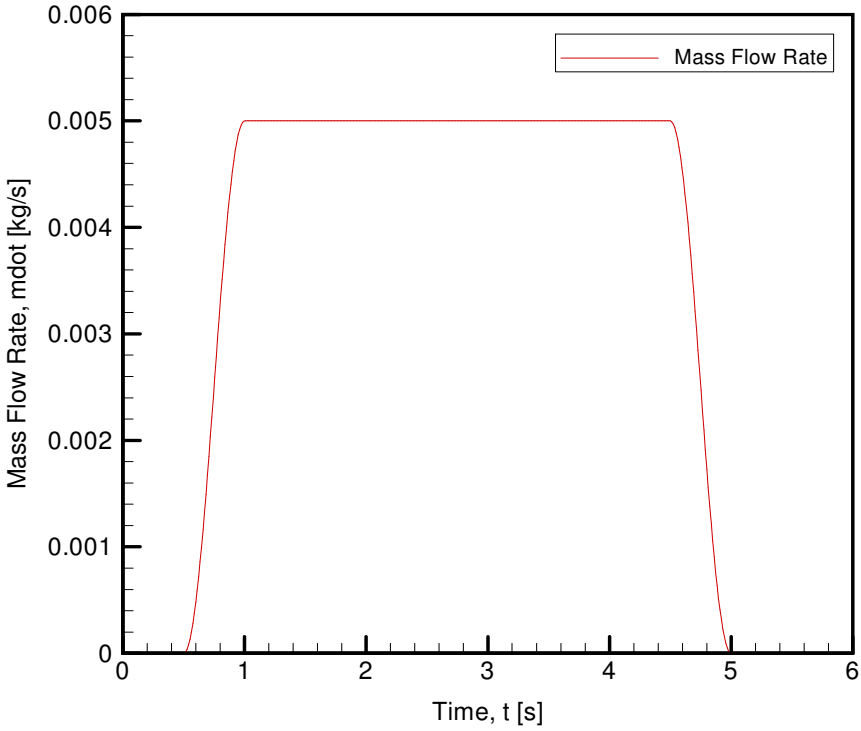

Figure 72- Mass Flow Rate histogram at the inlet of the 1-D model for Run 1D-H2-I.2

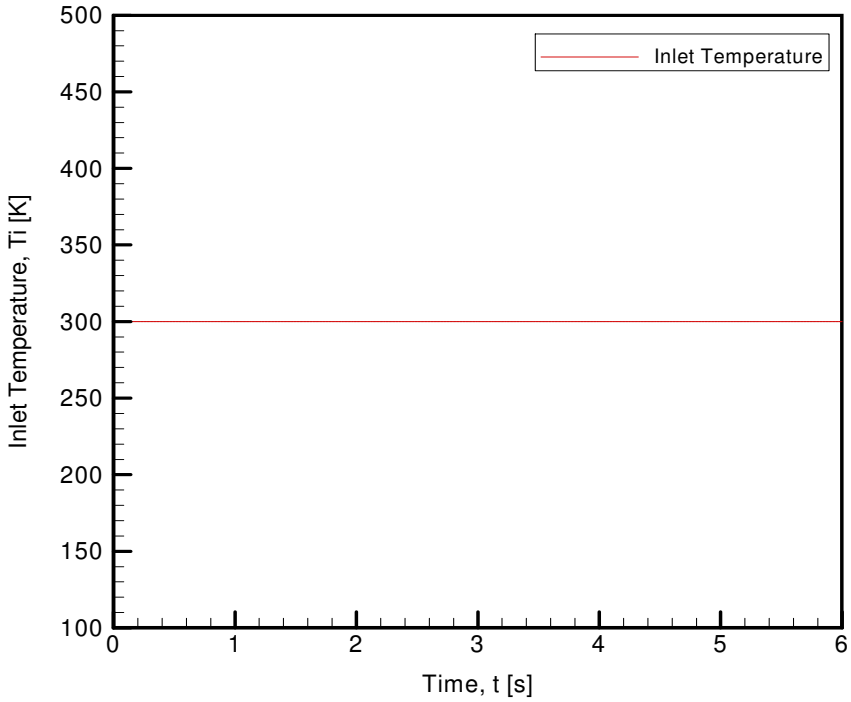

Figure 73- Temperature histogram at the inlet of the 1-D model for Run 1D-H2-I.2

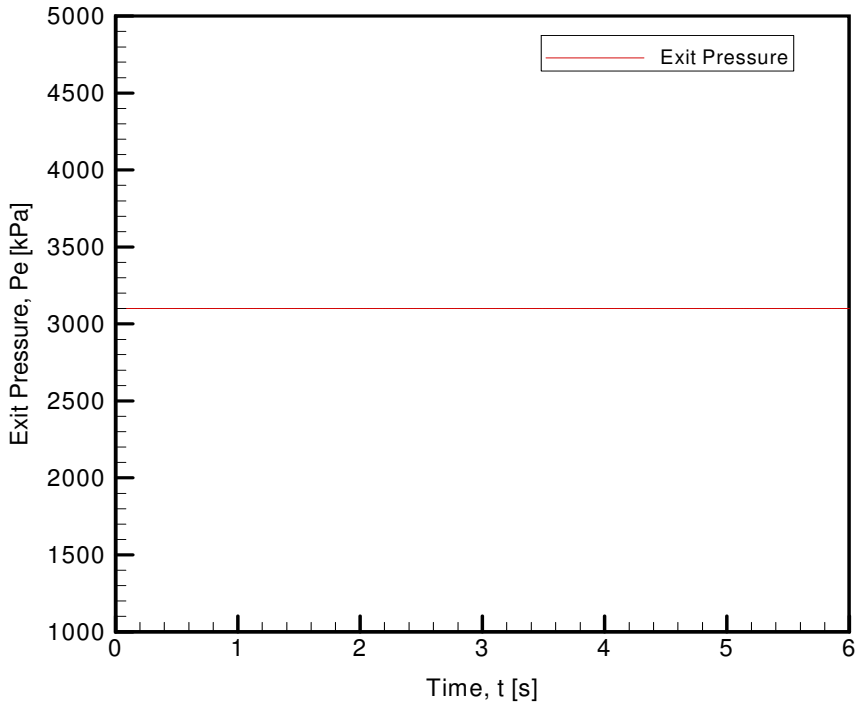

Figure 74- Pressure histogram at the exit of the 1-D model for Run 1D-H2-I.2

As the flow rate increases, the pressure at the inlet also gradually increases from initial 3.1 MPa at 0 seconds to 7.07 Mpa at 1.8 seconds. The pressure is maintained at this level for approximately 2.4 seconds. The flow is then shut down and the pressure goes back down to the original 3.1 MPa. The effects of mass flow inlet in pressure, temperature and velocity are recorded at the inlet and the exit of the channel.

At the inlet, the pressure is initially 3.1 MPa and since the density is directly proportional to pressure through ideal gas relation, the density also remains low for the first couple of seconds. During this period, the inlet velocity is at it max (around 340 m/s) because for constant mass flow rate and cross-sectional area, density is inversely proportional to velocity. Once the pressure gradually starts to increase, the velocity comes down and attains a constant value (approx. 180 m/s) for two seconds. Finally, the flow is shut down and the pressure goes back to

its original value of 3.1 MPa, resulting in the increase in velocity before the flow is completely static.

The histograms of pressure, velocity, and temperature at the inlet and the outlet are shown in the figures below.

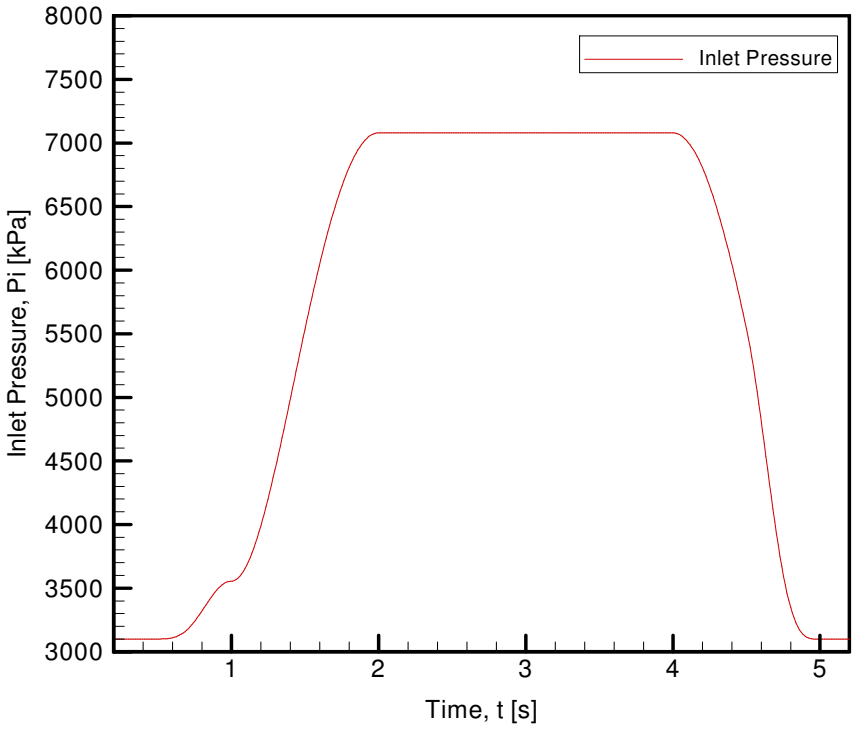

Figure 75- Pressure histogram at the inlet of the 1-D model for Run 1D-H2-I.2

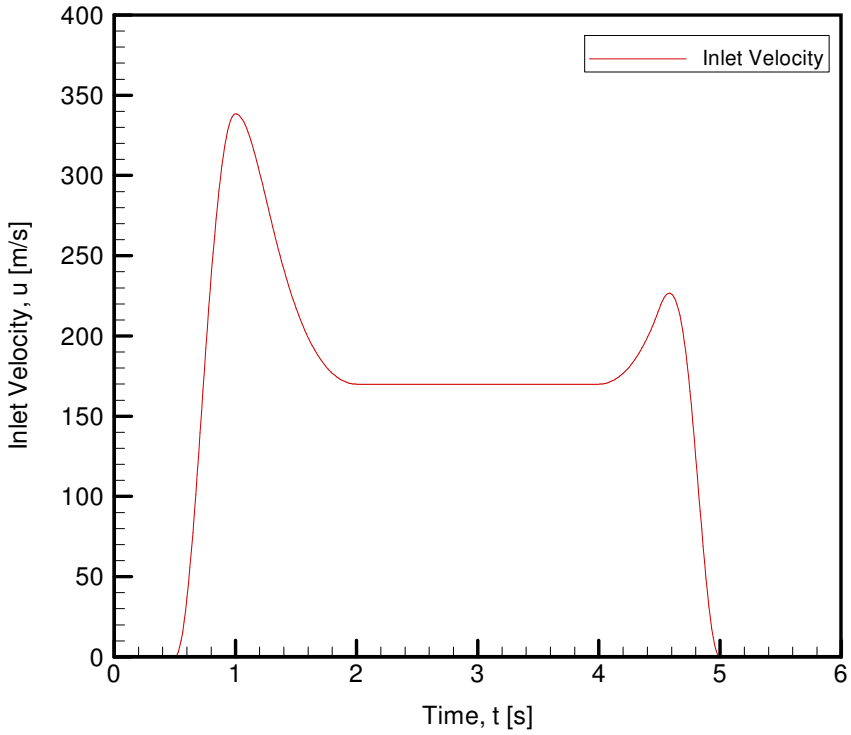

Figure 76- Velocity histogram at the inlet of the 1-D model for Run 1D-H2-I.2

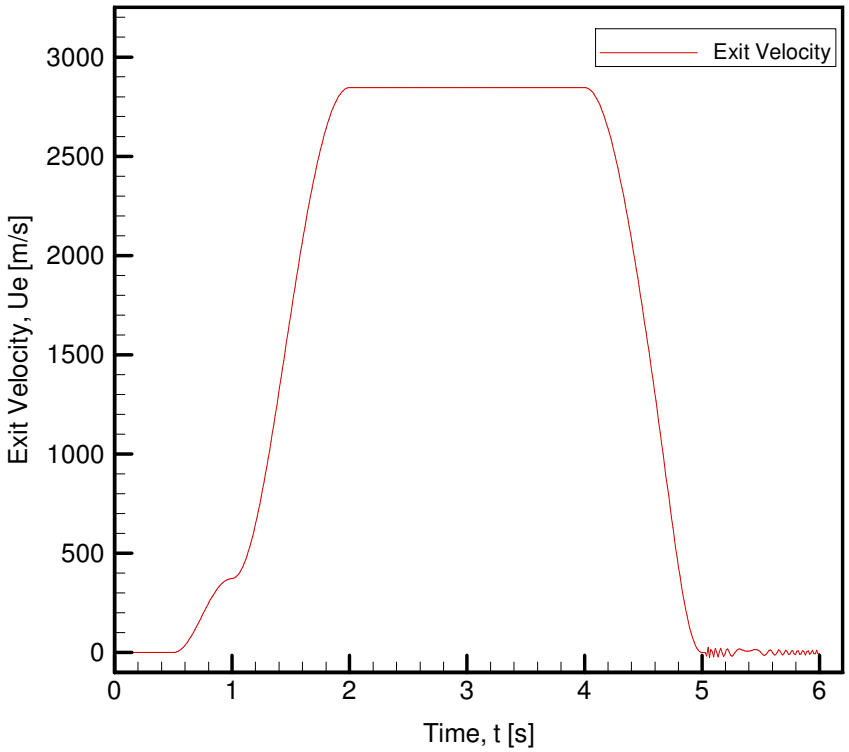

Figure 77- Velocity histogram at the exit of the 1-D model for Run 1D-H2-I.2

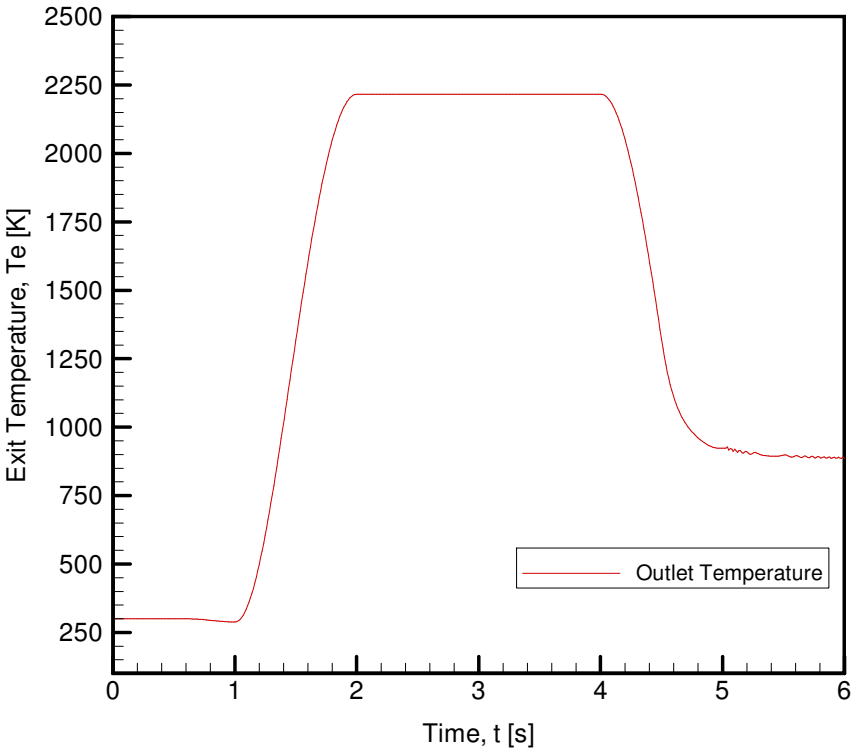

Figure 78- Fluid Temperature histogram at the exit of the 1-D model for Run 1D-H2-I.2

Chapter 10

Conclusion

The objective of this thesis research was to develop a mathematical model which could simulate the flow in a cooling channel of a NTR engine. The one-dimensional model was adopted which under similar initial and boundary conditions to that of the experimental NTR cooling channel generated similar results. The following conclusions are drawn from the study.

1. A modified MacCormack scheme was successfully employed to solve the governing differential equations of the unsteady, turbulent flow inside a cooling channel using second order accurate in time and finite difference approximation.
2. The results of the numerical study carried out using the mathematical model and the solution procedure proposed in this thesis fair well when compared to the results of the experimental case.
3. One-dimensional mathematical model showed no significant change in results during time increment and grid independence study.
4. There is negligible difference between the results from different models of the mesh independence study for three-dimensional CFD models.
5. There is a notable difference between the results of the variable property and the constant property case for a three-dimensional CFD models.
6. The temperature and velocities are higher for variable property case resemble more to the experimental values.

7. The experimental result has a higher mean temperature distribution along the length of the cooling channel as compared to that of the three-dimensional two-domain model.
8. The wall temperature distribution for the three-dimensional two-domain model is higher than the experimental case.
9. Comparison of mean fluid temperature between one-dimensional model, a three-dimensional two-domain model and the experiment shows that the three-dimensional model has greater resemblance to the experimental results.

Distributions of pressure, density, velocity and temperature for one-dimensional model and the 3-D one-domain model are compared. In Figure 61, the inlet pressure for the 3-D one-domain model is 8.30 MPa which is higher compared to the one-dimensional model's inlet pressure of 7.08 MPa. Also, the density of the fluid is also higher in case of the 3-D one-domain model compared to that of the one-dimensional model as shown in Figure 62. The 3-D one-domain model has an inlet density of 6.807 kg/m^3 whereas the one-dimensional model has 5.80 kg/m^3. The comparison of density distribution between the one-dimensional and the base model is given in Table 42. The inlet axial velocity for both one-dimensional and the 3-D one-domain model is 300 m/s. However, the 3-D one-domain model has an axial velocity 2921.21 m/s at the outlet and the one-dimensional model has an outlet axial velocity of 2846.60 m/s as shown in Figure 63. Finally, the mean fluid temperature distribution between the one-dimensional model and the 3-D one-domain model is shown in Figure 64. Both the models have an inlet fluid temperature of 300 K. With the non-uniform heat flux applied at the surface of the channel, the temperature of the fluid gradually increases along the length of the pipe. The maximum temperature of the fluid for one-dimensional and the 3-D one-domain model are 2253.74 K and

2056.84 K respectively. The mean fluid temperature at the outlet for the one-dimensional model is 2216.63 K and that for the 3-D model is 1989.1 K. The quantitative values of temperature along the length of the channel for both one-dimensional and base model are shown in Table 44.

A comparative study of temperature distributions between the experimental and 3-D two-domain model is conducted. The 3-D two-domain model is simulated with the benchmark initial and boundary conditions (Table 40) to achieve maximum accuracy with the experimental results. Mean fluid temperature and wall temperatures are compared between the two models. Table 46 presents the quantitative distribution of mean fluid temperature along the axial length of the channel in the experimental and the base model. The mean fluid temperatures in both the model gradually increases along the length of the channel. Both the models reach their respective maximum temperature at 1.1 meters of the channel. At this point, the experimental model reaches 2425 K and the base model is at 2312.17 K. The 3-D model has a deviation of 4.65 % from the experimental value. The mean fluid temperatures at the outlet for the experimental model and the base model are 2400 K and 2213.71 K respectively with a 7.7 % deviation. The results are graphically shown in Figure 65. The quantitative comparison of wall temperature along the axial length of the pipe for the experiment and the base model is presented in Table 47. The wall temperature of the experimental model at the inlet is 300 K whereas; the base model has a wall temperature of 324.55 K. The wall temperature for both the models reach maximum at 1.0 meter, where the 3-D model value has a deviation of 3.67 %. The experimental mode has a maximum wall temperature of 2550 K and the base model has the maximum wall temperature of 2643.81 K. The wall temperature of experimental model at the outlet is 2400 K and that of the base model is 2476.6 K and has a deviation of 3.19 % from the experimental value. The results are graphically compared in Figure 66.

Comparison of the results for the mean fluid temperature from all the models used in the present experiment with the experimental model is shown in Figure 67. The mean fluid temperatures at the inlet for all the models are very identical with a deviation of 0.23 %. The temperature in all the models gradually increases along the length of the channel. At 1.1 meters, the experimental model has the highest mean fluid temperature of 2425 K. At the outlet, the experimental model has the mean fluid temperature of 2400 K and the 3-D two-domain (base) model and the one-dimensional model have quite identical mean fluid temperature at the outlet with 2213.71 K and 2216.63 K respectively and a deviation of approximately 1.56 %. The quantitative comparison of mean fluid temperature distribution from the 1-D, 3-D Two-Domain, and the Experimental model is illustrated in Table 49. The comparison of the steady state predictions to the existing experimental results indicates that both models successfully predict the fluid temperature distribution in the NTR cooling channel. It is also concluded that the one-dimensional model is capable of predicting the thermal-hydrodynamic transients expected inside the coolant channels of the NTR engine in response to the variations in the power generation in the nuclear core and/or variations in the inlet gas flow rate due to anomalies in the turbo pumps.

Chapter 11

Recommendation

Although the one-dimensional and three-dimensional mathematical model were successful in predicting the results similar to the ones generated by the cooling channel of the NTR, further improvements and studies could be done to achieve higher accuracy in the results from the simulation.

1. A finer mesh should be utilized to obtain accurate results, especially at high heat fluxes.
2. In fully developed flow case study, a second run still was not fully developed. A third run can be conducted following the same procedure from the second run where the inlet conditions were taken from the outlet of the first run.
3. Present NTR systems can reach high temperature and velocity in the cooling channel. Therefore, the mathematical models can be simulated at higher heat flux to achieve higher fluid temperature.
4. Finally, the one-dimensional model only uses mass flow rate for the unsteady case to start-up and shutdown the simulation.

References

[1] Koenig, D.R., 1986. Experience Gained from the Space Nuclear Rocket Program (Rover). Los Alamos Report LA-10062-H, Los Alamos National Laboratory, Los Alamos, NM.

[2] Fittje, J.E. & Buehrle, R.J. 2006, "Conceptual engine system design for NERVA derived 66.7KN and 111.2KN thrust nuclear thermal rockets", AIP Conference Proceedings, p. 502.

[3] Fittje, J.E.ad, Schnitzler, B.G.bce , 2008, "Evaluation of recent upgrades to the NESS (Nuclear Engine System Simulation) code," 44th AIAA/ASME/SAE/ASEE Joint Propulsion Conference and Exhibit.

[4] Fittje, J.E., 2008, "Recent Upgrades to the NESS (Nuclear Engine System Simulation) Code," 44th AIAA/ASME/SAE/ASEE Joint Propulsion Conference and Exhibit.

[5] Emrich, W.J., 2006, "Non-Nuclear NTR Environmental Simulator," STAIF 2006, AIP, p.531-536.

[6] Finseth, J.L., 1991. Rover Nuclear Rocket Engine Program: Overview of Rover Engine Tests, Final Report, Sverdrup Technology, Inc.- MSFC Group, Contract NAS 8-37814, NASA, Marshall Space Flight Center, Science and Engineering.

[7] Litchford, R. J., Foote, J. P., Hickman, R., Dobson, C., & Clifton, S, 2007, "Long duration hot hydrogen exposure of nuclear thermal rocket materials." Paper presented at the Collection of Technical Papers - 43rd AIAA/ASME/SAE/ASEE Joint Propulsion Conference, 6056-6069.

[8] Pelaccio, D. G., 1994, Proceedings of the Workshop on Hydrogen Corrosion in Nuclear Thermal Propulsion Reactors, 10th Symposium on Space Nuclear Power and Propulsion, Albuquerque, NM.

[9] Pelaccio, D.G., El-Genk, M.S. & Butt, D.P. 1995, "Hydrogen corrosion considerations of carbide fuels for nuclear thermal propulsion applications", Journal of Propulsion and Power, vol. 11, no. 6, pp. 1338-1348.

[10] Litchford, R.J. , Foote, J.P., Clifton, W.B., Hickman, R.R., Wang, T.-S., Dobson, C.C. , 2011, "Hyperthermal environments simulator for nuclear rocket engine development," Nuclear and Emerging Technologies for Space 2011, NETS-2011, Pages 666-675.

[11] Swank, W.D. , Carmack, J., Werner, J.E., Pink, R.J., Haggard, D.C., Johnson, R. , 2007, "Hot hydrogen test facility," Space Technology and Applications International Forum: Space Renaissance: Inspiring the Next Generation, STAIF-2007, AIP Conference Proceedings, Volume 880, 2007, Pages 380-388.

[12] Emrich, W.J., 2008, "Nuclear Rocket Element Environmental Simulator-NTREES," STAIF 2008, AIP. Non-Nuclear NTR Environmental Simulator," STAIF 2006, AIP, p.531-536 (MSFC-679).

[13] Hall, M. L., Rider, W.J., and Cappiello. M.W., 1992, "Thermohydraulic Modeling of Nuclear Thermal Rockets: The Klaxon Code," Proceedings of Nuclear Technologies for Space Exploration, American Nuclear Society, Jackson Hole, WY

[14] Schmidt, E., Lazareth, O., and Ludewig, H., 1993, "Kinetic- A System Code For Analyzing Nuclear Thermal Propulsion Rocket Engine Transients," American Institute of Physics, Conference Proceedings 271, 1303

[15] Fittje, J.E., 2008, "Upgrades to NESS (Nuclear Engine System Simulation Code),"AIAA Joint Propulsion Conference, AIAA-2008-xxxx.

[16] Webb, J. A. and et al., 2011, "A Combined Neutronic-Thermal Hydraulic Model of a CERMET NTR Reactor," Proceedings of Numerical and Emerging Technologies for Space 2011, Paper No. 3276, Albuquerque, NM

[17] Akyuzlu, K.M., 2007, "Modeling of Instabilities Due to Coupling of Acoustic and Hydrodynamic Oscillations in Hybrid Rocket Motors," Proceedings of the 43st AIAA/ASME Joint Propulsion Conference and Exhibit, Paper No. 5367,Cincinnati, Ohio

[18] Akyuzlu, K.M., 2013, "Numerical Simulations of Thermal Hydrodynamic Transients in the Cooling Channels of a Nuclear Thermal Propulsion Engine," 49th AIAA Jet Propulsion Conference 2013 (paper accepted for publication.)

[19] Akyuzlu, K.M., 2012, "Analytical Investigation of Fluid-Structure Interactions in a Nuclear Thermal Rocket," Final Report, University of New Orleans -NASA SSC Contract No. NNS10AA92B.

[20] NIST Reference Fluid Thermodynamic and Transport Properties- REFPROP (2007), National Institute of Standards and technology, US Department of Commerce, Boulder, Colorado.

Appendices

Appendix I

Vector Form of Governing Differential Equations

For 1-D Model:

The continuity equation is given by:

$$\frac{D\rho}{Dt} + \rho\,\vec{\nabla}\cdot\vec{V} = 0 \tag{I.1}$$

The momentum equations are given by:

$$\rho\frac{D\vec{V}}{Dt} = \vec{g} - \vec{\nabla}p + \frac{\partial}{\partial x_j}[\mu(\frac{\partial u_i}{\partial x_j} + \frac{\partial u_j}{\partial x_i}) - \frac{2}{3}\delta_{i,j}\frac{\partial u_k}{\partial x_k})] \tag{I.2}$$

where,

$$\delta_{i,j} = \{ \begin{matrix} 1 & if & i=j \\ 0 & if & i\neq j \end{matrix}$$

The energy equation is given by:

$$\rho\frac{De}{Dt} + p\vec{\nabla}\cdot\vec{V} = \vec{\nabla}\cdot(k\,\vec{\nabla}T) + \Phi + \frac{\partial Q_s}{\partial t} \tag{I.3}$$

The equation of state for ideal gas is given by:

$$p = \rho R T \tag{I.4}$$

For 3-D CFD Model:

Continuity:

$$\frac{D\rho}{Dt} + \rho(\nabla . u) = 0 \qquad \text{(I.5)}$$

x-momentum equation:

$$\rho \frac{D\vec{u}}{Dt} = \rho\vec{g} - \vec{\nabla}P + \vec{\nabla}.\tau_{ij} \qquad \text{(I.6)}$$

r-momentum equation:

(I.7)

Energy equation:

$$\rho \frac{Di}{Dt} = -\vec{\nabla}.\vec{q} + \rho\vec{f}.\vec{u} + \vec{\nabla}.\left(\vec{\Pi}.\vec{u}\right) + \frac{\partial Q_s}{\partial t} \qquad \text{(I.9)}$$

Energy equation for the solid domain is given by:

$$q = -k\nabla T \qquad \text{(I.10)}$$

Appendix II

Differential Form of Governing Differential Equations

The continuity equation is given by:

$$\frac{\partial(\rho A)}{\partial t}+\frac{\partial}{\partial x}\left(\rho\, Au\right)=0 \tag{II.1}$$

The momentum equation in the x-direction is given by:

$$\frac{\partial}{\partial t}\left(\rho A\, u\right)+\frac{\partial}{\partial x}\left(\rho A\, u^{2}\right)=-\frac{\partial(PA)}{\partial x}-\tau'_{w}A \tag{II.2}$$

The energy equation is given by:

$$\frac{\partial}{\partial t}\left(\rho A\, c_{v}\, T\right)+\frac{\partial}{\partial x}\left(\rho\, Auc_{v}T\right)-PA\,\frac{\partial u}{\partial x}=\frac{\partial}{\partial x}(\,k\,A\frac{\partial T}{\partial x})+q_{w}A_{s} \tag{II.3}$$

Appendix III

Thermodynamic and Transport Properties for GH2

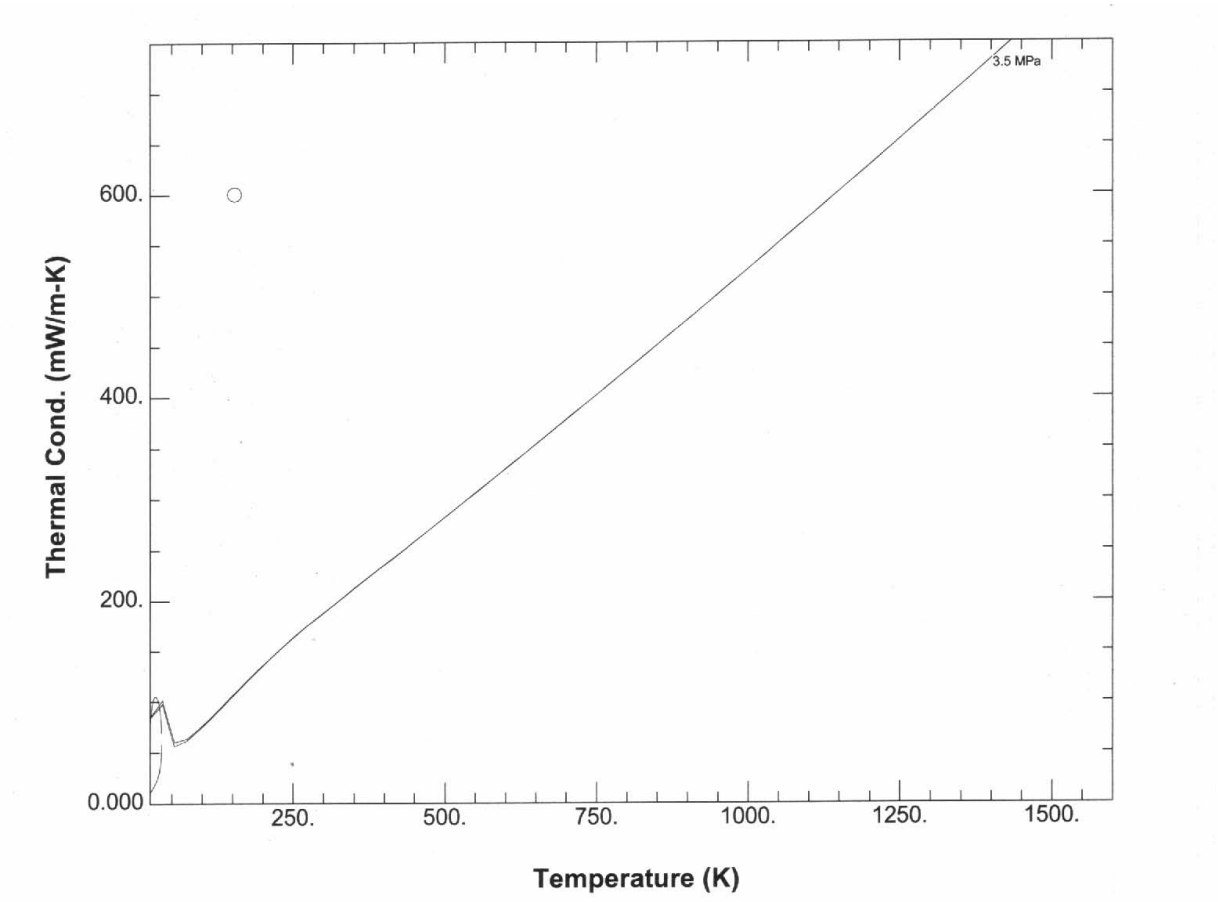

Figure A III -1 -Thermal Conductivity vs. Temperature for GH_2

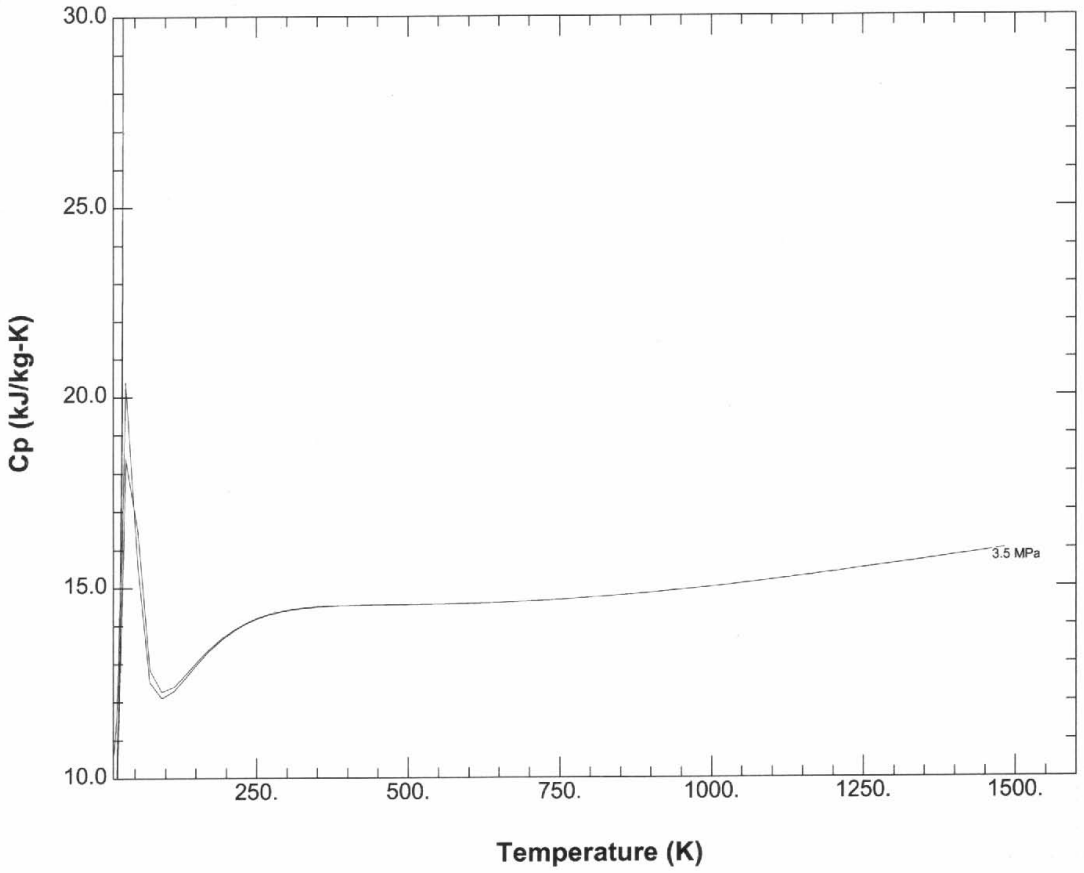

Figure A III- 2 - Specific Heat at Constant Temperature vs. Temperature for GH_2

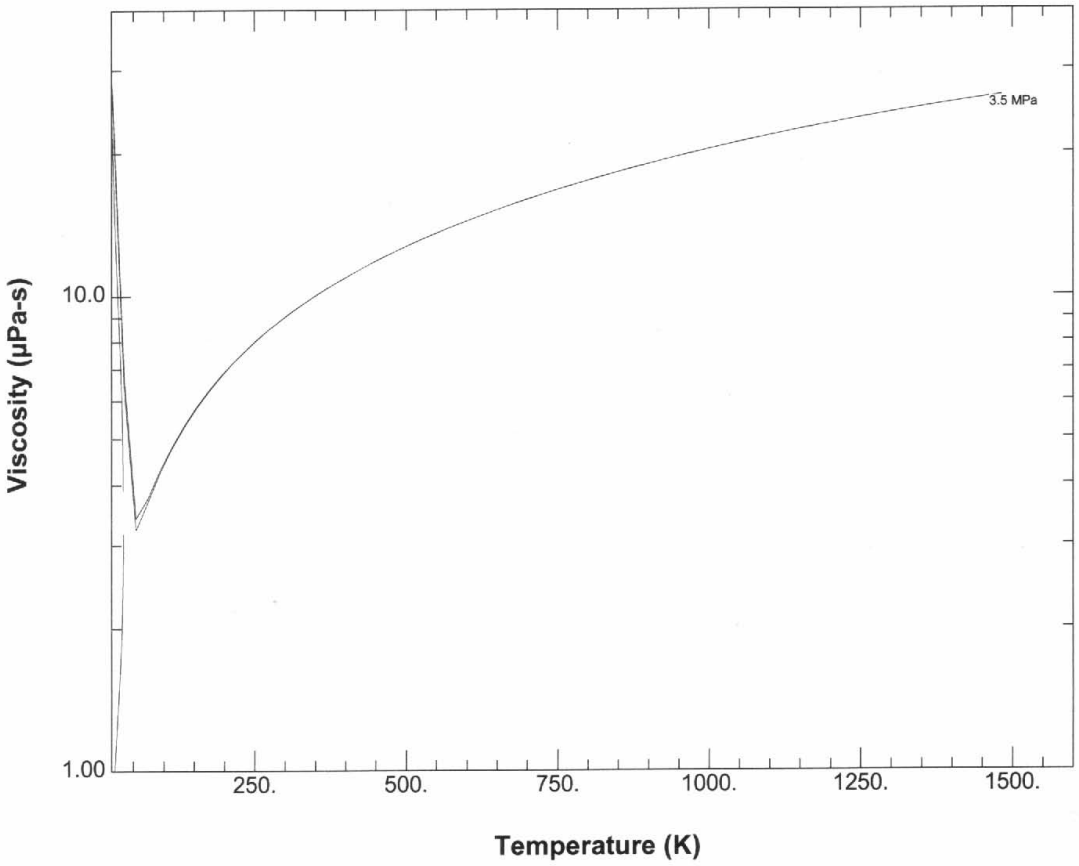

Figure A III- 3 - Viscosity vs. Temperature for GH_2

Appendix IV

Fluent Solver Settings for the 3-D CFD Model

Table A IV.1 shows complete configuration of Fluent for the present study.

Table A IV.1- Fluent Solver Settings

Problem Setup	Options			
General	Mesh	Scale		
		Check		
		Report Quality		
		Display		
	Solver	Type	Pressure-Based	
			Density-Based	
		Velocity Formulation	Absolute	
			Relative	
		Time	Steady	
			Transient	
	Gravity: Uncheck			
Models	Multiphase: Off			
	Energy: On			
	Viscous: Standard, k-e, Standard Wall Fn, Viscous Heating			
	Radiation: Off			
	Heat Exchanger: Off			
	Species: Off			
	Discrete Phase: Off			
	Solidification & Melting: Off			
	Acoustics: Off			
Materials	Fluid	Hydrogen (H_2)		
		Air		
	Solid: Aluminum, Steel			
Cell Zone Conditions	Zone: Inner Fluid	Material name	Hydrogen (H_2)	
			Air	
Boundary Conditions	Zone	Inlet Type: Mass-flow-inlet	Momentum	Reference Frame: Absolute
				Mass Flow Specification Method: Mass Flow Rate
				Mass Flow Rate (kg/s): 0.005
				Supersonic/Initial Gauge Pressure (MPa): 4.0
				Direction Specification Method: Direction Vector
				Coordinate System: Cartesian (X, Y, Z)
				X-Component of Flow Direction: 1
				Y-Component of Flow Direction: 0
				Z-Component of Flow Direction: 0
			Turbulence	Specification Method: Intensity and Hydraulic Diameter
				Turbulent Intensity (Fraction): 0.5
				Hydraulic Diameter (m): 0.00254
			Thermal	Total Temperature (K): 300
		Interior- Inlet Fluid		
		Outlet		Gauge Pressure (MPa): 3.0

		Type: pressure-outlet	Momentum	Backflow Direction Specification Method: Normal to Boundary		
				Radial Equilibrium Pressure Distribution		
				Target Mass Flow Rate		
			Turbulence	Specification Method: Intensity and Hydraulic Diameter		
				Turbulent Intensity (Fraction): 0.5		
				Hydraulic Diameter (m): 0.00254		
			Thermal	Total Temperature (K): 300		
		Surface Type: Wall	Momentum	Wall Motion	Stationary Wall	
					Moving Wall	
				Shear Condition	No Slip	
					Specified Shear	
					Specularity Coefficient	
					Marangoni Stress	
				Wall Roughness	Roughness Height (m): 0	
					Roughness Constant: 0.5	
			Thermal	Thermal Conditions	Heat Flux	Heat Flux (W/m2): 2200000
						Wall Thickness: 0
						Heat Generation Rate (W/m3): 0
						Shell Conduction: Uncheck
					Temperature	Temperature (K): 400
						Wall Thickness: 0
						Heat Generation Rate (W/m3): 0
						Shell Conduction: Uncheck
					Convection	
					Radiation	
					Mixed	
	Phase	Mixture				
	Type	Axis				
		Exhaust-fan				
		Inlet-vent				
		Intake-fan				
		Interface				
		Mass-flow-inlet				
		Outflow				
		Outlet-vent				
		Pressure-far-field				
		Pressure-inlet				
		Pressure-outlet				
		Symmetry				
		Velocity-inlet				
		wall				
Dynamic Mesh	Dynamic Mesh: Uncheck					
Reference Values	Compute From	Inner Fluid				
		Inlet				
		Interior- Inner Fluid				
		Outlet				
		Surface				
	Reference Values	All calculated with the boundary conditions provided.				

Solution			
Solution Methods	Pressure-Velocity Coupling	Scheme	SIMPLE
			SIMPLEC
			PISO
			Coupled
	Spatial Discretization	Gradient	Green-Gauss Cell Based
			Green-Gauss Node Based
			Least Squares Cell Based
		Pressure	Standard
			PRESTO!
			Linear
			Second Order
			Body Force Weighted
		Density	First Order Upwind
			Second Order Upwind
			QUICK
			Third-Order MUSCL
		Momentum	First Order Upwind
			Second Order Upwind
			Power Law
			QUICK
			Third-Order MUSCL
		Turbulent Kinetic Energy	First Order Upwind
			Second Order Upwind
			Power Law
			QUICK
			Third-Order MUSCL
		Turbulent Dissipation Rate	First Order Upwind
			Second Order Upwind
			Power Law
			QUICK
			Third-Order MUSCL
		Energy	First Order Upwind
			Second Order Upwind
			Power Law
			QUICK
			Third-Order MUSCL
Solution Control	Courant Number: 200		
	Explicit Relaxation Factors	Momentum: 0.75	
		Pressure: 0.75	
	Under-Relaxation Factors	Density: 1	
		Body Forces: 1	
		Turbulent Kinetic Energy: 1	
		Turbulent Dissipation Rate: 1	
		Turbulent Viscosity: 1	
		Energy: 1	
Monitors	Residuals, Statistics and Force Monitors	Residuals- Prints, Plots: 1e-08	
Solution Initialization	Compute from	All-Zones	
		Inlet	
		Outlet	
		Surface	
	Initial Values	Gauge Pressure (Pascal): Predicted Other values for initial velocity, temperature are calculated according to the given boundary conditions.	
Calculation Activities	Auto save every iteration		
Run Calculation	Check case Number of Iterations: 1000 Calculate		

Appendix V

List of Program Parameters – Common to all Runs

List of program parameters used in the program that are common to all runs:

L = 1.2 m

D = 0.00254 m

R = 4124.3 J/kg-K

k = 0.1554 W/m-K

c_p = 14065 J/kg-K

μ = 1.76 x 10^{-6} kg/m-s

Ti = 300 K

P_e = 3.1 MPa

m_{dot} = 0.005 kg/s

Appendix VI

List of Program Parameters – Specific to Each Run

List of parameters that are specific to the Base Run (3-D Two-Domain):

Mesh size: 212,577 cells

$dx = 1 \times 10^{-3}$ m

$dr = 5 \times 10^{-3}$ m

L = 1.2 m

D = 0.00254 m

t = 0.000125 m

T*i* = 300 K

P_i = 8.609 MPa (calculated)

m_{dot} = 0.005 kg/s

P_e = 3.1 MPa

$u_{i=}$ 141.818 m/s (calculated)

$T_{e=}$ 2076.79 K (calculated)

ΔT = 1776.79 K

Ma = 0.107 (calculated)

Appendix VII

Run Matrix for Numerical Simulation

Table A VI.1- 1-D Unsteady Model Run Matrix

Run Name	Study	
1D-H2-I	Time Increment, Δt [s]	
Common Run Parameters T_i = 300 K m_{dot} = 0.005 kg/s P_e = 3.1 MPa Q_{cst} = 22,000 kJ/s-m^2 IN = 41 C_f = 0.99	1.	$5x10^{-6}$
	2.	$1x10^{-6}$
	3.	$5x10^{-7}$
1D-H2-II	Mesh Independence, IN	
Common Run Parameters T_i = 300 K m_{dot} = 0.005 kg/s P_e = 3.1 MPa Q_{cst} = 22,000 kJ/s-m^2 $\Delta t = 5x10^{-6} - 1x10^{-6}$ C_f = 0.99	1.	31
	2.	41
	3.	51
1D-H2-III	Co-efficient of Friction, C_f	
Common Run Parameters T_i = 300 K m_{dot} = 0.005 kg/s P_e = 3.1 MPa Q_{max} = 22,000 kJ/s-m^2 $\Delta t = 5x10^{-6}$ sec	1.	0.3
	2.	0.55
	3.	0.99
1D-H2-IV	Heat Input, Q [kJ/s-m^2]	
Common Run Parameters T_i = 300 K m_{dot} = 0.005 kg/s P_e = 3.1 MPa $\Delta t = 5x10^{-6}$ sec C_f = 0.99	1.	Q = 0 [Adiabatic]
	2.	Constant Heat Flux, Q [kJ/s-m^2]
	2.a	1,600
	2.b	3,000
	2.c	7,000
	2.d	18,000
	3.	Variable Heat Flux, Q [kJ/s-m^2]
	3.a	18,000
	3.b	20,000
	3.c	22,000

*** Runs marked in red were chosen for the case studies.

Table A VI.2- 3-D One-Domain Steady State Model Run Matrix

Run Name	Study			File Name
Working Fluid GH_2				
3D-H2-1 DM- I	Mesh Independence			
Common Run Parameters T_i = 300 K P_e = 3.1 MPa m_{dot} = 0.005 kg/s Q_{max} = 22,000 kJ/s-m^2 5 layer mesh		Cell size, dx [m]	No. of Cells	
	1.	$1x10^{-3}$	200,400	mesh study_22.dl
	2.	$8x10^{-4}$	217,000	mesh study_22.dr
	3.	$5x10^{-4}$	348,000	variableheatflux_22mj.dr
3D-H2-1 DM- II	Mesh Independence [Different Layers]			
Common Run Parameters T_i = 300 K P_e = 3.1 MPa m_{dot} = 0.005 kg/s Q_{max} = 22,000 kJ/s-m^2 dx=$1x10^{-3}$		No. of Layers	No. of Cells	
	1.	5	200,400	mesh study_22.dl
	2.	10	320,400	mesh study_10lyr.dl
	3.	13	378,000	mesh study III-3.dl
3D-H2-1 DM-III	Heat Input, Q [kJ/s-m^2]			
Mesh Size: 348,000 Common Run Parameters T_i = 300 K P_e = 3.1 MPa m_{dot} = 0.005 kg/s	4.	Q = 0 [Adiabatic]		1-DMconstanthf0mj.dr
	5.	Constant Heat Flux, Q [kJ/s-m^2]		
	2.a	1,600		1-DMconstanthf1600kj.dr
	2.b	3,000		1-DMconstanthf3000kj.dr
	2.c	7,000		1-DMconstanthf7000kj.dr
	2.d	18,000		cst hf 18mj.dr
	2.e	22,000		cst hf 22mj.dr
	6.	Variable Heat Flux, Q [kJ/s-m^2]		
	3.a	18,000		variableheatflux_18mj.dr
	3.b	20,000		variableprop.dr
	3.c	22,000		variableheatflux_22mj.dr
3D-H2-1 DM-IV	Constant Wall Temperature, T_w [K]			
	4.	400		8-28i.dl
3D-H2-1 DM-V	Mass Flow rate, m_{dot} [10^{-3} x kg/s]			
Mesh Size: 348,000 Common Run Parameters T_i = 300 K P_e = 3.1 MPa m_{dot} = 0.005 kg/s Q_{max} = 22,000 kJ/s-m^2	4.	4.0		
	5.	5.0		variableheatflux_22mj.dr
	6.	6.0		
3D-H2-1 DM-VI	Turbulence Models			
Mesh Size: 348,000 Common Run Parameters T_i = 300 K P_e = 3.1 MPa m_{dot} = 0.005 kg/s Q_{max} = 22,000 kJ/s-m^2	1.	k-e		variableheatflux_22mj.dr
	2.	Spalart-Allmaras		SA-VI2.dr
	3.	k-omega		k-moega.dr
3D-H2-1 DM-VII	Physical Parameters			
Mesh Size: 348,000 Common Run Parameters T_i = 300 K P_e = 3.1 MPa m_{dot} = 0.005 kg/s	1.	k, Cp, $\nu = C^{st}$		Constant VII-1.dr
	2.	k, Cp, ν = Variable		variableheatflux_22mj.dr

Q_{max} = 22,000 kJ/s-m^2			
Working Fluid Air			
3D-A-1 DM-I	Heat Input, Q [kJ/s-m^2]		
Mesh Size: 348,000	1.	Q = 0 [Adiabatic]	-
Common Run Parameters	2.	Constant Heat Flux, Q [kJ/s-m^2]	
T_i = 300 K	2.a	500	1-13.dl
P_e = 3.0 MPa	2.b	700	1-14.dl
u_i = 70 m/s	2.c	1,000	1-15.dl
3D-A-1 DM-II	Constant Wall Temperature, T_w [K]		
Mesh Size: 200,400	1.	400	1-9.dl
T_i = 300 K	2.	500	1-10.dl
P_e = 3.0 MPa			
u_i = 70 m/s			

*** Runs marked in red were chosen for the case studies.

Table A VI.3- 3-D Two-Domain Steady State Model Run Matrix

Run Name	Study			File Name
Working Fluid GH_2				
3D-H2-2 DM- I	Mesh Independence			
Common Run Parameters T_i = 300 K P_e = 3.0MPa m_{dot} = 0.005 kg/s Q_{max} = 22,000 kJ/s-m^2		Cell size, dx [m]	No. of Cells	
	1.	5 x 10^{-3}	40,080	mesh study I-1.dr
	2.	2x10^{-3}	100,200	mesh study 2DM.dr
	3.	1x10^{-3}	212,577	variable non-uni_hf22.dr
3D-H2-2 DM-II	Mesh Independence [Different Layers in Fluid]			
		No. of Layers	No. of Cells	
Common Run Parameters T_i = 300 K P_e = 3.1 MPa m_{dot} = 0.005 kg/s Q_{max} = 22,000 kJ/s-m^2	7.	5	212,577	variable non-uni_hf22.dr
	8.	10	319,200	mesh study II-2.dl
	9.	13	386,400	mesh study II-3.dl
3D-H2-2 DM-III	Mesh Independence [Different Layers in Solid]			
Common Run Parameters T_i = 300 K P_e = 3.1 MPa m_{dot} = 0.005 kg/s Q_{max} = 22,000 kJ/s-m^2		No. of Layers	No. of Cells	
	1.	5	340,800	non-uni_400 5lyr.dr
	2.	8	403,200	non-uni_400 8lyr.dl
	3.	10	459,600	non-uni_400 10lyr.dr
3D-H2-2 DM-IV	Heat Flux, Q [kJ/s-m^2]			
Mesh size: 212,577 Common Run Parameters T_i = 300 K P_e = 3.1 MPa m_{dot} = 0.005 kg/s	1.	Q = 0 [Adiabatic]		constanthf0kj.dl
	2.	Constant Heat Flux, Q [kJ/s-m^2]		
	2.a	1,600		constanthf1600kj.dl
	2.b	3,000		constanthf3000kj.dl
	2.c	7,000		constanthf7000kj.dl
	2.d	18,000		cst hf18mj.dr
	2.e	22,000		cst hf 22mj.dl
	3.	Variable Heat Flux, Q [kJ/s-m^2]		
	3.a	18,000		variable non-uni_hf18.dr
	3.b	20,000		variable updt_non-uni_400.dl
	3.c	22,000		variable non-uni_hf22.dr
3D-H2-2 DM-V	Constant Wall Temperature, T_w [K]			
	5.	400		8-15i.dl
3D-H2-2 DM-VI	Inlet Temperature, T_i [K]			
Mesh size: 212,577 Common Run Parameters P_e = 3.1 MPa m_{dot} = 0.005 kg/s Q_{max} = 22,000 kJ/s-m^2	1.	200		inlet200
	2.	300		variable non-uni_hf22.dr
	3.	400		inlet400
	4.	500		inlet500
3D-H2-2 DM-VII	Mass Flow rate, m_{dot} [10^{-3} x kg/s]			
Mesh size: 212,577 Common Run Parameters T_i = 300 K P_e = 3.1 MPa Q_{max} = 22,000 kJ/s-m^2	7.	4.0		mdot4.dl
	8.	5.0		variable non-uni_hf22.dr
	9.	6.0		mdot6.dl
3D-H2-2 DM-VIII	Physical Parameters			
Mesh size: 212,577 Common Run Parameters T_i = 300 K	1.	k, Cp, $\nu = C^{st}$		constant VI-1.dr
	2.	k, Cp, ν = Variable		variable non-uni_hf22.dr

P_e = 3.1 MPa m_{dot} = 0.005 kg/s Q_{max} = 22,000 kJ/s-m^2			
3D-H2-2DM-IX	Material		
Mesh size: 212,577 Common Run Parameters T_i = 300 K P_e = 3.1 MPa m_{dot} = 0.005 kg/s Q_{max} = 22,000 kJ/s-m^2	1.	Aluminum	benchmark for Al.dl
	2.	Steel	benchmark for Steel.dl
3D-A-2DM-I	Working fluid Air		
Mesh size: 420,840 Common Run Parameters T_i = 300 K u_i = 70 m/s P_e = 3.0 MPa	1.	Q = 0 [Adiabatic]	FFF.1
	2.	Constant Heat Flux, Q [kJ/s-m^2]	FFF.1-3
	3.	Constant Wall Temperature, T_w [K]	FFF.2

*** Runs marked in red were chosen for the parametric study.

Vita

Sajan Bikram Singh was born on September 13, 1986 in Mahendranagar, Kanchanpur, Nepal. He received his bachelor's degree in mechanical engineering from the University of New Orleans, New Orleans, LA, USA in December 2010. He was admitted to the University of New Orleans as a graduate student in mechanical engineering. During the course of his study, he worked as a graduate teaching assistant and had a chance to assist in thermal sciences laboratory. His research interests include fluid mechanics, heat transfer and computational fluid dynamics. In December 2013, he was granted a Master of Science degree in mechanical engineering from the University of New Orleans.